Radiative Transfer and the Dynamics of Small-scale Magnetic Structures on the Sun

A Thesis
Submitted for the Degree of
Doctor of Philosophy
in the Faculty of Science

by

Rajaguru, S.

Department of Physics
Indian Institute of Science
Bangalore INDIA

June 1999

Declaration

I hereby declare that the work reported in this thesis is entirely original. It was carried out by me in the Department of Physics, Indian Institute of Science, and Indian Institute of Astrophysics, Bangalore under the Joint Astronomy Programme. I further declare that it has not formed the basis for the award of any degree, diploma, membership, associateship or similar title of any University or Institution.

Department of Physics
Indian Institute of Science
Bangalore 560 012, INDIA.

S.P.K Rajaguru.

(**S.P.K.Rajaguru**)
Candidate

Acknowledgements

I wish to express my sincere thanks to Professor Siraj Hasan, Indian Institute of Astrophysics for his support as my thesis supervisor. My association with him has been a source of much learning, especially the ways and means of scientific reasearch. I would specially like to thank him for patiently reading every word of this thesis and suggesting improvements in the presentation and style.

I thank Professor Venkatakrishnan for numerous useful discussions on the subject of this thesis and also for sharing his vast knowledge in solar physics. I thank Dr.Arnab Rai Choudhury for many scientific discussions. I thank Professor Gokhale for his course on 'Advanced Solar Physics' which was of immense use in acquainting me with modern reasearch problems in solar physics. I wish to thank the Joint Astronomy Programme coordinators Dr.Chanda J. Jog and Dr.Arnab Rai Choudhury.

I wish to thank the Supercomputer Education and Research Centre (SERC), IISc for the excellent computational facilities, where much of my research computations were done. I also wish to thank the Indian Institute of Astrophysics for computational, library and other essential facilities.

It is a pleasure to thank a lot of my friends, both at IISc and IIA, who have been a source of much enjoyment and fun: to name a few, Mahendra Prabhu and Bhuvanesh in my early days at IISc, Srikanth and Charu - my batchmates in JAP, and other friends: Rambho, R.D.Prabhu, Mangala, Dilip, Sivarani, Sankar, Ashish, Dharam, Amit, Sridharan, Jana, Krishna, Geetha, Preeti, Geetanjali, Arun, Pandey, Swara and many more.

Finally, and very importantly, I thank my parents and my brothers & sisters for all their love and support.

Preface

Observations have revealed that the surface distribution of the Sun's magnetic field is in an inhomogeneous concentrated form, ranging in size from small scale (sub-arc-second) intense flux tubes with diameter of around 100 km to sunspots with diameters of several thousand kilometers. Such a state of the magnetic field has been recognised as central to the structuring of the solar atmosphere, to the heating of the chromosphere and the corona and to a variety of active phenomena observed on the Sun. The identified processes, like the Parker's bouyancy instability, which account for the transport of the dynamo generated field from deep in the convection zone to the surface fail to explain the observed strengths, be it in the small scale structures or in the sunspots. The strengths in the range of 1-2 kG (kilogauss) for the small scale intense tubes and of about 3 kG for the sunspots are an order of magnitude higher than the equipartition values. Thus it has been recognised that the observed surface magnetic structures owe their formation, their distribution in size and strength to the local dynamics of the photopheric gas; in this respect it has been known that a convective instability termed -'convective collapse' operating inside weak field structures in the superadiabatic layers just below solar photosphere is responsible for the intensification of the structures into intense tube-like vertical structures. Furthermore, it has been found that the evolution of gaseous motions in these regions of the Sun is dynamically coupled to radiative energy exchange: radiation contributes to the heating or cooling of the gas and so affects the dynamics of the motion. In general, formation and maintanance of time dependent structures on the solar surface, like the granulation and the magnetic structures, are seen as a result of exchange of energy and matter in situations far from equilibrium. Hence a detailed study of the interaction between radiation and the hydrodynamics would give a physical explanation of the sizes of the structures that are seen. Such interactions are important for a study of the small scale magnetic structures as the length scales associated with these structures are comparable to the photon mean free paths. The study in this thesis is built on the above ideas in relation to the convective instability and wave-motions of the gas trapped inside the small scale magnetic structures. The stability characteristics of the usual magnetohydrodynamic wave-modes present in these structures, which are believed to play a crucial role in the heating of the chromospheric and coronal layers, are affected by radiative energy

exchange; lateral exchange of radiation by a flux tube with its surroundings is known to drive the magnetoacoustic slow mode overstable. In this thesis we thoroughly examine the character of such motions when the vertical radiative losses are self-consistently taken into account.

The main thrust of the thesis is on the effects of radiative processes on the wave modes in magnetic flux tubes. Since we are dealing solely with small-scale intense flux tubes, we adopt the *thin flux tube approximation* when solving the MHD (magnetohydrodynamic) equations. The coupling of the radiation field with the flux tube is provided by the energy equation, which incorporates the contribution due to radiative energy transport. Radiative transfer is treated in various levels of approximations: quasi-adiabatic, diffusion and finally in the generalised Eddington approximation. We examine the effects of radiative transfer on the wave modes using these approximations and delineate their validity. We study the development of the convective instability and the stabilizing influence of the radiation leading to a prediction of the size-strength relation for the tubes. We also examine in detail the character and development of the overstable modes and the thermal-convective modes.

The first part of Chapter I gives an overview of the present knowledge about the surface magnetic field of the Sun. In the second part, we outline our theoretical approach and develop the mathematical formulation that forms the basis for the investigation in this thesis, viz. the effects of radiative transfer on the dynamics of flux tubes, incorporating both vertical and horizontal energy transport; the latter involving heat exchange between the flux tube and the ambient medium.

In Chapter II, a general mathematical basis for the dynamics of gas confined in thin vertical flaring flux tubes embedded in a radiating fluid, treating the radiation to be diffusive, is presented followed by a brief overview of the earlier known treatments and results which are shown to emerge in the appropriate limits of the present treatment. This chapter also contains a quasiadiabatic analysis of the vertical radiative transport and simple analytical results are derived using a local stability analysis.

In Chapter III, we present general results on radiative transfer effects for magnetic flux tubes embedded in a polytropically stratified atmosphere. We enlarge the results of previous analyses and obtain a generalised necessary condition for the onset of convective instability in the presence of radiative heat diffusion. We calculate the frequencies and growth rates of the overstable modes that are set up due to the radiative exchange and show the existence of a Hopf bifurcation through which the overstable oscillations are set up.

In Chapters IV and V, we focus on intense flux tubes extending vertically through the photosphere and convection zone of the Sun. We choose a realistic stratification for the flux tube (and ambient

medium) based on a model atmosphere and also use realistic opacities from recent opacity tables. Chapter IV employs the diffusion approximation while in Chapter V a more refined treatment based on the generalized Eddington approximation is adopted. Size(flux)-strength relations for the tubes are derived and compared with the recent observational results. A comparison of the results of the diffusion and Eddington approximations are given in Chapter V.

In the final Chapter VI, we summarize the main results obtained in the thesis and highlight their contribution on our understanding of magnetic flux tubes on the Sun. We also critically assess the strengths and weaknesses of our work and suggest scope for further research.

Contents

Chapter 1

Introduction

This thesis presents a study of certain aspects of the physics of small-scale magnetic elements found on the Sun's surface layers. The major concern of the thesis is on the effects of radiative energy exchange on the convective and oscillatory motions of the gas inside these magnetic elements. A complete and comprehensive description of such effects would require consideration of the magnetohydrodynamic equations coupled to the radiative transfer equations; but owing to the complex nature of such systems, and for mathematical tractability, it is desirable that we employ suitable approximations that nevertheless capture the essential physics of the problem. As far as the magnetohydrodynamics is concerned, a reduced system of equations, that result from the so called *slender (or thin)-tube-approximation*, has proved to be extremely effective for the study of solar magnetic elements which are vertical tubes of diameter much less than the typical length scales such as the local pressure scale height. The treatment of radiative transfer too requires careful assessment of the physical system at hand: in the case of the Sun, the material below the photospheric layers is optically thick, where the diffusion approximation is valid. However, the photosphere, where there is a transition from the optically thick lower convecting medium to the optically thin higher chromospheric layers, ideally requires solving the radiative transfer equation for the specific intensity and thereby calculating the radiative flux. In view of the enormous computational effort needed to solve the full transfer equations and coupling them to the hydrodynamic equations, we resort to various levels of approximation ranging from the quasi-adiabatic approximation to the generalised Eddington approximation. The latter has been shown to yield both the optically thick and thin limits correctly (Unno and Speigel 1966). Comparison and delineation of the validity of these approximations of radiative transfer in relation to the coupling between the radiation field and hydrodynamics is one of our objectives in this thesis.

In Chapter II, a general mathematical basis for the dynamics of gas confined in thin vertical flaring flux tubes embedded in a radiating fluid, is presented, followed by a brief overview of the

earlier known treatments and results which are shown to emerge in the appropriate limits of the present treatment. This chapter also contains a quasi-adiabatic analysis of vertical radiative energy transport and the derivation of simple analytical results based on a local stability analysis. Chapters III and IV focus on more realistic and detailed treatments involving numerical solutions of the linear equations derived in Chapter II. In Chapter III, general results on radiative transfer effects for magnetic flux tubes embedded in a polytropically stratified atmosphere are presented, assuming the tube and the surrounding polytrope to be in radiative equilibrium. Chapter IV concentrates on an analysis applicable to small-scale magnetic structures extending vertically through the photosphere and the convection zone of the Sun based on a realistic model atmosphere. Size-strength relations and overstability criteria are derived for solar flux tubes. In Chapter V, the treatment for radiative tranfer used in Chapter IV is further refined to employ the generalised Eddington approximation. Realistic results are obtained for solar small-scale structures. Furthermore, a relation between the size and field strength, based on stability arguments, are derived and compared with observations. The final chapter summarizes the main results of this thesis and points to future directions.

In Section 1.1 below we take stock of the present knowledge about the Sun's magnetic field: how it is maintained, its general surface appearance and the well known properties that have been established both observationally and theoretically; the observational facts concerning the small scale magnetic fields and their physics are reviewed in section 1.2. Section 1.3 reviews the earlier results related to the problems chosen for study in this chapter.

1.1 Magnetic fields on the Sun

The Sun, being the closest star, gives us the opportunity to study in great detail a variety of stellar phenomena that occur over scales from only a hundred kilometers-the presently achieved resolution- to the scale of the whole star. The photosphere – the visible surface of the Sun that we see – is dominated by granulation and supergranulation, which is a direct manifestation of the underlying convective motions, and magnetic fields. The first demonstration that stars generate and maintain magnetic fields came from the discovery of the Zeeman effect in sunspots by Hale (1908); and the first detection of distinct magnetic structures in the solar photosphere outside sunspots was also reported by him (Hale 1922). Over the years, with improvements in our observational methods and the development of sophisticated instruments both on ground and on spacecrafts, it has become clear that the Sun organizes its magnetic fields in a hierarchy of structures which extends from large active regions with a size of 10^5 km down to the smallest magnetic flux concentrations with a diameter of the order of 10^2 km. These magnetic structures are now accepted to be central to the

structure and dynamics of the solar atmosphere and in all aspects of solar activity. They are also believed to play an essential role in the solution of the long standing problems of chromospheric and coronal heating.

Though much of the physical properties of these magnetic structures, such as their field strengths and sizes are determined mainly by the local properties of the photospheric matter and its dynamics, the overall global behaviour of Sun's magnetic field such as its origin and maintenance, the 11 year cycle are thought to be determined by a dynamo inferred to be operating at the interface between the convection zone and the radiative interior (e.g., Parker 1979, Procter et al 1993). The necessity of a dynamo for the Sun is evident from the fact that the resistive decay time of its magnetic field is of the order of only 10^9 years, much less than its age, and from the well-known behaviour of the solar cycle with a period of 22 years. The convection superposed on the solar differential rotation is thought to be the key factor responsible for the operation of the solar dynamo.

The observations of the behaviour of the large-scale field, combined with the theoretical models for the dynamo and the dynamical behaviour of the generated field, point to the following hypothetical picture: in the convection zone the dynamo generates a large scale field that consists of two 'tubes' of toroidal field, oppositely oriented in each hemisphere. A bouyancy instability causes the field to rise through the convection zone to break through the surface, thus forming bipolar active regions. These tubes apparently move to the equator in about 11 years and 'disappear', after which new tubes are generated at high latitudes in which the field direction is reversed. While the latitudinal migration of the emerged fields is almost explained by the differential rotation, the periodicity, and thus a mechanism to reverse the direction of the field, is thought to be provided by the turbulent convection.

As mentioned earlier, the surface properties of the magnetic structures, including the sunspots, are believed to be determined by the physical phenomena that occur locally, because the mechanisms invoked to explain the transport of the flux to the surface fail to explain the formation of sunspots with the observed field strengths as well as almost all known observed properties of the small scale elements. Nevertheless, there are successful models that explain the global properties such as the locations of the newly emerging bipolar regions over the solar cycle and the associated morphology of the sunspot pairs. Thus, though the formation and the sub-surface topology of the sunspot field in the Sun still remain long-standing puzzles in solar physics, the small scale magnetic elements, which possibly are a form of the recycled fields that diffuse out from the decaying active regions and spread over whole of the Sun's surface, are extensively researched, both observationally and theoretically. We review, in the following section, the current status of the physics of these elements.

1.2 Physics of small-scale magnetic fields

1.2.1 Observations

The Zeeman effect produces linear and/or cicular polarization in the wings of spectral lines and this is used to detect and measure the magnetic fields in the solar atmosphere. After the first detection of distinct magnetic structures outside of sunspots in 1922 by Hale, magnetographs that utilize the cicular polarization of the Zeeman components of spectral lines (Babcock and Babcock 1952, Kiepenheuer 1953) were built and the magnetic fluxes in active regions and in the network outlined by the supergranular velocity pattern were measured. Subsequently the observations of Sheeley (1966,1967) and Beckers and Schroter (1968) established the highly inhomogenous nature of the non-spot fields whose field strengths were much larger than the average field strengths derived from low spatial resolution measurements. Howard and Stenflo (1972), by comparing the magnetic response of different spectral lines, showed that more than 90% of the magnetic flux outside sunspots is in the form of strong (kilogauss) fields. Since the average field strengths were much smaller, this indicated that small magnetic structures with large field strength were surrounded by much less magnetised plasma. The intrinsic field strengths of unresolved magnetic filaments were determined to be in the range of $1-2$ kG by Stenflo (1973) with the introduction of a line-ratio technique. A number of later observations (see Solanki 1993 for a review and references therein) confirmed these results.

The development of sophisticated instruments like the Kitt Peak Fourier Transform Spectrograph/Polarimeter (FTS) (Brault 1978) made it possible to acquire synthetic Stokes profiles (I, V,and Q) for a large number of spectral lines simultaneously. These, together with inversion techniques using theoretical models of magnetic structures, led to the determination of many properties of the magnetic filaments (Solanki 1987, 1990, 1992; Stenflo 1989; Spruit et al. 1991). The important result has been that almost all filaments seem to share basically the same properties viz., magnetic field strength, temperature, diameter (Zayer et al. 1989,1990), leading to the concept of a unique small scale magnetic structure, the magnetic element, which constitutes the basic building block for magnetic fields in active regions and in the 'quiet' Sun network. Together with the complementary two-dimensional high-resolution magnetograms these data have demonstrated the relation between magnetic, flow and intensity structures and the interaction of magnetic fields with convective and oscillatory velocities in the solar photosphere.

The above discussed observations, as noted earlier, cover the active regions-also called the enhanced network and the quiet network: the magnetic elements which make up these structures outline the supergranular boundaries where the convective flows form the downdrafts. These elements are

bright in the continuum and in spectral lines and, are therefore, hotter than the mean photosphere at the same optical depth. The enhanced network exhibits itself as bright faculae seen at greater height; the elements are generally surrounded by rapid external downflows in their immediate environment. Apart from slight differences in the filling factor, the elements comprising both the enhanced and quiet network share uniform properties.

In addition to the distribution of the small scale fields into organised networks, there are also tiny elements of mixed polarity, possibly turbulent, weak fields which reside inside the network cells. Recent observations in the highly Zeeman sensitive infrared spectral lines (Stenflo et al. 1987; Livingston 1991; Zayer et al. 1989; Ruedi 1991; Lin 1995; Solanki et al. 1996) have determined the field strengths of these intrinsically weak fields. Very recent measurements of the small-scale fields (Meunier et al. 1998) indicate that the fraction of flux in these weak field structures maybe as high as about two-thirds of the total flux, in disagreement with the earlier measurements (Frazier and Stenflo 1972; Howard and Stenflo 1972; Stenflo 1973) which attributed over 90% of the flux to the strong kG tubes. The observations of Solanki et al. (1996) have shown that these weak field structures of intermediate field strenths (500-1000 G) are better described by flux tubes than by tangled turbulent fields; they also have obtained size(flux)-strength relations for these structures. Comparing their findings with theoretical predictions (Venkatakrishnan 1986), have led them to conclude that such structures represent tubes which have undergone partial convective collapse as a result of radiative smoothing effects. The study presented in this thesis examines in detail radiative transfer effects in flux tubes and provides a theoretical explanation for the two component distribution (strong and weak), in terms of physical parameters that control convective collapse.

1.2.2 Theoretical explanations

The explanations for the various observed properties of the small scale fields have come from a variety of theoretical approaches which are briefly reviewed below:

Magnetoconvection

Magnetoconvection is the study of the interaction between convection and magnetic fields and the focus is on isolating the basic physical processes that underlie the interaction: convective flows advect and concentrate the magnetic fields (Parker 1963, Weiss 1966) on the one hand, and on the other, the Lorentz force due to the magnetic field modify the stability criteria and the convective patterns (Chandrasekhar 1961). The formation and spatial locations with respect to the convective flow structures in the photosphere of the solar magnetic elements have been explained in terms of

a *flux expulsion* mechanism found in the studies of magnetoconvection (Proctor and Weiss 1982, Nordlund 1984, Weiss 1981, Hurlburt and Toomre 1988) - a kind of "phase separation" between field-free, convecting plasma and magnetic almost stagnant regions. This mechanism involves the sweeping of field lines from the center of convecting cells to their vertices by the fluid motions.

MHD of thin flux tubes

A magnetic flux tube, i.e. a bundle of magnetic field lines whose conception date back to Michael Faraday, is in the solar context a 'roundish' magnetic element separated from its non-magnetic environment by a tangential discontinuity with a surface current. Its diameter at the photosphere is usually very small compared to all relevant spatial scales; this enables one to considerably simplify the MHD equations to a quasi-one-dimensional form called the *thin flux tube approximation (TFA)* (Roberts and Webb 1978). The analysis in the present work is mainly based on this approximation and the mathematical procedure of deriving the set of equations is outlined in Section 1.31. As the action of gravity and the effects of compressibility are captured in the simplest way, this approximation has been extensively used in the study of dynamical instabilities and wave-motions of gas confined in magnetic elements. It is generally believed that field intensification in a moderate flux tube occurs through a mechanism, called *convective collapse*. This process has been studied analytically (Webb and Roberts 1978) and numerically (Spruit and Zweibel 1979; Unno and Ando 1979; Hasan 1983,1984,1985; Venkatakrishnan 1983,1985). We generalize the earlier treatments by including an energy equation which makes it possible to focus on the influence of radiative exchange on the flux tube dynamics, enabling us to make quantitative predictions that can be compared with observations of small scale magnetic elements. Generation and propagation characteristics of MHD wave modes in a flux tube geometry, which play a crucial role in heating the upper atmosphere, have been extensively studied using the *TFA*. Our analysis provides a natural extension to this work through the inclusion of radiative transfer effects.

Numerical simulations

Both static models with sophisticated treatments of radiative transfer (Steiner 1990,1994; Steiner and Stenflo 1990; Pizzo et al.1991,1993; Hasan and Kalkofen 1994; Hasan, Kalkofen and Steiner 1999) and time-dependent two-dimensional simulations with realistic physics (Grossman-Doerth et al. 1989; Shibata et al.1990; Knolker et al.1991; Steiner et al.1997) have been developed for magnetic elements that enable a comparison with observations. These studies aim to describe the quasi-stationary phase of magnetic elements self-consistently including force balance and dynamics,

energy transport by radiation and flows, and interaction with the environment.

1.2.3 Formation of magnetic elements

Magnetic fields, generated by a dynamo localized deep inside the convection zone migrate upwards and emerge in the photosphere and form the bipolar active regions by the combined action of bouyancy, instabilities, and convective flows (Moreno-Insertis 1992). However, the predicted field strengths for the magnetic flux elements that arrive at the surface are lower than those observed. It, therefore, appears, that an additional mechanism is required to further intensify the field through a local process confined to the shallow surface layers. Two mechanisms that offer plausible explanations for concentrating the field are: flux expulsion and convective collapse.

Flux expulsion

The magnetic Reynolds number $R_m = vL/\eta_m$, where v is the magnitude of typical velocity of the solar plasma, L is a typical length scale and η_m is the magnetic diffusivity, is much larger than unity for the solar plasma in view of its very high electrically conductivity; in such situations the solution to the kinematic MHD problem, namely the solution of the MHD induction equation:

$$\frac{\partial \mathbf{B}}{\partial t} = \nabla \times (\mathbf{v} \times \mathbf{B}) + \eta_m \nabla^2 \mathbf{B} \tag{1.1}$$

for a given velocity field has been shown (Parker 1963) to represent a state where the magnetic field is excluded from the regions of closed streamlines; this solution gives values for the strength of the expelled field which is proportional to the magnetic Reynolds number. In reality the backreaction of the field due to the Lorentz force will limit the field strength; this happens when the Lorentz force becomes of the order of the inertial force, i.e.

$$\frac{1}{4\pi}(\nabla \times \mathbf{B}) \times \mathbf{B} \approx \rho \mathbf{v}.\nabla \mathbf{v} \tag{1.2}$$

where ρ is the mass density of the fluid. Using the above equation we can estimate the equipartition field strength as follows:

$$\frac{\mathbf{B^2}}{4\pi} \approx \rho \mathbf{v^2} \tag{1.3}$$

which gives

$$B \approx v(4\pi\rho)^{1/2} \equiv B_{eq} \tag{1.4}$$

Thus, in general, flux expulsion can not amplify the field to values which exceed significantly the equipartition limit B_{eq} defined above. For typical values of $v = 2$ km s^{-1} for the horizontal velocity

and $\rho = 3 \times 10^{-7}$ g cm^{-3} (for the solar photosphere), $B_{eq} \approx 400$ G which is much less than the observed fields strengths of $1 - 2$ kG range.

Dynamical calculations have shown that a convecting high magnetic Reynolds number fluid permeated by a magnetic field concentrates the magnetic flux into filaments between the convection cells (Weiss 1966, Galloway et al. 1978, Weiss 1981, Kerswell and Childress 1992) much like the phenomenon of 'intermittency' for magnetic fields in turbulent flow (Kraichnan 1976, Orszag and Tang 1979, Meneguzzi et al. 1981). The observed network pattern of magnetic field in the solar photosphere with magnetic flux located predominantly in the granular and supergranular downflow regions (Title et al.1987) has been qualitatively captured in the numerical simulations of a magnetised compressible stratified fluid (Nordlund 1983,1986; Hurlburt et al. 1984; Hurlburt and Toomre 1988).

Convective collapse

It has been suggested by Parker (1978) that the further amplification of the field above the equipartition value could occur through the *superadiabatic effect*, which results from a downflow in a magnetic element. This mechanism relies on the superadiabatic stratification of the sub-photospheric layers and on the flow being thermally shielded from the ambient medium. Consequently, a small downflow inside a magnetic element is further accelerated, and the ensuing evacuation of the upper layers of the tube requires the magnetic pressure to increase to maintain pressure balance with the surroundings. The final state is a flux tube with intense fields. Theoretical verification of such a convective instability for a flux tube which is initially in magnetostatic and temperature equilibrium with the surroundings has been done both in the linear limit (Webb and Roberts 1978, Spruit and Zweibel 1979, Unno and Ando 1979) and by non-linear calculations (Hasan 1983, 1984, 1985; Venkatakrishnan 1983,1985). The sufficient condition for stability against convection in the presence of a uniform vertical magnetic field in an arbitrary stratification (Gough and Taylor 1966) is given by:

$$\delta < \left(1 + \frac{\gamma\beta}{2}\right)^{-1} \tag{1.5}$$

where $\delta = \nabla - \nabla_a$ is the superadiabaticity, ∇ and ∇_a being the logarithmic and adiabatic temperature gradients respectively, $\beta = 8\pi p/B^2$ the ratio of gas to magnetic pressure and γ is the ratio of specific heats assumed constant. A similar condition has been derived for a thin flux tube (Webb and Roberts 1978). For the Sun, using a model atmosphere where δ, γ and μ-the mean molecular weight vary over depth, Spruit and Zweibel (1979) have found that the critical value of β for stability is $\beta_c = 1.83$, which corresponds to a field strength (at $\tau_{5000} = 1$ inside the tube) of

about 1300 G, which is in fair agreement with the observed values.

The efficiency of convective collapse described above is determined by the degree of superadiabaticity that the downflow achieves; it is easily realised that, for the small scale structures of sizes of the order of 10^2 km in the solar photosphere, radiation acts as a dominant source of non-adiabaticity: the radiative exchange time scale is comparable to dynamical time scale such as the free-fall time at the photospheric and sub-photospheric driving layers. Such effects of radiation have been studied using approximate treatments (Hasan 1986, Venkatakrishnan 1986). They have demonstrated the stabilizing influence of radiation on the convective mode and the overstable nature of the oscillatory motions that would be stable in the absence of radiation. Venkatakrishnan (1986), using an isothermal stratification and the diffusion approximation for radiation, has derived a relation for the size(flux)-strength distribution for the flux tubes. In this thesis, by a more realistic treatment of radiation transport in a medium with a realistic stratification, we quantiatively examine the linear stability and properties of the convective and oscillatory motions in solar flux tubes.

1.2.4 Wave-motions

The dynamical properties of the magnetic elements are empirically inferred from an analysis of the net circular polarization (Stokes V-profiles) of a spectral line: flows, non-stationary turbulent motions and oscillatory motions within the tubes and external downflows are derived from the zero-crossing wavelength, wing width and asymmetry of the observed Stokes V-profiles, respectively (Solanki 1986, Keller et al.1990, Solanki and Stenflo 1984, Solanki 1989, Grossmann-Doerth et al.1991). The asymmetry is seen in amplitude and area of the Stokes V-profile and often the amplitude shows larger asymmetry than the area: this has been interpreted as the result of oscillations in the interior of magnetic elements (Solanki 1989, Grossman-Doerth et al. 1991). The waves in thin flux tubes can be identified with a longitudinal mode (sausage mode) and a transversal tube mode (kink mode), respectively (Spruit 1981, Herbold et al.1985, Thomas 1985, Roberts 1986, 1991; Ryutova 1990).

Various studies (e.g., Cowling 1957, Chandrasekhar 1961) have revealed that radiative energy exchange can drive overstable oscillations. For the case of a flux tube, radiative exchange with the exterior medium makes the *longitudinal mode* overstable (Hasan 1986). We, in this thesis, examine the properties of this mode using a comprehensive treatment of radiative transfer. Our analysis has important implications for wave-propagation in magnetic structures and for heating of the solar chromosphere.

1.3 MHD and radiative transfer in magnetic elements

There are a variety of astrophysical situations where the hydrodynamics of the motion of a magnetized gas is strongly coupled to radiative energy transport: radiation contributes to the heating or cooling of the gas and so affects the dynamics of the motion. Examples range from stellar atmospheres, accretion discs to early universe. Considering the fact that observations of almost all astrophysical phenomena are made through their effect on the spectrum of radiation they emit, it is important to understand the interplay between the radiation field and the gas.

The basis for our treatment of the dynamical effects of the radiation is provided by the energy equation which relates any two of the thermodynamic fluctuations, e.g, pressure and temperature, through the fluctuation in the divergence of the energy flux. The net energy dissipation rate, in general, has contributions from all possible mechanisms of energy transfer viz., radiation, convection, conduction etc. In this study we deal with those situations where radiative energy transport dominates over all the other means of energy transfer. We begin with the general equations and then derive a set of equations which are applicable for a study of small amplitude waves and instabilities in a one dimensional gravitationally stratified medium. The geometry of the magnetic field is taken to be that of a vertical flaring slender tube in pressure equilibrium with the surroundings. Thus the field strength is depth dependent; the reason for this choice is two-fold: first, the complicated MHD equations get reduced to a more tractable simplified set, and secondly we appeal to the observational fact that about 90 % of the surface magnetic flux, excluding sunspots, on the Sun is in the form of discrete small scale tube-like vertical structures.

1.3.1 Magnetohydrodynamics of slender tubes in a radiating fluid

MHD equations

The gross physical evolution and dynamics of astrophysical as well as laboratory plasmas is conveniently described by magnetohydrodynamics (MHD), with the basic assumption that the the electrons and ions, that comprise the plasma, behave collectively so as to satisfy the criteria for a fluid-description (Braginsky 1965, Landau and Lifshitz 1984, Cowling 1955). The MHD model essentially describes how inertial, magnetic, gravitational, and pressure gradient forces interact. The equations of MHD are (e.g. Landau and Lifshitz 1984):

$$\frac{\partial \rho}{\partial t} + \nabla . \rho \mathbf{v} = \mathbf{0} \tag{1.6}$$

$$\rho \frac{\partial \mathbf{v}}{\partial t} + \rho(\mathbf{v}.\nabla)\mathbf{v} = -\nabla \mathbf{p} + \rho \mathbf{g} + \frac{(\nabla \times \mathbf{B}) \times \mathbf{B}}{4\pi} + \eta \nabla^2 \mathbf{v} \tag{1.7}$$

where η is the coefficient of viscosity and the last term on the right hand side of equation(1.7) is the viscous force per unit volume.

$$\frac{\partial \mathbf{B}}{\partial t} = \nabla \times (\mathbf{v} \times \mathbf{B}) + \eta_{\mathrm{m}} \nabla^2 \mathbf{B} \tag{1.8}$$

To these equations an equation of state which relates the pressure p, density ρ and temperature T of the fluid and the equation of heat transfer is added:

$$p = p(\rho, T) \tag{1.9}$$

The latter is, for the present case,

$$\rho T \left(\frac{\partial s}{\partial t} + \mathbf{v}.\nabla s \right) = \sigma'_{ik} \frac{\partial v_i}{\partial x_k} - \nabla.\mathbf{F} + \frac{c^2}{16\pi^2\sigma} (\nabla \times \mathbf{B})^2 \tag{1.10}$$

where s is the entropy per unit mass of the fluid, σ'_{ik} is the viscous stress tensor and $\mathbf{F}$ is the energy flux vector; the quantity on the left hand side in the above equation represents the heat generated per unit time and volume in a frame moving with a fluid element. The right hand side in the above equation is the energy dissipated per unit time and volume: the first term denotes viscous dissipation, the second term denotes the energy that flows out from a fluid element and the third term denotes Joule dissipation. The above equation of heat transfer, which also states the conservation of energy, can be rewritten in a convenient form using the thermodynamic relation for a gas with ionization gradients

$$s = \frac{c_v}{\chi_T} ln(p\rho^{-\Gamma_1}) + const. \tag{1.11}$$

as

$$\frac{d}{dt}(lnp) - \Gamma_1 \frac{d}{dt}(ln\rho) = \frac{\chi_T}{\rho c_v T} \left[\sigma'_{ik} \frac{\partial v_i}{\partial x_k} - \nabla.\mathbf{F} + \frac{c^2}{16\pi^2\sigma} (\nabla \times \mathbf{B})^2 \right] \tag{1.12}$$

where

$$\Gamma_1 = \frac{\chi_\rho c_p}{c_v}$$

$$\chi_\rho \equiv \left(\frac{\partial lnp}{\partial ln\rho} \right)_T = 1 - \left(\frac{\partial ln\mu}{\partial ln\rho} \right)_T$$

$$\chi_T \equiv \left(\frac{\partial lnp}{\partial lnT} \right)_\rho = 1 - \left(\frac{\partial ln\mu}{\partial lnT} \right)_\rho$$

c_p and c_v are the specific heats at constant pressure and at constant volume respectively and μ is the mean molecular weight; for a gas with no ionization gradients , i.e. with μ constant, we have $\chi_\rho = \chi_T = 1$ and $\Gamma_1 = \gamma = c_p/c_v$. The above equation provides the necessary coupling of the matter to the radiation through the term that contains the flux of energy $\mathbf{F}$ and thus forms the basis for the present treatment of the interaction between the hydrodynamics and the radiative energy

transport. The treatment of radiation and the determination of the radiative flux is discussed in the section on radiative transfer.

We ignore the viscous forces in the momentum equation, viscous and Joule dissipation in the energy equation and resistive diffusion of the magnetic field in the induction equation. The only departure from the ideal MHD description is thus due to the inclusion of radiation in the energy equation. The magnetic field hence is 'frozen' into the plasma and this is in general a good approximation for the solar plasma as the electrical conductivity is sufficiently high.

Thin tube equations

Small-scale magnetic elements found on the Sun can be regarded as magnetic flux tubes with diameters very small compared to all relevant spatial scales. For such a field geometry the MHD equations stated in the previous section can be cast in a very simple, quasi-one-dimensional form, using the *thin flux tube approximation (TFA)* (Roberts and Webb 1978; Spruit 1981; Ferriz-Mas and Schussler 1989).

These equations are (*A derivation of them is given in Appendix A*):

$$\frac{\partial}{\partial t}\left(\frac{\rho}{B}\right)+\frac{\partial}{\partial z}\left(\frac{\rho v}{B}\right)=0 \tag{1.13}$$

$$\rho\left[\frac{\partial v}{\partial t}+v\frac{\partial v}{\partial z}\right]=-\frac{\partial p}{\partial z}-\rho g \tag{1.14}$$

$$p+\frac{B^2}{8\pi}=p_e \tag{1.15}$$

$$\frac{\partial p}{\partial t}+v\frac{\partial p}{\partial z}-\frac{\Gamma_1 p}{\rho}\left[\frac{\partial \rho}{\partial t}+v\frac{\partial \rho}{\partial z}\right]=-\frac{\chi_T}{\rho c_v T}\nabla.\mathbf{F} \tag{1.16}$$

$$Ba^2=const. \tag{1.17}$$

The physical justification of the TFA is based on the fact that all quantities pertaining to the gas inside the tube vary weakly with r, except at $r=R$, the tube-ambient medium interface. Equation (1.15) states that the total pressure which is the sum of the magnetic and gas pressures inside the tube, is equal to the external pressure. This warrants that the time scale for the pressure adjustment over the cross-section of the tube in response to the external pressure changes is small compared to the times scales of the processes that the equations are used to decribe. The pressure adjustment takes place approximately on a time-scale for a magneto-acoustic wave to cross the tube, which is typically a few seconds for a solar magnetic element.

The right hand side of the energy equation (1.16) allows for the possibility of the tube exchanging radiative energy with the oustside medium. In the present thin tube approximation the divergence of the energy flux is:

$$\nabla.\vec{\mathbf{F}} = 2F_{r1} + \frac{dF_z}{dz} \tag{1.18}$$

where F_{r1} is first order term in the expansion of the radial component of the flux and r is the radial coordinate; the above expression is written for a cylindrical coordiante system (r, ϕ, z). [1].

Radiative transfer

The total energy flux vector $\mathbf{F}$ in the energy equation (1.16) may be written as

$$\mathbf{F} = \mathbf{F_R} + \mathbf{F_C} + \mathbf{F_M} \tag{1.19}$$

where $\mathbf{F_R}$ is the radiative flux, $\mathbf{F_C}$ is the convective flux, and $\mathbf{F_M}$ is a 'mechanical' flux which must be invoked to explain any non-thermal heating of the atmospheric layers. As mentioned earlier, since our main concern is on the energy exchange due to radiation, we will ignore any perturbations in the convective and the 'mechanical' fluxes. We assume that the Eulerian perturbations of these non-radiative fluxes are negligible, although in the equilibrium configuration these fluxes may be important.

We start off with a static equilibrium configuration. Any semi-empirical model like the VAL (Vernazza-Avrett-Loeser) model which reproduces the real atmosphere on the Sun in an average (in time) sense can be considered as a static model. In such situations the equilibrium energy equation is of the form:

$$\nabla.\mathbf{F} = \nabla.(\mathbf{F_R} + \mathbf{F_C} + \mathbf{F_M}) = 0 \tag{1.20}$$

Thus while using the real model stratifications for the solar atmosphere, we implicitly assume that the above equation expressing energy conservation is satisfied.

The radiative flux $\mathbf{F_R}$, in general, has to be determined by solving the radiative transfer equation, applicable to the problem on hand. We write down here the radiative transfer equation in its general form and then reduce it under the various approximations that we shall employ: we show how the various forms which are used for optically thick, optically thin and intermediate cases of optical depth are derived in the various limits. For a medium that absorbs as well as scatters, the radiation field in the equilibrium state satisfies:

$$\mu \frac{\partial I_\nu(z,\mu)}{\partial z} = -(\kappa_{a,\nu} + \kappa_{s,\nu})\rho I_\nu + \kappa_{a,\nu}\rho B_\nu + \kappa_{s,\nu}\rho J_\nu \tag{1.21}$$

where $I_\nu(z,\mu)$ is the specific intensity at position z for a frequency ν at the angle $\theta = cos^{-1}\mu$ from the vertical; local thermodynamic equilibrium (LTE) and isotropic scattering have been assumed;

[1] Regularity at $r = 0$ and symmetry of the problem demands that radial components of vectors retain only the odd terms while the scalars and axial components of vectors the even terms, in the expansion about the axis [26]

$\kappa_{s,\nu}$ and $\kappa_{a,\nu}$ are the monochromatic scattering and absorption coefficients, respectively, B_ν is the Planck function and

$$J = \int_0^\infty J_\nu d\nu = \frac{1}{4\pi}\int_0^\infty \oint I_\nu d\Omega d\nu \tag{1.22}$$

is the mean intensity and the integration is over solid angle Ω. We introduce higher moments of the specific intensity, as follows:

$$H = \int_0^\infty H_\nu d\nu = \frac{1}{4\pi}\int_0^\infty \oint \mu I_\nu d\Omega d\nu \tag{1.23}$$

$$K = \int_0^\infty K_\nu d\nu = \frac{1}{4\pi}\int_0^\infty \oint \mu^2 I_\nu d\Omega d\nu \tag{1.24}$$

here H is related to the radiative flux by

$$F_R = 4\pi H \tag{1.25}$$

and K is related to the radiation pressure. We restrict our treatment to the *grey* case , where $\kappa_{a,\nu} = \kappa_a$ and $\kappa_{s,\nu} = \kappa_s$ are assumed to be independent of ν. Then the integration of the transfer equation (1.21) over μ and ν yields

$$\nabla.\mathbf{F_R} = \frac{dF_R}{dz} = 4\pi\kappa_a\rho(\mathcal{B} - J) \tag{1.26}$$

where $\mathcal{B} = \sigma T^4/\pi$ is the frequency-integrated Planck function and σ is the Stefan-Boltzmann constant. Determination of J requires solving the frequency integrated form of the transfer equation (1.21) over adequate number of directions for the rays, i.e. the μ-points; in the presence of scattering the transfer equation contains J and thus is an integro-differential equation. For mathematical tractability we neglect the scattering terms in the transfer equation (1.21) which results in the following simpler form:

$$\mu\frac{\partial I(z,\mu)}{\partial z} = \kappa\rho(\mathcal{B} - I) \tag{1.27}$$

We consider two methods of solving the above form of transfer equation:

Two stream approximation:

In this approximation we assume that the entire radiation field can be represented by radiation travelling along two anti-parallel beams tilted at an angle θ with the vertical; for the upward and downward beams, we have

$$\mu\frac{\partial I^+}{\partial \tau} = \mathcal{B} - I^+ \tag{1.28}$$

$$-\mu\frac{\partial I^-}{\partial \tau} = \mathcal{B} - I^- \tag{1.29}$$

where we have defined optical depth along the vertical, increasing downward, by

$$d\tau = \kappa\rho dz \tag{1.30}$$

In terms of I^+ and I^- the moments J, H, and K have the representations

$$J = \frac{1}{2}(I^+ + I^-) \tag{1.31}$$

$$H = \frac{\mu}{2}(I^+ - I^-) \tag{1.32}$$

$$K = \mu^2 J \tag{1.33}$$

and the addition and subtraction of the two equations (1.28) and (1.29) yield ,respectively

$$\frac{\partial H}{\partial \tau} = \mathcal{B} - J \tag{1.34}$$

$$\frac{\partial J}{\partial \tau} = -\frac{H}{\mu^2} \tag{1.35}$$

The above two equations can be combined into an useful form which forms the basis of the Feautrier finite-difference method for the numerical solution of J given $\mathcal{B}$:

$$\mu^2 \frac{\partial^2 J}{\partial \tau^2} = J - \mathcal{B} \tag{1.36}$$

The conventional Eddington approximation is obtained by considering two anti-parallel beams which have $\mu = \pm 1/\sqrt{3}$. In this case the above equation (1.36) becomes,

$$\frac{1}{3}\frac{\partial^2 J}{\partial \tau^2} = J - \mathcal{B} \tag{1.37}$$

Variable Eddington Factor Method :

Here we form moments of the transfer equation (1.21) and replace the angular dependence in terms of the variable Eddington factors; in terms of the moments defined earlier in equations (1.23) and (1.24) we write down the zeroth and first moments of the transfer equation (1.21) :

$$\frac{dH}{dz} = \kappa\rho(\mathcal{B} - J) \tag{1.38}$$

$$\frac{dK}{dz} = -\kappa\rho H \tag{1.39}$$

The above procedure of forming moments leads to, at each step, one less equation than unknowns, and this process is arrested by introducing the variable Eddington factors which also close the system of equations provided they are known:

$$f = \frac{K}{J} \tag{1.40}$$

The Eddington factors f are not known and the standard technique (Auer and Mihalas 1970) is their determination by iteration, starting from an initial guess which may be taken to correspond to the classical Eddington approximation with $f = 1/3$.

1.3.2 Diffusion approximation

When the medium is locally homogeneous, the radiation field attains near isotropy at large optical depths, as in the interiors of stars, and this combined with the fact that matter is in LTE, i.e. the source function equals the Planck function B, leads to a simple expression for the radiative energy flux, relating it to the local temperature gradient as follows: approximation:

$$F_R = -\frac{4\pi}{3\kappa_R \rho}\frac{\partial \mathcal{B}}{\partial T}\frac{\partial T}{\partial z} = -\frac{16\sigma T^3}{3\kappa_R \rho}\frac{\partial T}{\partial z} \tag{1.41}$$

where κ_R is the Rosseland mean absorption coefficient defined by the relation

$$\frac{1}{\kappa_R} \equiv \frac{\int_0^\infty \frac{1}{\kappa_\nu}\frac{\partial \mathcal{B}_\nu}{\partial T} d\nu}{\int_0^\infty \frac{\partial \mathcal{B}_\nu}{\partial T} d\nu} \tag{1.42}$$

In this approximation, radiative energy transport is essentially like heat conduction, with an 'effective heat conductivity' given by $16\sigma T^3/3\kappa_R\rho$.

For the case of a thin tube which exchanges radiation diffusively with the surroundings, the components of the flux that enter (1.18) are easily found to be:

$$F_{R,r1} = -r\frac{8\pi \mathcal{B}_2}{3\kappa_R \rho} \tag{1.43}$$

$$F_{R,z} = -\frac{4\pi}{3\kappa_R \rho}\frac{d\mathcal{B}}{dz} \tag{1.44}$$

where $\mathcal{B}_2$ is the second order term in the expansion of $\mathcal{B}$ about the axis of the tube and is estimated in an approximate fashion by using the relation

$$\mathcal{B}(a, z) = \mathcal{B}_e(z) \tag{1.45}$$

This yields ,

$$\mathcal{B}_2 = \frac{\mathcal{B}_e - \mathcal{B}}{a^2} = \frac{\sigma(T_e^4 - T^4)}{\pi a^2} \tag{1.46}$$

where $\mathcal{B}_e$ in the above equation denotes the Planck function of the external radiation field.

1.3.3 Generalised Eddington approximation

As noted earlier the Eddington approximation corresponds to taking, in the one dimensional plane-parallel case, $f = K/J = 1/3$ for the Eddington factor which this leads to the following expression for the radiative energy flux:

$$F_R = 4\pi H = -\frac{4\pi}{3\kappa\rho}\frac{\partial J}{\partial z} \tag{1.47}$$

which has been generalised to the three-dimensional case (Unno and Spiegel 1966) :

$$\mathbf{F_R} = 4\pi H = -\frac{4\pi}{3\kappa\rho}\nabla J \tag{1.48}$$

We note that in the case of radiative equilibrium the flux $\mathbf{F_R}$ has zero divergence and equation (1.26) implies $J = \mathcal{B}$. Thus, in radiative equilibrium, the Eddington approximation leads to the diffusion approximation (1.41). For the case of a thin flux tube which has lateral radiative exchange with the surroundings, the above generalised Eddington approximation (1.48) gets reduced to a simple quasi-one-dimensional form.

Having discussed the relevant equations as well as the different levels of approximation, we are now in a position to undertake a linear stability analysis of thin flux tubes, with the effects of radiative energy transport included. The ensuing chapters are devoted to such an investigation.

Chapter 2

Radiative Diffusion and Instability in Slender Magnetic Flux Tubes. I. Mathematical Formulation and Quasi-adiabatic Analysis

2.1 Introduction

The convective stability or instability of a gravitationally stratified gas like the solar plasma, in the absence of any dissipative (viscous, radiative or conductive) forces, is determined by the Schwarzschild criterion which states that the medium is stable against the convective motions if prevailing gradients in temperature is smaller than the adiabatic gradient. Here, we note that the Schwarzschild criterion involves signs as well as the amplitudes of the temperature gradients, and this will be clear in the context at which it is used. Thus, for subadiabatic gradients any mechanical perturbation in the fluid dies down if it is incompressible while in a compressible medium it is maintained as a stable mode of acoustic type driven by the pressure forces when there are no dissipative processes operating. A dissipative mechanism that can be operative in the gas, in the presence of an restoring force, introduces an oscillatory instability, or overstabilty (Chandrasekhar 1961), even if the medium is convectively stable(Refer to Appendix B, Section B.2 for further discussion). Thus in the presence of a magnetic field which imparts a 'pressure' to the ionized plasma through its Lorentz force, the magnetoacoustic oscillations can get amplified, even if the medium is stable against convection. This is characteristic of any dissipative mechanism operative in a gas and the energy that feeds in such amplification comes from the energy sources that cause the dissipation. In a radiating fluid the energy could be drawn from the energy in the radiation.

Quite apart from such modifications introduced by a dissipative process on the convective properties

of a gas, a magnetic field can modify the stability properties of the gas in a fundamental way which is independent of the dissipative processes: due to the Lorentz force exerted on the plasma by the magnetic field, cross-field motions of the plasma are inhibited and this leads to an overall stabilizing influence of the magnetic field against the convective motions (Biermann 1941); this results in the modification of the Schwarzschild criterion. As already mentioned in Chapter 1, a sufficient condition for stability in an adiabatic fluid with a uniform vertical field in an arbitrary stratification is given by equation (1.5), which is also valid for a thin flux tube (Webb and Roberts 1978). A violation of the condition for a thin tube, as is known, is a collapsed tube of higher field strength as against the formation of overturning convective cells in the uniform unbounded field case. Thus, for the present case of a magnetic tube which is maintained by pressure equilibrium with the surroundings and with a strength that is in dynamic equipartition with the field free convective flows, the instability can be triggered by a downflow as discussed by Parker (1978). The ensuing evacuation of the top layers causes the field strength to increase to maintain lateral pressure balance. Thus, we expect an unstable tube to eventually achieve a new equilibrium state with a higher field strength, given approximately by the critical strength for convective stability. This self-limiting behaviour of the instability was later confirmed by Hasan (1984), using a detailed time development study of the instability.

Turning now to the effects of non-adiabaticity due to radiation – the main focus of the present study – it is well known that for a uniform vertical field, overstability exists even for field strengths greater than the critical strength for stability against the overturning convective motions(Chandrasekhar 1961). The convective and oscillatory modes have been identified as two limiting forms of the same mode, the slow magnetoacoustic mode. Overstability shows a complicated dependence on the stratification of the medium, the magnetic field strength and on whether the disturbances are optically thin or thick (Kato 1966). There are contradictory results, as to the dependence of the overstability on the field strength, obtained from treatments which use optically thick and thin limits. Thus, in the Boussinesq limit, overstability has been shown to persist below a certain critical field strength, which is determined by the degree of superadiabaticity (or the Rayleigh number), irrespective of whether the perturbation is optically thick or thin as long as the viscosity and the electrical resistivity are neglected (Chandrasekhar 1961; Kato 1966). On the other hand, for a compressible gas, the behaviour of the overstable mode crucially depends on the optical thickness of the perturbation: for optically thin perturbations, it has been shown to persist even at infinite field strengths (Syrovatskii and Zhugzhda 1967) while in the optically thick regime it gets damped above a certain limiting field strength (Kato 1966).

For a magnetic tube, the aforementioned behaviour is exhibited by the longitudinal sausage mode,

which is an axisymmetric mode of a thin flux tube. It turns out that the dominant non-adiabaticity in thin tubes arises from the lateral diffusion of radiation from the surroundings. At the photosphere, the time scales for convective instability and lateral heat exchange are comparable. The latter depends upon the horizontal dimensions of the tube, and consequently the final 'collapsed state' arising due to the stability has a size (and hence magnetic flux) dependence. There have been simplified treatments (Hasan 1986, Venkatakrishnan 1986) of such non-adiabatic effects on the collapse both in the linear limit and through the numerical simulation of the thin flux tube equations. Venkatakrishnan (1986), assuming an isothermal atmosphere with a constant radiative conductivity and with an ad hoc inclusion of superadiabaticity that is necessary for the collapse, obtained a dispersion relation for the collapse instability with radiative exchange in the diffusion approximation. Hasan (1986), using a more realistic treatment based on Newton's law of cooling for radiative exchange (applicable both in the optically thin and thick limits), studied the instability for polytropic and realistic (based on a model solar atmosphere) stratifications. Both these studies have exhibited the stabilizing influence on convective instability of radiative exchange of the tube with its surroundings.

In the present study, by using a more realistic treatment that includes both vertical and horizontal radiative losses, we self-consistently model the influence of radiative energy transport on the convective stability of a thin tube. We begin our analysis by adopting the diffusion approximation, which despite its limitations, allows us to qualitatively capture many of the physical effects associated with radiative energy transport. We carry out a systematic study with an aim of thoroughly examining the nature and properties of convectively unstable and overstable motions in thin flux tubes. The analysis will be gradually refined in the ensuing chapters.

2.2 Mathematical formulation

2.2.1 Equilibrium

Let us consider an initial equilibrium state of a slender magnetic flux tube embedded in a plane-parallel stratified atmosphere subject to a constant gravitational acceleration $g\mathbf{e}_z$, where $\mathbf{e}_z$ is a unit vector along the z-axis assumed to point into the Sun. This configuration is taken to be in hydrostatic and energy equilibrium with equal temperatures in the flux tube and the external atmosphere at each height. The hydrostatic and pressure balance conditions are,

$$\frac{dp}{dz} = \rho g \tag{2.1}$$

$$p + \frac{B^2}{8\pi} = p_e \tag{2.2}$$

On account of the assumption of temperature balance between the tube and the surroundings the net radiative flux across the tube, i.e. the radial component $F_{R,r}$ of the radiative flux is zero in the equilibrium. Consequently, there is no net heat flux across the tube in the equilibrium. The above assumptions lead to the energy equations (1.16) and (1.18) taking the following form:

$$\nabla.\mathbf{F} = 2F_{r1} + \frac{dF_z}{dz} = \frac{dF_z}{dz} = 0 \tag{2.3}$$

with

$$T = T_e \tag{2.4}$$

The radius of the flux tube is found from the flux conservation condition

$$Ba^2 = \text{constant} \tag{2.5}$$

The condition of temperature equilibrium implies that $\beta = 8\pi p/B^2$ is constant with depth. Hence, it can be easily shown, that the internal pressure and density are reduced by a constant factor, $\beta/(1+\beta)$ of the external pressure and density respectively.

In the external atmosphere, the hydrostatic and energy equilibrium conditions yield:

$$\frac{dp_e}{dz} = \rho_e g \tag{2.6}$$

$$\nabla.\mathbf{F_e} = \frac{dF_{z,e}}{dz} = 0 \tag{2.7}$$

2.2.2 Linear stability: perturbed equations

Small amplitude fluctuations are imposed on the equilibrium configuration, described above. We linearize the thin tube equations (1.13), (1.14), (1.15), (1.16) and (1.18) given in Chapter 1. It is assumed that the external atmosphere is unaffected by the motions inside the tube. Specifically, we neglect the Eulerian perturbations in the external pressure and in the non-radiative energy fluxes, such as the convective energy flux. With these assumptions, small amplitude perturbations inside the tube obey the following equations:

$$\frac{\partial \xi}{\partial z} = \frac{B'}{B} - \frac{\rho'}{\rho} - \left[\frac{d(\ln\rho)}{dz} - \frac{d(\ln B)}{dz}\right]\xi \tag{2.8}$$

$$\frac{\partial^2 \xi}{\partial t^2} = -Hg\frac{\partial}{\partial z}\left(\frac{p'}{p}\right) - g\left(\frac{p'}{p} - \frac{\rho'}{\rho}\right) \tag{2.9}$$

$$\frac{B'}{B} = -\frac{\beta}{2}\frac{p'}{p} \tag{2.10}$$

$$\frac{\partial}{\partial t}\left(\frac{p'}{p}\right) - \Gamma_1 \frac{\partial}{\partial t}\left(\frac{\rho'}{\rho}\right) + \frac{N^2\Gamma_1}{g}\frac{\partial \xi}{\partial t} = -\frac{\chi_T}{\rho c_v T}\nabla.\mathbf{F}' \tag{2.11}$$

where ξ denotes the vertical displacement, H is the pressure scale height and N^2 is the Brunt-Väisälä frequency,

$$N^2 = g\left[\frac{1}{\Gamma_1}\frac{d\ln p}{dz} - \frac{d\ln \rho}{dz}\right] \tag{2.12}$$

The divergence of the flux perturbations, i.e. the perturbation of the equation (1.18) is written as

$$\nabla.\mathbf{F}' = \frac{4KT}{a^2}\frac{T'}{T} + F_z\frac{\partial}{\partial z}\left(\frac{F_z'}{F_z}\right) + \frac{dF_z}{dz}\frac{F_z'}{F_z} \tag{2.13}$$

where the first term on the right hand side corresponds to lateral heat exchange due to thermal fluctuations and the second and third terms describe the effects of perturbations in the vertical radiative energy flux (F_z and F_z' hereafter, denote the vertical radiative flux and its perturbation respectively). The lateral and vertical flux perturbations have been obtained from the relations (1.43), (1.44) and (1.46). Thus the perturbed energy equation takes the form

$$\frac{\partial}{\partial t}\left(\frac{p'}{p}\right) - \Gamma_1 \frac{\partial}{\partial t}\left(\frac{\rho'}{\rho}\right) + \frac{N^2\Gamma_1}{g}\frac{\partial \xi}{\partial t} = -\frac{4K\chi_T}{\rho c_v a^2}\frac{T'}{T} - \frac{F_z\chi_T}{\rho c_v T}\frac{\partial}{\partial z}\left(\frac{F_z'}{F_z}\right) - \frac{\chi_T}{\rho c_v T}\frac{dF_z}{dz}\frac{F_z'}{F_z} \tag{2.14}$$

We note here that the form of the lateral exchange term in the present diffusion approximation is more general than that derived from Newton's law of cooling (which crudely allows only for heat exchange in the horizontal direction). It turns out that the radiative exchange represented by Newton's law of cooling is a special case of the expression (equations [1.43] and [1.46]) derived for the present case (see also Herbold et al [1985]). From equation (1.41) we find:

$$\frac{F_z'}{F_z} = \left(\frac{d\ln T}{dz}\right)^{-1}\frac{\partial}{\partial z}\left(\frac{T'}{T}\right) + 4\frac{T'}{T} - \left(\frac{\kappa'}{\kappa} + \frac{\rho'}{\rho}\right) \tag{2.15}$$

The full set of linear stability equations has the property that all the coefficients are functions of z alone and this permits the Fourier decomposition in time of all the fluctuating variables, i.e. with the time dependence in the separable form $f'(z)exp(-i\omega t)$, for a typical perturbation variable $f'(z,t)$. It is convenient to cast the system of equations in non-dimensional form. We scale z in terms of the total length of the tube L and the time by the free fall time over L which is $(L/g)^{1/2}$. This results in the following equations (see Appendix A for a detailed derivation):

$$\frac{d\xi}{dr} = \frac{1}{H}\left(\frac{dH}{dr} - \frac{1}{2}\right)\xi - \left(\frac{\beta}{2} + \frac{1}{\chi_\rho}\right)\frac{p'}{p} + \frac{\chi_T}{\chi_\rho}\frac{T'}{T} \tag{2.16}$$

$$\frac{d}{dr}\left(\frac{p'}{p}\right) = \frac{\Omega^2}{H}\xi - \frac{(\chi_\rho - 1)}{\chi_\rho H}\frac{p'}{p} - \frac{\chi_T}{\chi_\rho H}\frac{T'}{T} \tag{2.17}$$

$$\frac{d}{dr}\left(\frac{T'}{T}\right) = \frac{dlnT}{dr}\left[\kappa_p + \frac{1}{\chi_\rho}\right]\frac{p'}{p} - \frac{dlnT}{dr}\left[4 - \kappa_T + \frac{\chi_T}{\chi_\rho}\right]\frac{T'}{T} + \frac{dlnT}{dr}\frac{F_z'}{F_z} \tag{2.18}$$

$$C\frac{d}{dr}\left(\frac{F_z'}{F_z}\right) = -i\Omega\frac{N^2\Gamma_1}{\chi_T}\xi + i\Omega\frac{(\gamma-1)}{\chi_T}\frac{p'}{p} + (4\epsilon - i\Omega\gamma)\frac{T'}{T} - C\frac{dlnF_z}{dr}\frac{F_z'}{F_z} \tag{2.19}$$

where

$$r = \frac{z}{L} \tag{2.20}$$

$$\Omega = \omega\tau_d \tag{2.21}$$

$$\tau_d = \left(\frac{L}{g}\right)^{1/2} \tag{2.22}$$

All the quantities appearing in the above equations are dimensionless; the displacement ξ and the scale height H are in units of L; the Brunt-Väisälä frequency is in units of $1/\tau_d$; C is the nonadiabaticity parameter which is the ratio of the free-fall time τ_d and the thermal time-scale τ_{th} (Jones 1970; Antia and Chitre 1979):

$$C = \frac{\tau_d}{\tau_{th}} \tag{2.23}$$

where,

$$\tau_{th} = \frac{\rho c_v T L}{F} \tag{2.24}$$

The time-scale τ_{th} represents the thermal time-scale in which radiative relaxation takes place over the length of the tube, F is the magnitude of the vertical component of the radiative flux, ϵ is given by

$$\epsilon = \frac{\tau_d}{\tau_r} \tag{2.25}$$

where,

$$\tau_r = \frac{\rho c_v a^2}{K} \tag{2.26}$$

is the lateral radiative exchange time-scale, K is the radiative conductivity and a is the radius of the tube.

The above system of coupled equations, in general, is intractable analytically. We, therefore, attempt numerical solutions and these form the subject of the next two chapters. However, before doing this it is instructive to consider certain limiting cases to make contact with earlier work.

2.3 Previous analyses

2.3.1 Adiabatic case

The adiabatic limit occurs when $\tau_r \to \infty$ and $C \to 0$, which results in the following equations (Spruit and Zweibel 1979):

$$\frac{d\xi}{dz} = \left[\frac{1}{H}\left(\frac{dH}{dz} - \frac{1}{2}\right) - \frac{N^2}{g}\right]\xi + \left[\frac{(\gamma-1)}{\gamma\chi_\rho} - \frac{\beta}{2} - \frac{1}{\chi_\rho}\right]\frac{p'}{p} \tag{2.27}$$

$$\frac{d}{dz}\left(\frac{p'}{p}\right) = \frac{(\omega^2 + N^2)}{gH}\xi + \frac{(1-\Gamma_1)}{\Gamma_1 H}\frac{p'}{p} \tag{2.28}$$

This adiabatic system of equations has the property that the differential operator acting on the eigenvalue ω^2 (note that ω appears only in quadratic form) is *Hermitian* and hence ω^2 is real: thus ω can only take either real or purely imaginary values. Consequently, the tube can exhibit either stable oscillations or be monotonically unstable (convective instability).

For polytropic stratifications the adiabatic system (2.27) and (2.28) gets simplified yielding the following equation for the displacement ξ, in the following non-dimensional form:

$$\frac{d^2\xi}{dr^2} + \frac{1}{2\zeta}\frac{d\xi}{dr} + \frac{1}{\zeta}\left[\frac{\Omega^2}{\gamma} + \frac{\mathcal{N}^2}{2} + \frac{\beta}{2}(\Omega^2 + \mathcal{N}^2)\right]\xi = 0 \tag{2.29}$$

where $\mathcal{N}$ and Ω are the non-dimensional Brunt-Väisälä frequency and the eigen frequency respectively(scaled in terms of the inverse of the free-fall time τ_d):

$$\mathcal{N}^2 = N^2\tau_d^2 = \frac{\delta}{\zeta} \tag{2.30}$$

$$\Omega = \omega\tau_d \tag{2.31}$$

and

$$\zeta = 1 + \frac{r}{m+1} \tag{2.32}$$

where m is the polytropic index (see Section 3.2 for details about polytropic stratifications). The above equation is amenable to an analytic solution in terms of the Bessel function (Webb and Roberts 1978; Hasan 1986). Necessary and sufficient conditions for stability have been derived by Webb and Roberts (1978) both for a tube of infinite and finite extents. The mathematical properties of the solutions and the spectrum of eigenvalues have been studied in detail by the above mentioned authors and we refer the interested reader to these papers. We summarize the main results: a polytropically stratified tube of infinite extent has a continuous spectrum of positive eigenvalues Ω^2 if the following necessary and sufficient condition is satisfied:

$$\left(\frac{1-m}{2}\right)^2 - 2\delta(1+\beta) > 0 \tag{2.33}$$

When the above condition is violated, there is convective instability. The eigenvalues in this case form a continuous spectrum.

For a tube of finite depth d, with closed boundary conditions at the ends, the equation (2.29) forms a regular Sturm-Liouville system with only discrete eigenvalues. Thus there no longer exists a continuous spectrum of eigenvalues for Ω^2. The necessary and sufficient condition for the existence of unstable solutions now is

$$e^{2\pi/s} < \frac{H(d)}{H(0)} \tag{2.34}$$

where,

$$s^2 = 2\delta(1+\beta) - \left(\frac{1-m}{2}\right)^2 \tag{2.35}$$

2.3.2 Newton's law of cooling

In the limit $\tau_{th} \to \infty$, i.e. as $C \to 0$, the energy equation given by equation (2.19) becomes an algebraic relation among $\xi, p'/p$ and T'/T:

$$-\frac{N^2\Gamma_1}{g\chi_T}\xi + \frac{(\gamma-1)}{\chi_T}\frac{p'}{p} - (\gamma + i\frac{4}{\omega\tau_r})\frac{T'}{T} = 0 \tag{2.36}$$

This equation is applicable when the only non-abiabaticity is due to lateral exchange of radiation between the tube and its surroundings; note that τ_r is the thermal relaxation time in the optically thick limit, which follows from the following exact formula (first derived by Spiegel 1957) by replacing the inverse of the wavenumber k by a, the tube radius, and taking the limit of $\kappa\rho a \to \infty$ (Hasan 1986):

$$\tau_s = \frac{c_v}{16\kappa\sigma T^3}\left[1 - (\kappa\rho a)cot^{-1}(\kappa\rho a)\right]^{-1} \tag{2.37}$$

The optically thin limit($\kappa\rho a \ll 1$) in the above formula gives:

$$\tau_{thin} = \frac{c_v T}{16\kappa B} \tag{2.38}$$

Now the use of equation (2.36) to replace the temperature perturbations in the equations (2.16) and (2.17) leads to the following second order system:

$$\frac{d\xi}{dz} = \left[\frac{1}{H}\left(\frac{dH}{dz} - \frac{1}{2}\right) - \frac{\gamma\omega\tau_r N^2}{(\gamma\omega\tau_r + i4)g}\right]\xi + \left[\frac{\omega\tau_r(\gamma-1)}{\chi_\rho(\gamma\omega\tau_r + i4)} - \frac{\beta}{2} - \frac{1}{\chi_\rho}\right]\frac{p'}{p} \tag{2.39}$$

$$\frac{d}{dz}\left(\frac{p'}{p}\right) = \left[\frac{\omega^2}{g} + \frac{\gamma\omega\tau_r N^2}{(\gamma\omega\tau_r + i4)g}\right]\frac{\xi}{H} + \frac{1}{H}\left[\frac{1}{\chi_\rho} - 1 - \frac{\omega\tau_r(\gamma-1)}{\chi_\rho(\gamma\omega\tau_r + i4)}\right]\frac{p'}{p} \tag{2.40}$$

This system is the same as that obtained by Hasan (1986); the above two equations are the first order form of his equation (13).

For a background polytropic stratification the above two equations get simplified and can be written in the following form satisfied by ξ,

$$\zeta^2 \frac{d^2\xi}{dr^2} - L\zeta \frac{d\xi}{dr} + (M\zeta + N)\xi = 0 \tag{2.41}$$

where

$$L = \frac{1}{1+m}\left[\frac{1-m}{2} + \frac{i\Omega\gamma}{q}\right] \tag{2.42}$$

$$M = \left(1 + \frac{\beta}{2}\right)\Omega^2 + i\frac{(\gamma-1)\Omega^3}{q} \tag{2.43}$$

$$N = \frac{(1-m)}{2(1+m)^2} - \frac{\delta\gamma}{q}\left(1 + \frac{\beta}{2} + \frac{i}{(m+1)}\right)\Omega + \frac{(m-1)(1-\gamma)}{2(m+1)q}\Omega \tag{2.44}$$

$$q = 4\epsilon_p - i\Omega\gamma \tag{2.45}$$

The above equation is identical to the equations of Webb & Roberts (1980) and Hasan (1986) and has an analytical solution in terms of the Bessel function (Abramowitz and Stegun 1965). In the limit $\epsilon_p \to 0$ (the adiabatic limit) the above equation reduces to the equation (2.29) derived earlier. Equation (2.41) admits the formal solution,

$$\xi = p^{1-L}[AJ_s(p) + BY_s(p)] \tag{2.46}$$

where J and Y denote the Bessel functions,

$$p^2 = 4M\zeta \tag{2.47}$$

$$s^2 = (1-L)^2 - 4N \tag{2.48}$$

and A and B are constants to be determined by the boundary conditions,

2.4 Quasi-adiabatic approximation for a thin flux tube

2.4.1 Derivation of the equations

Rather than dealing with the full set of equations given in Section (2.2.2), in this chapter we adopt the quasi-adiabatic approxmation, which qualitatively captures the physical effects associated with both vertical and horizontal energy transport. However, it has the advantage that the number of differential equations is reduced effectively to two. In the subsequent chapters, we consider the full set of equations.

We begin by writing the equations in terms of Lagrangian perturbations, which are related to the Eulerian perturbations as follows:

$$f' = \delta f - \xi\frac{df}{dz} \tag{2.49}$$

where δf is the Lagrangian perturbation. The linear equations (2.8), (2.9), (2.14) and (2.15), with a time dependence of the form $e^{\omega t}$, in Lagrangian form are:

$$\frac{d\xi}{dz} = \frac{(1+\beta)}{2H}\xi - \left(\frac{\beta}{2} + \frac{1}{\Gamma_1}\right)\frac{\delta p}{p} + \frac{\chi_T}{\Gamma_1 c_v}\delta s \tag{2.50}$$

$$\frac{d}{dz}\left(\frac{\delta p}{p}\right) = \left[\frac{1+\beta}{2H} - \frac{\omega^2}{g}\right]\frac{\xi}{H} - \left(1+\frac{\beta}{2}\right)\frac{1}{H}\frac{\delta p}{p} \tag{2.51}$$

$$\omega\frac{\delta s}{c_v} = -\frac{1}{\rho c_v T}\delta\left(\frac{dF_R}{dz}\right) - \frac{4}{\tau_R}\frac{\delta T}{T} + \frac{4}{\tau_R}\frac{dlnT}{dz}\xi \tag{2.52}$$

$$\frac{\delta F_R}{F_R} = \left(\frac{dlnT}{dz}\right)^{-1}\frac{d}{dz}\left(\frac{\delta T}{T}\right) - \frac{d\xi}{dz} + \left[4 + \frac{\chi_T}{\chi_\rho} - \kappa_T\right]\frac{\delta T}{T} - \left[\kappa_p + \frac{1}{\chi_\rho}\right]\frac{\delta p}{p} \tag{2.53}$$

where δs is the Lagrangian entropy perturbation and we have used the following thermodynamic identity to replace $\delta\rho/\rho$:

$$\frac{\delta\rho}{\rho} = \frac{1}{\Gamma_1}\frac{\delta p}{p} - \frac{\chi_T}{\Gamma_1 c_v}\delta s \tag{2.54}$$

We also make use of the following identity in our subsequent analysis:

$$\frac{\delta T}{T} = \frac{\chi_\rho}{\Gamma_1 c_v}\delta s + \nabla_a\frac{\delta p}{p} \tag{2.55}$$

The quasi-adiabatic approximation is now effected by using the adiabatic relations among the variables to evaluate the right hand side of the equation (2.53) which determine the vertical flux perturbations. This amounts to replacing $\delta T/T$ by the adiabatic relation

$$\frac{\delta T}{T} = \nabla_a\frac{\delta p}{p} \tag{2.56}$$

and $d\xi/dz$ by the equation (2.50) with δs equated to zero; this procedure yields the following approximation for the vertical flux perturbations in terms of the vertical displacement ξ and pressure perturbation $\delta p/p$:

$$\frac{\delta F_R}{F_R} = \frac{D_1(z)}{L}\xi + D_2(z)\frac{\delta p}{p} \tag{2.57}$$

where

$$D_1(z) = b(z) - \omega^2\tau_d^2 a(z) \tag{2.58}$$

$$a(z) = \frac{\nabla_a}{\nabla} \tag{2.59}$$

$$b(z) = -\frac{(1+\beta)L}{2H}\frac{\delta}{\nabla} \tag{2.60}$$

$$D_2(z) = \frac{H}{\nabla}\frac{d\nabla_a}{dz} - \frac{\nabla_a}{\nabla} + \frac{\beta}{2}\frac{\delta}{\nabla} + \frac{1}{\Gamma_1} + \left[4 - \kappa_T + \frac{\chi_T}{\chi_\rho}\right]\nabla_a - \kappa_\rho - \frac{1}{\chi_\rho} \tag{2.61}$$

Noting that

$$\delta\left(\frac{dF_R}{dz}\right) = \frac{d\delta F_R}{dz} - \frac{dF_R}{dz}\frac{d\xi}{dz} \tag{2.62}$$

we have the energy equation (2.52) in the form,

$$(\gamma\omega\tau_d + 4\epsilon)\frac{\delta s}{c_v} = \frac{\gamma D_3(z)}{H}\xi + \gamma D_4(z)\frac{\delta p}{p} \tag{2.63}$$

where $D_3(z)$ and $D_4(z)$ are the dimensionless functions,

$$D_3(z) = C(c(z) - \omega^2\tau_d^2 d(z)) + 4\epsilon\nabla \tag{2.64}$$

$$D_4(z) = C(u(z) - \omega^2\tau_d^2 w(z)) - 4\epsilon\nabla_a \tag{2.65}$$

and,

$$c(z) = H\frac{db}{dz} + \frac{(1+\beta)L}{2}\left(\frac{b}{L} + \frac{D_2}{H}\right) + L\frac{dlnF_R}{dz}\left(\frac{Hb}{L} - \frac{1+\beta}{2}\right) \tag{2.66}$$

$$d(z) = a\left(\frac{1+\beta}{2} + H\frac{dlnF_R}{dz}\right) + H\frac{da}{dz} + D_2 \tag{2.67}$$

$$u(z) = L\frac{dD_2}{dz} + \left(\frac{dlnF_R}{dz} - \frac{2+\beta}{2H}\right)LD_2 + \left(\frac{\beta}{2} + \frac{1}{\Gamma_1}\right)\left(L\frac{dlnF_R}{dz} - b\right) \tag{2.68}$$

$$w(z) = -\left(\frac{\beta}{2} + \frac{1}{\Gamma_1}\right)a \tag{2.69}$$

and ϵ and C are the ratios defined earlier in the last section.

Thus the entropy perturbations have been written in terms of the dynamical perturbations ξ and $\delta p/p$ as given by equation (2.63); the coefficients D_3 and D_4 as given by the equations (2.64) and (2.65) reveal that in the limit τ_{th} tending to infinity, i.e. when the vertical radiative exchange between the fluid elements is negligible the first two terms in the right hand side of these equations become zero and the third term in both equations represent solely the effects of lateral exchange.

Substituting for the entropy perturbations in equation (2.50) and using the relation (2.63) we have, along with the perturbed momentum equation (2.51), the following system of equations in the quasi-adiabatic approximation:

$$\frac{d\xi}{dz} = \left[\frac{1+\beta}{2} + \frac{\chi_T}{q\chi_\rho}D_3(z)\right]\frac{\xi}{H} - \left[\frac{\beta}{2} + \frac{1}{\Gamma_1} - \frac{\chi_T}{q\chi_\rho}D_4(z)\right]\frac{\delta p}{p} \tag{2.70}$$

$$\frac{d}{dz}\left(\frac{\delta p}{p}\right) = \left[\frac{1+\beta}{2H} - \frac{\omega^2}{g}\right]\frac{\xi}{H} - \left(1 + \frac{\beta}{2}\right)\frac{1}{H}\frac{\delta p}{p} \tag{2.71}$$

where

$$q = \gamma\omega\tau_d + 4\epsilon \tag{2.72}$$

In the limit $\tau_{th} \to \infty$, $C \to 0$ and the above equations get reduced to the case where the only non-adiabaticity is through the lateral exchange of radiation. The above two equations can be combined into a single second order equation for ξ:

$$\frac{d^2\xi}{dz^2} + \frac{P}{2H}\frac{d\xi}{dz} + \left(\frac{R}{H^2} + \frac{Q}{H}\right)\xi = 0 \tag{2.73}$$

where,

$$P = 1 - 2\left(\frac{\chi_T D_3}{q\chi_\rho} + \frac{HM'}{M}\right) \tag{2.74}$$

$$R = I(\nabla - 1) + \frac{M}{2} + \frac{\beta}{2}(M - I) \tag{2.75}$$

$$Q = \frac{IM'}{M} - I' - \frac{M\Omega^2}{L} \tag{2.76}$$

$$I = \frac{1+\beta}{2} + \frac{\chi_T}{q\chi_\rho}D_3(z) \tag{2.77}$$

$$M = \frac{\beta}{2} + \frac{1}{\Gamma_1} - \frac{\chi_T}{q\chi_\rho}D_4(z) \tag{2.78}$$

Here the prime symbol denotes a derivative with respect to z (e.g. $M' \equiv dM/dz$). The above second order differential equation does not lend itself to an analytic solution. However, when the equilibrium atmosphere is a polytrope, it is possible to construct an analytic solution. *Polytropic stratification*

For a polytrope, ∇ and F_R are constants; we further assume that γ, τ_r and μ are constants; thus ∇_a and the superadiabaticity δ become constants and hence the functions $a(z)$ and $D_2(z)$ become constants. This leads to the following simplification:

$$D_2 = \frac{\beta}{2}\frac{\delta}{\nabla} + \left(4 - \kappa_T - \frac{1}{\nabla}\right)\nabla_a - \kappa_p \tag{2.79}$$

and

$$c(z) = H\frac{db}{dz} + \frac{(1+\beta)L}{2}\left(\frac{b}{L} + \frac{D_2}{H}\right) \tag{2.80}$$

$$d(z) = a\frac{1+\beta}{2} + D_2 \tag{2.81}$$

$$u(z) = -\frac{2+\beta}{2H}LD_2 - \left(\frac{\beta}{2} + \frac{1}{\gamma}\right)b \tag{2.82}$$

The equation (2.73) is still analytically intractable because the coefficients P, Q and R are functions of z. It is seen that the functions $c(z)$ and $u(z)$, which enter in the above coefficients, vary approximately as $1/H$, and consequently become negligibly small in the deep layers (where H becomes very large) compared to $\omega^2\tau_d^2 d$ and $\omega^2\tau_d^2 w$. Hence, to a first approximation P, Q and R can effectively be regarded constant in equation (2.73). With these further simplificiations, the equation now reduces to a form which resembles the Bessel equation and is similar in structure to the equation derived by Webb and Roberts(1980) and Hasan (1986). It should, however, be noted that the present equation contains the effects of vertical radiative losses, which are incorporated in the quasi-adiabatic analysis. We, therefore, find that equation (2.73) has the following solution:

$$\xi = p^{1-P}[AJ_s(p) + BY_s(p)] \tag{2.83}$$

where

$$p^2 = 4RH \tag{2.84}$$

$$s^2 = (1-P)^2 - 4Q \tag{2.85}$$

The coefficients A and B depend upon the boundary conditions. We can now in principle determine the eigen frequencies of the system. Before doing this, it is instructive to carry out a 'local analysis' in order to gain a physical understanding of the various effects embodied in equation (2.73). This leads to a dispersion relation which enables us to delineate various effects.

2.4.2 Solutions in the local approximation

In the so-called 'local' approximation, the coefficients of the displacement and their derivatives in equation (2.73) are assumed to vary weakly with depth; this corresponds to assuming a locally constant atmosphere. Thus, the various quantities appearing in the equations have values corresponding to a particular location in the atmosphere, and here for convenience we redefine the scaling length L to be the local scale height H. Therefore, the length scale appearing in the thermal time scale τ_{th} is the local scale-height and hence C is the ratio of the local free-fall time $\tau_d = (H/g)^{1/2}$ to the local thermal time scale. Further, we neglect contributions from the perturbations in the opacity to the dynamic perturbations, *i.e.* there is no κ-mechanism operating inside the flux tube confined gas. Under these approximations, the various coefficients in the equation (2.73) become constants and the application of rigid boundary conditions $\xi = 0$ at $z = 0$ and at $z = D$ where D is the length of the tube, leads to the following dispersion relation for the dimensionless eigenvalue $\Omega = \omega\tau_d$:

$$S_4\Omega^4 + \Omega^3 + S_2\Omega^2 + S_1\Omega + S_0 = 0 \tag{2.86}$$

where,

$$S_4 = -C\frac{\nabla_a}{\gamma\nabla} \tag{2.87}$$

$$S_2 = \epsilon\eta_2 + C\sigma_2 \tag{2.88}$$

$$S_1 = \frac{\gamma}{\delta_c}\left[b_0 - \frac{(1+\beta)\delta}{2}\right] \tag{2.89}$$

$$S_o = \epsilon\eta_o + C\sigma_o \tag{2.90}$$

and,

$$\eta_2 = \frac{4}{\delta_c}\left(1+\frac{\beta}{2}\right) \tag{2.91}$$

$$\sigma_2 = \frac{\delta}{\delta_c\nabla}\left[\frac{(1+\beta)}{2}\nabla_a + \frac{\nabla}{2} + \frac{1}{8}\right] + \frac{1}{\gamma}\frac{\nabla_a}{\nabla} + \frac{1+\beta}{2}\left[\nabla - \frac{(2\beta+3)}{4}\right]\frac{1}{\delta_c} - Q_r\left[\frac{2}{\gamma} - \frac{1}{4}\frac{\nabla_a}{\delta_c\nabla}\right] \tag{2.92}$$

$$\eta_o = \frac{4b_0 + \nabla(1-4\nabla)}{\delta_c} \tag{2.93}$$

$$\sigma_o = -\frac{(1+\beta)}{4\delta_c}\left[\frac{1}{4} + \nabla + (1+\beta)\nabla_a\right]\frac{\delta}{\nabla} + Q_r\frac{1+\beta}{2\delta_c}\left[\delta\left(1+\frac{1}{4\nabla}\right) + \nabla + \frac{1}{\gamma} - \frac{3}{4}\right] \tag{2.94}$$

$$b_0 = \frac{1}{16} + \frac{n^2\pi^2H^2}{D^2} \tag{2.95}$$

n being the harmonic order of the perturbations. In the above,

$$Q_r = H\frac{d\ln F_R}{dz} \tag{2.96}$$

which is a measure of vertical radiative losses (equivalently, a measure of departure from radiative equilibrium) and is negative because $|F_R|$ decreases as z increases. The greater the radiative losses the larger the magnitude of Q_r. In the limit $C\rightarrow 0$, i.e. when the vertical radiative transfer is switched off, the above dispersion relation becomes a cubic equation which describes the effects of horizontal exchange alone; further it is seen that taking the limit of isothermal background stratification, which can be done by replacing the temperature derivative ∇ by zero, the dispersion relation reduces to the following form:

$$\Omega^3 + s_2\Omega^2 + s_1\Omega + s_o = 0 \tag{2.97}$$

where

$$s_2 = \frac{4\epsilon}{\delta_c}\left(1+\frac{\beta}{2}\right) \tag{2.98}$$

$$s_1 = \frac{\gamma}{\delta_c}\left[b_0 - \frac{(1+\beta)(1-\gamma)}{2\gamma}\right] \tag{2.99}$$

$$s_o = \frac{4\epsilon b_0}{\delta_c} \tag{2.100}$$

$$\delta_c = 1 + \frac{\gamma\beta}{2} \tag{2.101}$$

The above dispersion relation is the same as the one derived by Venkatakrishnan (1986) based on horizontal radiative exchange in an isothermal atmosphere. If the isothermal approximation is not imposed, i.e. if $\nabla \neq 0$, the $C \to 0$ limit of (2.86) differs from the above isothermal limit in two ways. Firstly, there is an additional term that multiplies ϵ in the inhomogeneous term and it is equal to $\nabla(1 - 4\nabla)$. The latter is negative if $\nabla > 1/4$, which means that if the vertical temperature gradient is greater than 1/4 the horizontal heating effect parameterized by ϵ is reduced. Physically this explains the fact that the radiation available for smoothing out the horizontal temperature inhomogeneities is reduced because of the increased vertical temperature stratification which tries to channel more radiation in the vertical direction. Thus it is seen that the isothermal approximation overestimates the horizontal heating effects. Secondly, δ in the isothermal case is replaced by the negative of the adiabatic gradient ∇_a. Hence, to simulate a superadiabatic gradient which is necessary for the convective collapse, γ has to be assumed to take values less than unity. The thermal exchange time in the horizontal direction (which depends upon the radius a) is controlled by the parameter ϵ. It may be noted that the non-adiabatic effects are contained in the coefficients of even powers of Ω in the dispersion relations and further, in the equation (2.97), the factors multiplying ϵ are all positive. The above equation, which brings out in a simple way the size dependent collapse of the tubes, has been solved numerically and a relationship between the size and strength for stable solar tubes has been derived by Venkatakrishnan (1986). Here, we derive an approximate analytic relation between ϵ (i.e. the size of the tube) and critical values of β at which the convective instability sets in, through a simple analysis of the transition from oscillatory to convective behaviour contained in the solutions of (2.97).

The limit $\epsilon = 0$ in (2.97) gives the adiabatic solution,

$$\Omega_{ad} = \pm(-s_1)^{1/2} \tag{2.102}$$

which shows that if s_1 is positive, i.e. if β is less than a critical value $\beta_c = 2b_o/\delta - 1$, then the tube is convectively stable and exhibits undamped oscillations with frequency Ω_{ad}. If the tube is of infinite extent, the following condition for convective instability is arrived at,

$$\delta > \frac{1}{8(1+\beta)} \tag{2.103}$$

which is identical to the relation derived by Roberts and Webb (1978). Thus the adiabatic eigenvalues Ω_{ad}^2 are real, negative or positive values corresponding to a convective (monotonically growing)

or a oscillatory (stable) mode, respectively. The inclusion of radiative exchange brings out two new effects: (*i*) Ω_{ad}^2 becomes complex transforming the adiabatic oscillatory mode into a growing mode or introducing damping to the convective mode, and (*ii*) a new thermal mode corresponding to the third solution of the dispersion relation (2.97). To order ϵ, the solution for the thermal mode can easily be found and it is given by,

$$\Omega_3 = -\frac{s_o}{s_1} \tag{2.104}$$

Since s_o is always positive, the thermal mode is damped when s_1 is positive and growing when it is negative; this means that the thermal mode is destabilised when the stratification is convectively unstable, i.e. either when the field strength is less than the abiabatic stability limit ($\beta > \beta_c$) or when the superadiabaticity $\delta \leq 0$, and it is damped otherwise. This thermal mode and its above stated behaviour have been noted earlier (Hasan 1986).

The other two solutions of (2.97), which concern the above stated effect (*i*), are given by, to first order in ϵ,

$$\Omega_{1,2} = \Omega_{ad} + \frac{s_o - s_1 s_2}{2 s_1} \tag{2.105}$$

It is easily noted from the above solutions that, to first order in ϵ, the lateral radiative exchange introduces either damping or amplification without affecting the frequencies of the oscillatory mode and thus does not determine the transition from oscillatory to convective behaviour which is still set by the adiabatic limit. This shows that the size dependent onset of the convective instability of a tube is an effect of order at least two in ϵ. Such a dependence between ϵ and β_c can be derived by examining the cubic relation (2.97)'s discriminant which determines the transformation of complex conjugate solutions (oscillatory mode) to two real valued solutions. This discriminant is given by (Abramovitz and Stegun 1965),

$$k = q^3 + r^2 \tag{2.106}$$

where

$$q = \frac{1}{3} s_1 - \frac{1}{9} s_2^2 \tag{2.107}$$

$$r = \frac{1}{6}(s_1 s_2 - 3 s_o) - \frac{1}{27} s_2^3 \tag{2.108}$$

To leading order in ϵ,

$$k \approx \frac{s_1^3}{27} - \frac{s_1^2 s_2^2}{108} - \frac{s_o s_1 s_2}{6} + \frac{s_o^2}{4} \tag{2.109}$$

which shows that the deviation of k from the value it obtains in the adiabatic limit is of order ϵ^2 and higher; thus the non-adiabatic contributions to the oscillatory mode's frequencies are of order atleast two in ϵ, as also noted earlier from the solutions (2.105) which are of order ϵ. The points in the $\epsilon - \beta$ space at which the oscillation frequency becomes zero and the convective mode sets in

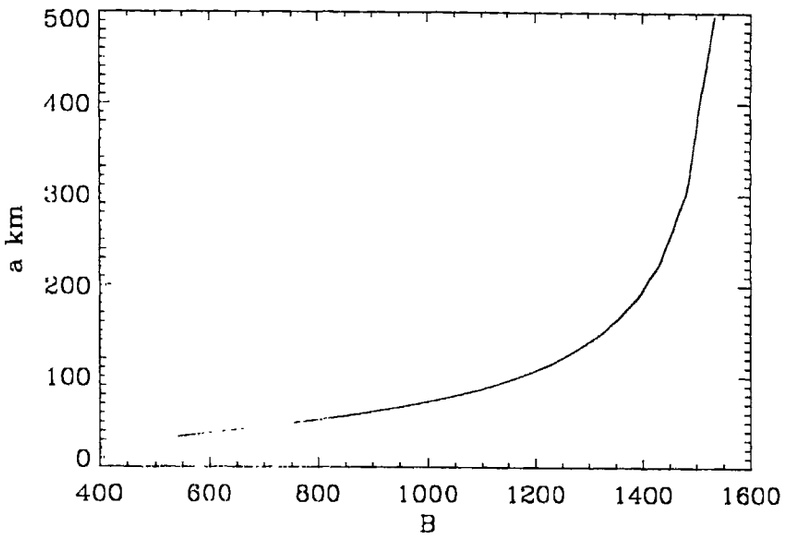

Figure 2.1: Photospheric radius a (km) of the flux tubes as a function of their field strengths B (G), calculated from the relation (2.110) using values for the various quantities representative of the solar surface layers

is given by $k = 0$. Thus the loci of solutions $k = 0$ in the $\epsilon - \beta$ space demarcate the stable tubes from the convectively unstable ones. Examination of the various terms in the expression (2.109) for k shows that the second term takes very small values compared to the other ones in the relevant range of values for β, and thus can be neglected. The relation between ϵ and the critical values of β that satisfies $k = 0$ can then be written as,

$$\epsilon^2 = -\frac{s_1^3 \delta_c^2}{9b_o[48b_o - 8(1+\beta/2)s_1]} \tag{2.110}$$

With ϵ expressed in terms of the tube's radius a, using the definitions (2.25) and (2.26), the above equation gives a relation between tube radius a and field strength needed for convective stability.

Application of relation (2.110) to the solar flux tubes requires correct values for the various parameters that characterize the solar superadiabatic surface layers; for example, the value of the radiative conductivity K crucially determines the size dependence of the convective collapse, through its appearance in the lateral radiative exchange time scale τ_r. From an improved version of the convection zone model of Spruit (1977) (see Hasan, Kneer and Kalkofen 1998) we find the following values for the various quantities representing the superadiabatic layer: the thermometric conductivity K_r=K/ρc_v=1 $\times$ $10^{11} cm^2 s^{-1}$, H=150 km, and $\delta \approx 0.2$ which represents an average over the depth extent of D=1500 km which includes a thin layer of peak superadiabaticity of about 0.4. The

quoted value of K thus corresponds to this layer of maximum superadiabaticity. With these values for the various solar quantities, the relationship between tube radius a and field strength B obtained from the relation (2.110) is plotted in Fig.(2.1). This plot shows that tubes of radii above about 100 km have field strengths above a kG and their strength is very weakly dependent on the size, whereas smaller tubes have a large range in the field strength from about the equipartition value of 400 G to 1 kG. These smaller tubes thus represent the regime wherein radiative heating from the surroundings is capable of inhibiting their collapse. The larger tubes experience ineffective heating within the dynamical collapse time-scale and thus undergo collapse almost adiabatically achieving a field strength close to that set by the adiabatic limit.

Solutions of the quartic relation

The inclusion of vertical radiative transfer, as captured in the quartic relation (2.86), modify the characteristics of the convective and oscillatory modes described above through the terms containing the parameter C which appear additively with those containing the lateral radiative exchange parameter ϵ in the coefficients S_o and S_2; also, the fourth root of the quartic relation corresponds to a new thermal mode which owes its origin purely to vertical radiative effects. Examining the various terms in the expressions for σ_2 and σ_o, we find that the dominant contributions are from the terms containing the vertical radiative loss function Q_r and this leads to the following simplifications:

$$\sigma_2 \approx -2Q_r - \frac{1+\beta}{2} \tag{2.111}$$

$$\sigma_o \approx Q_r \tag{2.112}$$

The above simplified expressions reveal immediately the signs of the contributions by σ_2 and σ_o to S_2 and S_o respectively: as Q_r is negative, with roughly a value of -5 that corresponds to the solar superadiabatic surface layers, σ_2 is always positive for the relevant range of values of β and σ_o is always nagative. The above nature of the contributions of σ_2 and σ_o help in quantifying the effects of the vertical losses, in the following analysis that we present.

We analyse the effects of terms containing the vertical radiative transfer parameter C by expanding the solutions Ω of the quartic relation (2.86) about the solutions Ω_0 of the cubic equation obtained by putting $C = 0$ in (2.86), and retaining only corrections upto first order in C. We find that,

$$\Omega = \Omega_0 + \frac{\alpha S_4 - \sigma_2 \Omega_0^2 - \sigma_o}{3\Omega_0^2 + 2\epsilon\eta_2\Omega_0 + S_1} C \tag{2.113}$$

where,

$$\alpha = (S_1 - \epsilon^2\eta_2^2)\Omega_0^2 + \epsilon(\eta_o - \eta_2 S_1)\Omega_0 - \epsilon^2\eta_o\eta_2 \tag{2.114}$$

The fourth solution of the quartic relation, that represents a thermal mode arising purely out of

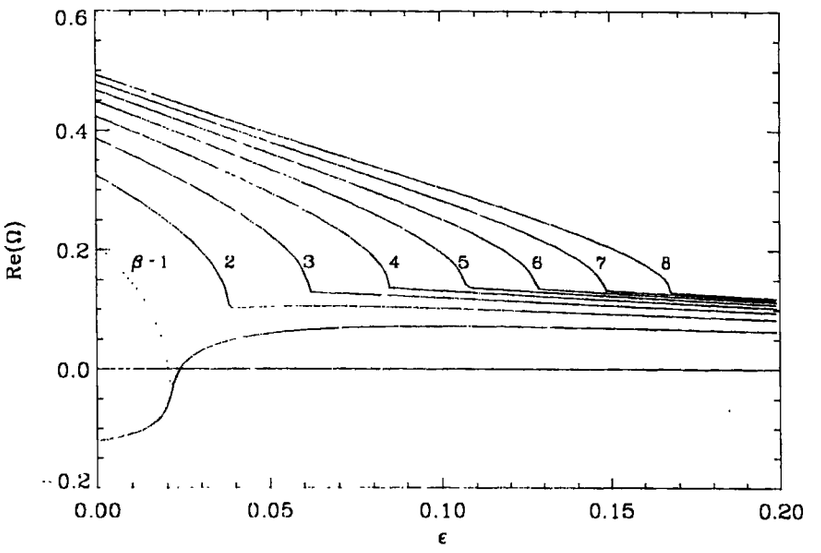

Figure 2.2: Re(Ω), i.e growth rate scaled by the inverse of free-fall time τ_d, as a function of ϵ for different values of β starting from 1 to 8

inclusion of the vertical radiative transfer, is given by (to order ϵ and C)

$$\Omega_4 = -\frac{1}{S_4} + \epsilon\eta_2 \tag{2.115}$$

Now, we examine the corrections to Ω_0, as given by (2.113), arising purely out of vertical radaitive transfer by switching of the lateral radiative exchange, i.e. by putting $\epsilon = 0$. Thus, we find the corrections ω_c to the adiabatic eigenvalues Ω_{ad} due to the vertical radiative losses alone:

$$\omega_c = \left[S_1 S_4 - \sigma_2 + \frac{\sigma_o}{S_1}\right]\frac{C}{2} \tag{2.116}$$

The above relation, in combination with the relations (2.112) and (2.111) which establish the signs of σ_o and σ_2, shows that, since S_4 is negative, a convectively stable (positive S_1) tube's oscillations are damped (ω_c is negative) while the convective instability (negative S_1) of a tube is enhanced (ω_c is positive), by the vertical radiative losses. Thus we have established that vertical radiative losses act against the lateral heating effects. Having identified the different physical effects contained in the general dispersion relation (2.86), we present, in the following section, numerical solutions and the detailed behaviour of the modes under study.

2.4.3 Numerical solutions of the dispersion relation

The values for various parameters that enter the relation (2.86), representing the equilibrium atmosphere, are chosen from a realistic model atmosphere of the Sun (see Chapter IV for a description of the solar model used). From this model, we make the following choice for the various parameters to represent the superadiabatic layer (driving the instability) on the Sun: $\delta \approx 0.3$, $C = 0.004$, $H = 150$ km and $Q_r = -5$. For this set of parameters, the scaled growth rates $\mathrm{Re}(\Omega)$ as a function of ϵ for different values of the magnetic field strength (parameterized by β) are shown in Fig.(2.2), with $D = 1200$ km. The cusps in the curves mark the locations where the overstable mode gets transformed into the convective mode and these are the points where the discriminant k changes sign. Positive values of S_1 correspond to oscillatory overstable solutions with growth rates that vary slowly with ϵ. The overstability is reduced as β decreases or when the field strength increases. It is seen that for $\beta = 1$ the overstability growth rates decrease as ϵ decreases, i.e as the tube size increases, and they become negative at a critical value of ϵ (size). It should be noted that the destabilisation in the form of a monotonic growing mode that appears in the regime of strong fields (small β) and thick tubes (small ϵ), shown in Fig.(2.2) as a dotted part of the curve for $\beta = 1$, is due to a thermal instability caused entirely by the vertical radiative losses. This is the mode given by the solution (2.104) which becomes unstable for positive S_1(convectively stable stratification or strong tubes) and negative S_o (vertical losses dominant). This purely thermal instability is related to a similar instability first studied by Defouw (1970).

To appreciate better the effects of vertical radiative transport we also present solutions of the dispersion relation for different values of C, with the same values for the other parameters. Figures (2.3) and (2.4) correspond to solutions for $\beta = 1$ and $\beta = 7$ respectively. Considering first the case of $\beta = 1$ shown in Fig.(2.3), where the dotted curves correspond to positive values of S_1 and negative values of S_o and thus represent the monotonically growing solution given by equation (2.104). This thermal instability occurs in the convectively stable strong field limit ($\beta = 1$, $S_1 > 0$) and as expected, its growth rate increases as C increases, i.e. as the vertical radiative transport and losses increase. As a function of ϵ, growth rates for the mode decreases as the horizontal exchange increases (as ϵ increases), i.e. as the tube size decreases. Thus, physically, this mode represents the purely thermally driven downflow due to the cooling associated with the vertical radiative losses and this downflow gets decelerated as the tube size decreases, i.e. as ϵ increases. These competing influences of vertical and horizontal energy exchanges are clear in Fig.(2.3). For the cases marked as a, b and c, the horizontal heating effects win over the vertical radiative losses within the relevant ranges of ϵ: the growth rate of the thermal mode becomes negative at a particular value of ϵ which depends on the value of C. As C decreases this critical value of ϵ decreases, the limit of C and

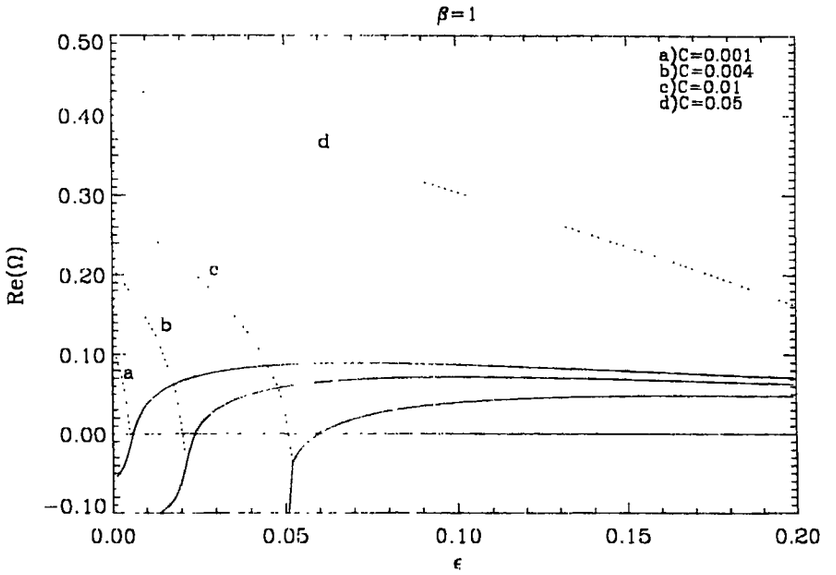

Figure 2.3: Re(Ω) as a function of ϵ for different values of C and $\beta = 1$

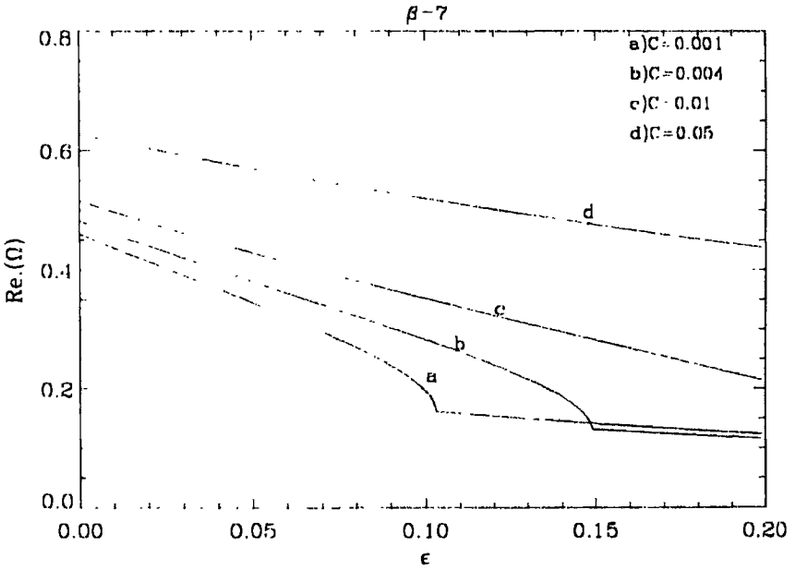

Figure 2.4: Re(Ω) as a function of ϵ for different values of C and $\beta = 7$

$\epsilon \to 0$ being the zero growth rate adiabatic limit. For sufficiently large values of C, for example the case d with $C = 0.05$ in Fig.(2.3), the growth rate of the thermal mode dominates for the values of ϵ considered by us. This regime of values for C, though is not realistic, has been shown for illustrative purposes. The solid parts of the curves show the oscillatory mode given by the solution (2.105). Here, the vertical radiative transport and losses act to damp the oscillations: as C is increased the growth rates decrease and the critical values of ϵ at which the growth rates cross zero being larger for larger values of C. This represents the fact that there has to be more heat gain (ϵ higher) than the vertical losses for the oscillations to grow.

Fig.(2.4) depicts the oscillatory and convective behaviour of a weak tube ($\beta = 7$). Here, the tube is convectively unstable if its size is greater than a particular limit, i.e. if ϵ is less than a particular limit. The critical size is smaller (critical ϵ is larger) for larger values of C establishing the destabilizing action of the vertical radiative losses on the convective mode. For sufficiently large values of C the tube is always convectively unstable irrespective of the size, as shown by the case d in Fig.(2.4). The flatter overstable parts of the curves show the opposite effect, namely a reduction in the oscillatory growth rate as C increases (see the cases a and b in the figure).

2.5 Conclusions

We have developed in this chapter a consistent mathematical formulation to study the effects of radiative energy exchanges on the unstable motions in a thin flaring flux tube with both vertical and horizontal radiative losses. After a brief review of the known results for the adiabatic and non-adiabatic cases (the latter based on Newton's law of cooling), we have derived the equations for a thin flux tube in the quasi-adiabatic approximation. We have obtained analytic solutions in the limiting case of a polytropic stratification. A dispersion relation, that generalises earlier work based solely on lateral heat exchange, has been derived adopting a local approximation. We have shown that vertical radiative losses have important dynamical consequences for the evolution of gas confined in magnetic flux tubes. The convective downflows are shown to accelerate faster due to the cooling associated with the vertical radiative losses thereby verifying theoretically the viability of thermal origin of the convective collapse (Parker 1978) as the cause of the intense magnetic tubes on the Sun. We have also shown the existence of a thermal instability which owes its existence entirely due to the vertical radiative transport; a thick tube which is not subject to efficient lateral radiative heating but which has a source of vertical radiative losses is shown to develop a downflow due to this pure thermal instability.

As regard the overstable motions, our results have demonstrated that the driving due to the hori-

zontal exchange is countered by the vertical radiative losses; this is the familiar radiative damping associated with the wave-motions in a radiating atmosphere. A realistic criterion for the existence of overstable motion has been derived in terms of the parameters describing the vertical transport and lateral heating from the surroundings.

The analytical results derived in this Chapter are from a local analysis of the relevant equations and thus they are strictly valid only in the limit of small length scales for the perturbations. However, the phyiscal effects brought out here are general and are most likely to remain in a detailed exact study. Thus having obtained basic physical insight into the range of phenomena that are expected in intense vertical magnetic flux tubes, we turn in the ensuing Chapters to a more general and refined analysis of the equations.

Chapter 3

Radiative Diffusion and Unstable Motions in Slender Magnetic Flux Tubes. II. Solutions for polytropes

In this Chapter, we turn to the numerical solutions of the full non-adiabatic system of equations, derived in Chapter 2, for polytropic equilibrium stratifications. Polytropes are idealized models of stellar atmospheres with a linear temperature profile. Often polytropes are used in the study of stellar structure, which involves solving the hydrostatic and the continuity equations (but not the energy equation) that lead to the well known Lane-Emden equation (Chandrasekhar 1939). However, polytropic models with a net flux (constant) can be constructed if the opacity is constrained to vary in accordance with energy and mechanical equilibrium conditions. The main sources of unstable motions that we are interested in are due to the super-adiabatic stratification and the radiative energy transport. The polytropic index m, for a fixed value of the adiabatic index γ, provides a measure of the super-adiabaticity while the constant radiative conductivity or the constant radiative flux of the polytrope provides a easy parameterization of the radiative effects or non-adiabaticity. The above simple properties of the polytropes make possible a detailed study of the pattern of the convective and overstable motions in a flux tube and its dependence on the polytropic index and degree of non-adiabaticity (by a suitable parameterization described in the next section). We examine such general aspects of the flux tube behaviour in this Chapter, before taking up a study, in the following chapters, for specific conditions on the sun.

3.1 Equilibrium: Polytropic stratification

Let us assume that the atmosphere surrounding the flux tube is a truncated polytrope with a surface corresponding to $z = 0$ which we choose to be the base of the photosphere. It should be noted that

the pressure, density and temperature are finite at $z = 0$, in contrast to a true polytrope where all these variables vanish at its surface. We further assume that in the energy equilibrium condition (2.7), energy transport occurs solely through radiation, which implies that the atmosphere is in radiative equilibrium. We model the opacity variation of the polytrope by a power law

$$\kappa = \kappa_o \rho^{\ell} T^{\nu} \tag{3.1}$$

where ℓ and ν are constants. It is easily seen that, in the present case of diffusive transport of radiative energy, the equations (1.41) and (2.7) imply a constant radiative conductivity $K = 16\sigma T^3/3\kappa\rho$ which together with the hydrostatic condition (2.6) and the assumed form for the variation of opacity given by (3.1) lead to the following relation among $m-$ (polytropic index), ℓ and ν:

$$m = \frac{3-\nu}{1+\ell} \tag{3.2}$$

In the equilibrium atmosphere, the thermodynamic variables have the following form:

$$T_e = T_o \zeta \tag{3.3}$$

$$p_e = p_o \zeta^{m+1} \tag{3.4}$$

$$\rho_e = \frac{p_o}{H_o g} \zeta^m \tag{3.5}$$

$$F_e = -K_e \frac{dT_e}{dz} = -K_e \frac{\mu g}{R} \frac{1}{m+1} = -\sigma T_{eff,\odot}^4 = const. \tag{3.6}$$

where

$$\zeta = 1 + \frac{r}{m+1} \tag{3.7}$$

with r=z/H_o being the dimensionless depth scaled by $H_o = RT_o/\mu g-$ the pressure scale height at the surface(z=0). The logarithmic temperature gradient is thus $\nabla = 1/1 + m$.

The thermodynamic variables for the tube, which satisfy the equations (2.1), (2.2), (2.3) and (2.4), are given by:

$$T = T_e \tag{3.8}$$

$$p = \frac{\beta}{1+\beta} p_e \tag{3.9}$$

$$\rho = \frac{\beta}{1+\beta} \rho_e \tag{3.10}$$

$$F = -K\frac{dT}{dz} = -\left(\frac{1+\beta}{\beta}\right)^{1+l} K_e \frac{dT}{dz} = -\left(\frac{1+\beta}{\beta}\right)^{1+l} F_e = const. \tag{3.11}$$

Thus the atmosphere inside the tube is also a polytrope but shifted by a constant factor with respect to the external polytrope.

As it will become clear from the results that we present later in the chapter, the important quantity that determines the effects of radiation is the radiative conductivity K, a constant in the present case. Its value for a polytrope of given index is set, in the present assumption of radiative equilibrium, by the constant flux that traverses the polytrope in the vertical direction. The more the radiative flux (or equivalently larger the radiative conductivity) greater the non-adiabaticity (i.e., the departure from adiabatic conditions). This is clear from the expressions (2.24) and (2.26) for the radiative time-scales τ_{th} and τ_r, respectively, introduced in Chapter 2. Thus the values taken by the dimensionless non-adiabaticity parameters C and ϵ, given by eqns.(2.23) and (2.25) respectively, for a polytrope of given index, are essentially controlled by the amount of radiative flux that traverses the polytrope. One of the properties of polytropes is the independence of the equilibrium stratification on the details of the energy transport mechanisms, i.e. the energy flux through the polytrope does not determine its stratification, in contrast with real stellar models. Thus, one can arbitrarily choose a value for the constant energy flux that flowing through the polytrope, as long as the opacity variation and the polytropic index satisfy the condition (3.2) which is the requirement for the equilibrium to remain polytropic. We take advantage of this situation to arbitrarily vary the amount of non-adiabaticity due to radiation by introducing a parameter α which measures the radiative flux F_r in the polytrope in units of the solar flux $F_{\odot}$.

$$F_r = \alpha F_{r,\odot} = -\alpha\sigma T_{eff,\odot}^4 \tag{3.12}$$

In reality, the radiative flux is a rapidly decreasing function of the depth z as most of the energy in the deeper layers is transported by the convection. This situation would correspond to a depth dependent α. Thus, a constant value for α, required for a polytrope, could be taken to represent an average over depth of variation in α that one encounters in real cases.

In terms of α, the parameters C and ϵ now read as,

$$C = \alpha\frac{\tau_d}{\tau_{th}} \tag{3.13}$$

$$\epsilon = \alpha\frac{\tau_d}{\tau_r} \tag{3.14}$$

Here, it is to be noted that C and ϵ are still depth dependent owing to the appearance of the density ρ and opacity κ in the radiative time-scales. The above way of controlling the non-adiabaticity due to radiation through the constant multiplication factor α has been employed by Shibahashi and Osaki (1981) (see also Saio, Wheeler and Cox 1984) in their non-adiabatic treatments of non-radial oscillations in stars.

3.2 Linear stabílity analysis

3.2.1 Equations

The general non-adiabatic system of equations that describes the linear evolution of small amplitude fluctuations, derived in Chapter 2 (equations [2.16], [2.17], [2.18], [2.19]), takes the following form for the background polytropic stratification described in the previous Section:

$$\frac{d\xi}{dr} = -\left(1+\frac{\beta}{2}\right)\frac{p'}{p} + \frac{T'}{T} + \frac{(1-m)}{2\zeta(1+m)}\xi \tag{3.15}$$

$$\frac{d}{dr}\left(\frac{p'}{p}\right) = -\frac{1}{\zeta}\frac{T'}{T} + \frac{\Omega^2}{\zeta}\xi \tag{3.16}$$

$$\frac{d}{dr}\left(\frac{T'}{T}\right) = \frac{(1+\ell)}{(1+m)\zeta}\frac{p'}{p} - \frac{(5+\ell-\nu)}{(1+m)\zeta}\frac{T'}{T} + \frac{1}{(1+m)\zeta}\frac{F_z'}{F_z} \tag{3.17}$$

$$C\frac{d}{dr}\left(\frac{F_z'}{F_z}\right) = -i\Omega\mathcal{N}^2\gamma\xi + i\Omega(\gamma-1)\frac{p'}{p} + (4\epsilon - i\Omega\gamma)\frac{T'}{T} \tag{3.18}$$

It is to be noted that the depth coordinate z has been scaled in terms of the pressure scale height H_o at $z = 0$ as against the scaling, with respect to L - the total length of the tube -, done in the last chapter. Thus the dynamical time scale τ_d now reads as follows:

$$\tau_d = \left(\frac{H_o}{g}\right)^{1/2} \tag{3.19}$$

which is the free fall time over one pressure scale height at $z = 0$. The quantity $\mathcal{N}^2$ is the non-dimensional Brunt-Väisälä frequency (scaled in terms of the inverse of the free-fall timeτ_d). All the other quantities in the above equations are the same as those defined in the last chapter. With the assumed time dependence of the form $e^{-i\omega t}$, the growth rates of the modes are the imaginary parts of ω, which we denote as η, so that

$$\eta = Im.(\Omega) \tag{3.20}$$

As a function of the depth coordinate r, the lateral radiative time-scale τ_r can be written as

$$\tau_r = \frac{R\rho_o a_o^2}{(\gamma-1)K}\zeta^{(m-1)/2} \tag{3.21}$$

where we have used the definition,

$$(\gamma-1)c_v = R \tag{3.22}$$

It should be noted that the above form of variation for τ_r, for the present case of a polytrope in radiative equilibrium, is brought about only by the depth dependence of density and the tube radius and not through the depth dependence of opacity whose variation is such as to keep the radiative conductivity K a constant.

The two sources driving convective and the oscillatory motions are respectivley, the super-adiabatic temperature stratification and the pressure forces (which includes the magnetic pressure) that is parameterized by β. The strengths of these sources are set, in the present case of a polytrope, by: the ratio of specific heats γ, the opacity exponents ℓ and ν, the radiative conductivity K and the polytropic index m. For a given value of m, all the above quantities are constants. Fixing a value for one of the opacity exponents, e.g. choosing a value for ℓ, automatically sets the value of ν which determines the temperature dependence of opacity, for a polytrope of given index, through the relation (3.2) which is a requirement for the stratification to remain polytropic. In other words, a polytrope with a constant radiative flux, i.e. a polytrope in radiative equilibrium, is constrained to have a opacity variation dictated by the relation (3.2). It is easily noted that the perturbations in the opacity through the thermodynamic perturbations vanish for the choice of $\ell = -1$ and $\nu = 3$. Thus the κ-mechanism which extracts energy from the radiation to drive the oscillations overstable is not operative for this particular choice of values for ℓ and ν. Accordingly, we choose two different values for ℓ: $\ell = -1$ and 1 which through the relation (3.2) determine the values for ν as a function of the polytropic index m. The super-adiabaticty, which is a constant for a polytrope, is set by the values of the polytropic index m and γ. We fix a value of $\gamma = 1.2$, representative of solar-type stratifications, and thus the variation in the convective driving force is parameterized by the polytropic index: a smaller value for the polytropic index gives a larger super-adiabaticity. Finally, we vary α, as introduced in the last section, to control the effects of radiation. We study the pattern of the convective and oscillatory instabilities as a function of α: $\alpha = 0$ leads to the adiabatic limit while $\alpha = 1$ retains the full non-adiabaticity corresponding to the case of a radiating polytrope with a flux of $F = F_0$ traversing the whole depth.

3.2.2 Boundary conditions

It has been widely noted in the literature, mainly for adiabatic studies (Webb and Roberts 1978) and also in the case of radiative exchange with Newton's law of cooling (Hasan 1984,1986; Takeuchi 1993, 1995), that the linear equations are sensitive to the boundary conditions, particularly the lower one. Calculations yielding a stability limit for a particular value ofβ with a closed mechanical boundary condition at the bottom, have been criticized by Nordlund (1980), who pointed out that a open lower boundary leads to convectively unstable solutions however strong the magnetic

field. This contradicts the observational inference that the strong field elements with a finite β, typically around a value of 1, are convectively stable with a life-time exceeding the turn over time in granules. Such criticisms are not relevant for polytropes, with a constant super-adiabaticity, because in a polytrope the driving force of the convective motions is the same throughout the atmosphere: depending on the chosen amount of super-adiabaticity, for a particular β, there is always a critical depth for the tube such that tubes with depth smaller than this critical value are convectively stable (Webb and Roberts 1978). Thus a polytropic tube having finite super-adiabaticty and with a open lower boundary will always be convectively unstable however strong the field is. Hence, the analysis of the effects of the nature of the lower boundary mechanical condition is meaningful only for the case of a variable driving force over the depth of the tube, i.e. for temperature stratifications which are non-linear and hence a depth dependent super-adiabaticity. We take up this issue in the next chapter where we consider the realistic stratifications of solar magnetic tubes. Here, we consider only closed mechanical boundary conditions.

The boundary conditions that we employ at the top boundary (r=0) are:

$$\xi = 0 \tag{3.23}$$

$$\frac{F_z'}{F} = 4\frac{T'}{T} \tag{3.24}$$

and at the bottom boundary:

$$\xi = 0 \tag{3.25}$$

$$\frac{T'}{T} - \frac{\gamma - 1}{\gamma}\frac{p'}{p} = 0 \tag{3.26}$$

where the last condition is the adiabatic condition, which is chosen to mimic the situation at large depths in the solar convection zone. We fix the lower boundary at a depth of 5000 km below the photospheric surface.

3.2.3 Numerical solution

The linear equations stated in the previous section are solved numerically by approximating the derivatives by finite differences. The insertion of the boundary conditions in the difference equations leads to a homogeneous, tridiagonal system of equations which constitute a generalized eigenvalue problem. The eigenvalues are determined by finding the roots of a determinantal equation. Muller's method is used for locating the complex roots. Determinants are evaluated efficiently using Gaussian elimination with partial pivoting and the eigenvectors are calculated using inverse iteration (Wilkinson and Reinsch,1971).

3.3 Results and discussion

As stated in the previous sections the parameters determining the evolution of a perturbation are the polytropic index m, which determines the amount of super-adiabaticity for a given value of γ, the surface radius a_o of the tube, the plasma β and the value of radiative conductivity K whose value is in turn parameterized by α which, for a given polytropic index, is the ratio of the total vertical energy flux $F = \sigma T_{eff}^4$, where T_{eff} is the surface value of the temperature for the truncated polytrope, to the chosen value of actual constant radiative flux that traverses the polytrope.

We study the stability characteristics of the system of equations by varying α for a tube of given field strength strength (i.e β), super-adiabaticity (m) and radius (a_o). We distinguish between two 'kinds' of overstability: one which developes when there is a finite super-adiabaticity and is termed as *convective overstability*, and the other which exists even under adiabatic and sub-adiabatic stratifications which is the *classical overstability*. These two kinds can be traced to the properties of the same mode, which is the slow magnetoacoustic mode or the sausage tube mode. The latter kind can be traced solely to radiative energy transport, whereas the former is due to the combined influence of convective and radiative effects. In the following Subsection we present and discuss the results for the classical overstability. Sections (3.3.2) and (3.3.3) contain the results and discussions for the convective mode. In Section (3.3.4), we discuss the results for the convective overstability.

3.3.1 Classical overstability- dependence on radiative conductivity

In the absence of radiative energy exchange and other non-adiabatic processes, oscillations, once excited in a convectively neutral atmosphere, remain undamped. For a compressible unmagnetised gas these essentially correspond to a stable spectrum of acoustic modes, while a magnetised gas can support, in general, the usual MHD wave modes viz., the *fast*, *slow* magnetoacoustic modes and the *Alfven* mode. The longitudinal tube mode in a thin flux tube corresponds to the MHD slow mode. This tube mode has also a stable spectrum in the absence of radiative and other dissipative effects (Webb and Roberts 1978). Introduction of any non-adiabatic effects due to radiation or any other kind of dissipative processes lead to either damping or amplification of the oscillations and also considerably modify the propagation characteristics. Here we demonstrate that longitudinal oscillations in an adiabatically stratified polytropic tube can become damped or amplified depending on the amount of radiative flux that traverses the atmosphere or equivalently depending on the value of radiative conductivity. Moreover, depending on the strength and the size of the tube, the tube mode selects a particular value for the radiative conductivity at which it has a maximum growth rate. The growth rates, in general, for this kind of overstable mode,

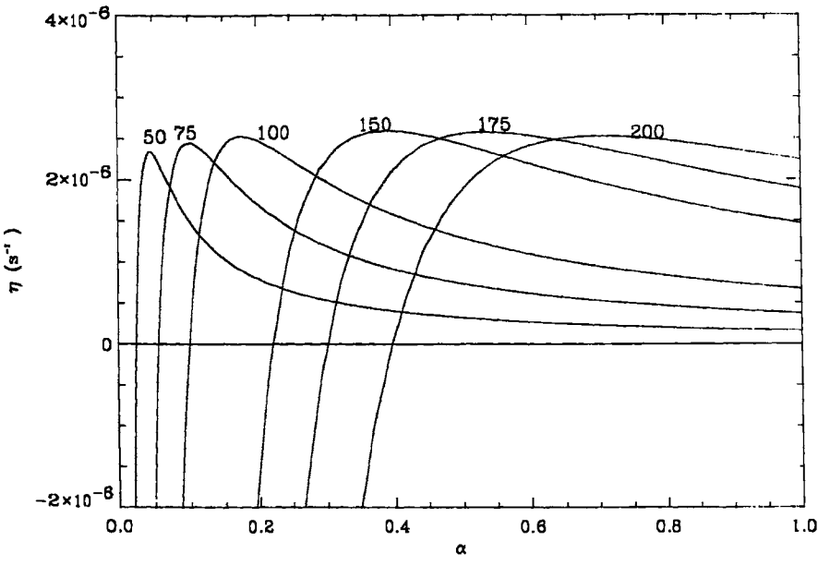

Figure 3.1: Growth rates, η (s^{-1}), of the overstable mode as a function of the non-adiabaticity parameter α for a convectively neutral stratification, i.e. for $m = 1.5$ and $\gamma = 5/3$; the numbers by the side of the curves denote the surface radius a_o of the tubes.

i.e. for the convectively stable stratification, are much smaller than those which are set up in a convectively unstable atmosphere. Thus, for example, a tube of size 100 km at the surface with a plasma $\beta = 1$ has a typical growth rate of the order of 10^{-6} s^{-1} for adiabatic stratifications $(m = 3/2)$ while the convectively overstable mode has a growth rate of the order of 10^{-3} s^{-1}. Fig. (3.1) depicts the growth rates η of the overstable modes as a function of α for tubes of surface radii a_o ranging from 50 km to 200 km and for a representative value of $\beta = 1$. The numbers besides the curves denote the surface radius a_o in km. The regime of negative values for η, i.e. the damping of the mode, is the one where the radiative conductivity K (equivalently the radiative flux) is small making the thermal time-scale τ_{th} very large compared to the oscillation period. Here, the radiative exchange acts to remove the energy in the oscillations at a small rate (the damping rate is of the order of 10^{-6} s^{-1}). But as α increases, i.e. as K and the radiative flux F increases, the damping rate decreases and at a critical value of α, which depends on a_o and β, η crosses zero and the mode becomes unstable. We note that the damping here is different from the one that arises when there are net radiative losses arising out of radiative non-equlibrium in the atmosphere, as we showed in the last chapter: such radiative losses always act to damp the oscillations in contrast to the situation here where the vertical radiative exchange between the oscillating elements damps or amplify the oscillations depending on the amount of non-adiabaticity.

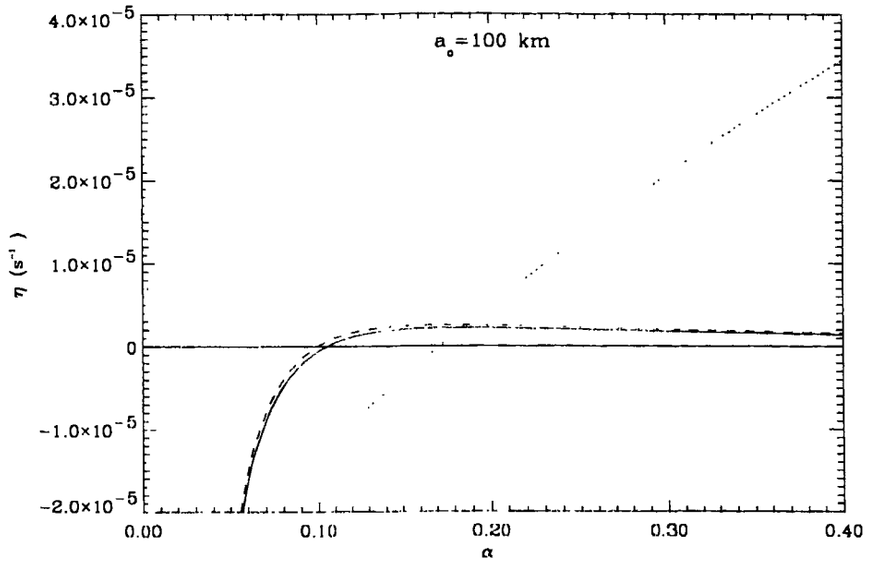

Figure 3.2: Comparison of the instability behaviour between the cases when (i) when there is no horizontal exchange (dotted curve), (ii) when there is only horizontal exchange (solid curve) and (iii) for the full solution (dot-dashed curve).

The growth rates attain a maximum for a particular value of α, which depends upon the radius and β, indicating that non-adiabatic effects are not linearly dependent on the amount of radiative flux available to produce overstability: there is an optimum value for the radiative conductivity and hence the radiative flux to make the tube oscillations grow as a function of time. Since an increase in α increases both the lateral exchange time-scale τ_r and the thermal time scale τ_{th}, the effects of increasing α are the same as that obtained when a_0 is decreased, in so far as radiative exchange between the tube and its surroundings are concerned. This fact is reflected in the shifts of the peak growth rates towards larger α as a_0 increases: the horizontal radiative exchange time is larger for a larger tube and hence the amount of non-adiabaticity, here equivalently the value of α, required to attain the maximum growth rate that a smaller tube attains at a smaller α is higher. Thus one can guess that the behaviour of the growth rates attaining a maximum at a particular value of α is mainly due to the size dependent horizontal exchange, quite similar to the horizontal wave-number (k) dependent behaviour seen in studies of radiative transfer effects on the 2-D convective perturbations in a field-free atmosphere (Bohm and Richter 1960, Spiegel 1962, 1964) or in a uniform field geometry (Antia and Chitre 1979). We make this clear by comparing the growth rates obtained when horizontal radiative exchange is switched off with those obtained when only horizontal exchange is allowed. In the former case, there is no size dependence and thus

varying α amounts to varying only τ_{th}; in the latter case, we have chosen a tube of size $a_o = 100$ km and have varied α. The results are shown in Fig. (3.2). In the absence of horizontal exchange (dotted curve in the figure) the growth rate monotonically increases as α increases while for the case of horizontal exchange alone (solid curve), the growth rates attain a maximum at a particular value of α, very much the same as that is obtained when both horizontal and vertical exchanges are included (the dot-dashed curve). It is also seen that the dominant non-adiabatic contribution is from the horizontal exchange as there is very little difference between the solid and dot-dashed curves.

3.3.2 Convective instability criteria: modifications due to radiative transport

The modifications, introduced by the radiative exchange, to the adiabatic stability criterion in the $\beta - m$ space are shown in Figs. (3.3a) and (3.3b). These figures contain both the convective instability (solid curves) and the overstability (dashed curves) criteria. Here, let us consider the radiative effects only on the convective instability, leaving a discussion on overstability criteria to Section (3.3.4). The dot-dashed curve in these figures represents the adiabatic stability criterion (2.34) derived by Webb and Roberts(1978), i.e. the points on these curves are the critical points which satisfy the equality in (2.34). The portion to the left of this curve in the $\beta - m$ space is convectively unstable region while that on its right is stable. The dotted curve in the figures demarcate the sub-adiabtic and super-adiabatic regions: since we have used a representative value of $\gamma = 1.2$ this demarcation lies at a value of polytropic index $m = 5$ which is a adiabatically stratified (convectively neutral) polytrope. Thus, this dotted curve denotes the Schwarzschild criterion which holds for an unmagnetised gas. Fig. (3.3a) contains the stability criteria for a tube of surface radius $a_o = 100$ km for two different values of the non-adiabaticity parameter α; the left panel is for $\alpha = 0.01$ and the right one is for $\alpha = 0.05$. Comparison of these two cases reveal the stabilizing influence of radiation on the convective instability of the tube: the more the value of α the less is the area of the convectively unstable region in the $\beta - m$ space. Similar comparison in Fig. (3.3b), which is for a smaller tube of $a_o = 50$ km, shows that the radiative effects are stronger so much so that there is no convective instability at all for $\alpha = 0.05$. Thus, for $\alpha = 0.05$ a tube of size $a_o = 50$ km does not collapse to form a stronger tube and shows only overstability. Also a comparison of the cases for the same value of α in Fig. .(3.2a) and (3.2b) reveals the size-dependent influence of radiation on the convective instability: the larger the tube-size the closer is the convective instability criterion to the adiabatic instability criterion.

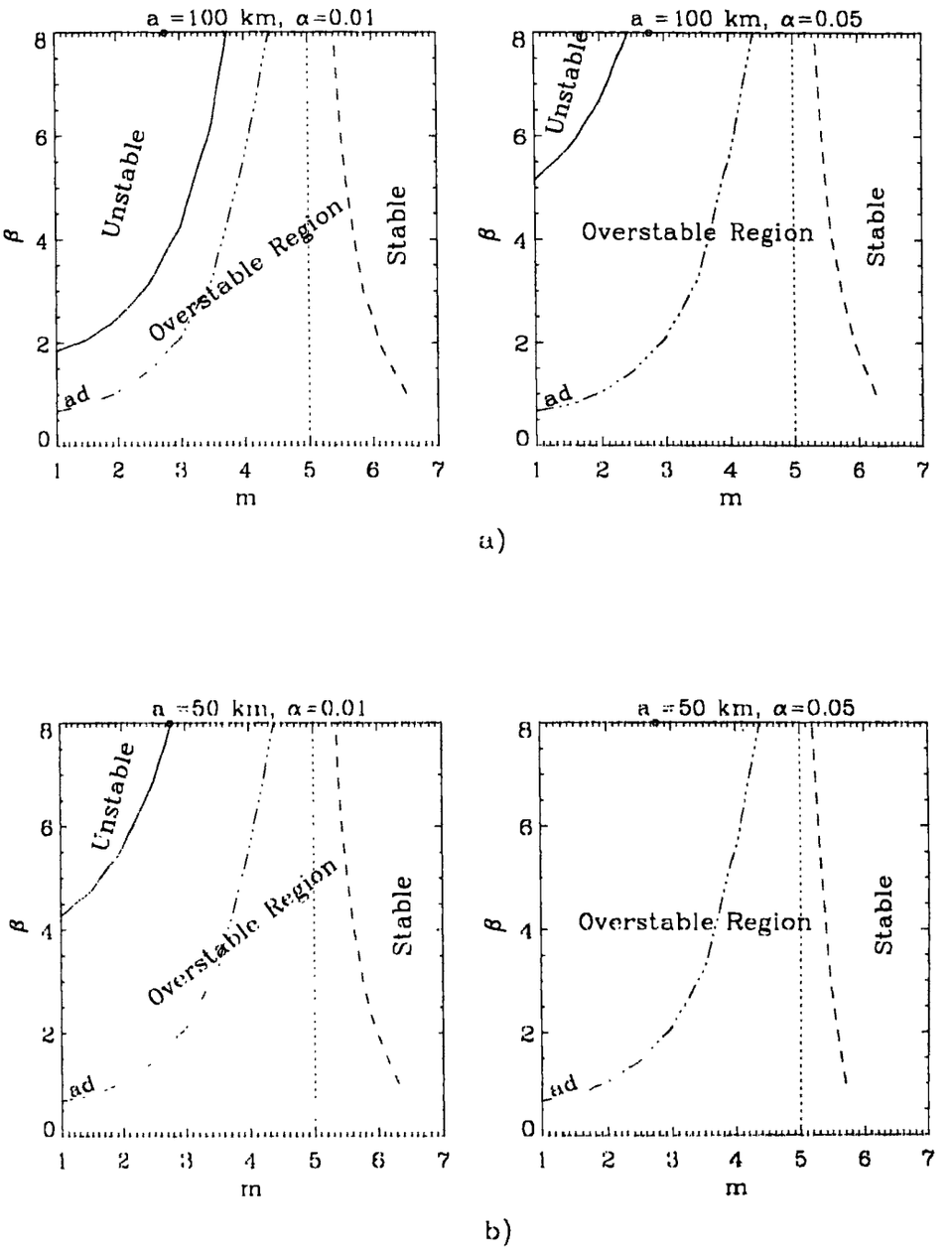

Figure 3.3: Stability Criteria in the β-m space: a) for a tube of surface radius a_o = 100 km and b) a_o = 50 km. The label 'ad' refers to the adiabatic stability criterion. The solid curve is the convective instability criterion and the dashed curve is the overstability criterion. The dotted curve divides the space into super-adiabatic (left) and sub-adiabatic (right) regions

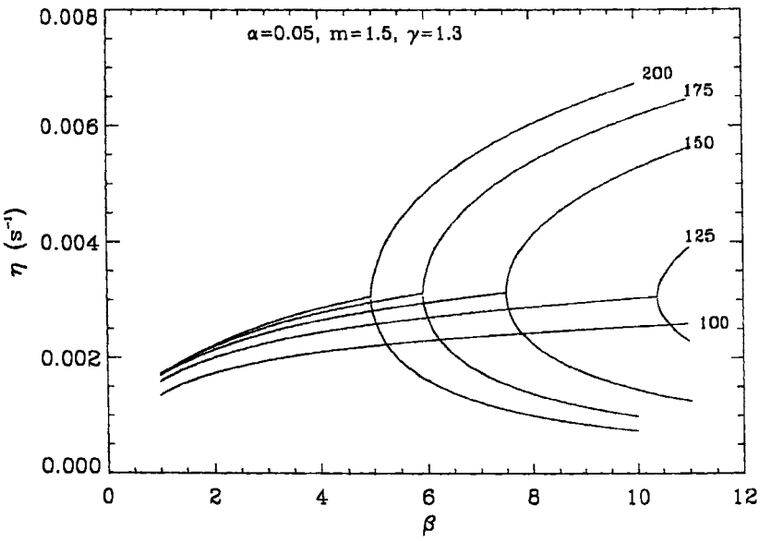

Figure 3.4: Growth rates, η (s^{-1}) of overstable and convective modes as a function of β for different values of the tube radius. The numbers by the side of the curves denote the radii in kms at $z = 0$. The polytropic index $m = 1.5$, $\gamma = 1.3$ and $\alpha = 0.05$

3.3.3 Convective instability: dependence on the radius and field strength of the tube

The general pattern of the instability behaviour as a function of the plasma β, as modified by the presence of radiative energy exchange, is similar to that which has been brought out in simplified treatments involving only the lateral exchange either in the optically thin limit (Newton's law of cooling) (Hasan 1986) or in the thick limit (Venkatakrishnan 1986) and also in studies of radiative effects on convective motions in a uniform laterally unbounded magnetic fields (Syrovatskii and Zhugzhda 1968, Antia and Chitre 1979). The growth rate of the overstable slow tube mode increases as the plasma β increases, while the frequency of the mode decreases, until it gets transformed into two purely growing monotonic convective modes at a particular value of β which depends on the radius of the tube and at which the period of the overstable mode becomes infinite. The vertical diffusion of radiation does not change such a behaviour but the growth rates and the location at which the mode transformation takes place are affected.

In Fig. (3.4), the growth rates of the fundamental mode, which is the most unstable, are shown as a function of plasma β for tubes of different sizes. The values of the polytropic index m, adiabatic index γ and the control parameter for non-adiabaticity α used for this set of curves are respectively, 1.5, 1.3 and 0.05. The bifurcation of the growth rate curve, at a particular value of β, into two curves

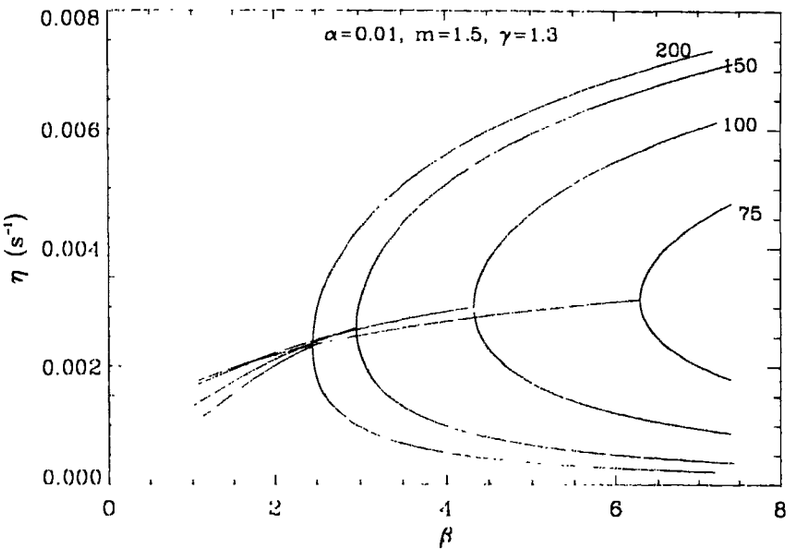

Figure 3.5: The same as previous Fig. (3.4) with $\alpha = 0.01$

mark the location where the overstable mode gets transformed into two purely growing monotonic convective modes. The upper branch corresponds to the usual convective mode whose growth rate increases as the plasma β increases, i.e. as the field strength decreases. The lower branch is a consequence of the radiative effects (Hasan 1986) which can be called a thermal-convective mode and has a characteristic that its growth rate decreases as the field strength decreases: this can be explained as a consequence of the decreasing influence of the radiation for weaker fields because weaker fields are less transparent than the stronger ones. For the above same values of m and γ i.e., for the same amount of super-adiabaticity which is the driving force of the convective stability, the instability behaviour for $\alpha = 0.01$ i.e., for a smaller amount of non-adiabaticity due to radiation, is shown in Fig. (3.5).

The helioseismologically determined sound speed variation in the surface layers of the sun is closely reproduced by a polytrope of index 3.85 (Bogdan et al. 1996). For this value of polytropic index, the convective stability limit of β around a value of 1 in the adiabatic case corresponds to a value of $\gamma = 1.1$. We repeat the calculations for this choice of values for m and γ. As a representative behaviour of this polytrope, the growth rate curves are shown in Fig. (3.6) for a value of $\alpha = 0.02$. Here we have shown only the normal convective mode which branches out from the overstable part.

The above expalined behaviour is also seen in the growth rate-radius plane, shown in Fig. (3.7): here we plot the growth rates as a function of the surface radius a_0 for various values of β. The

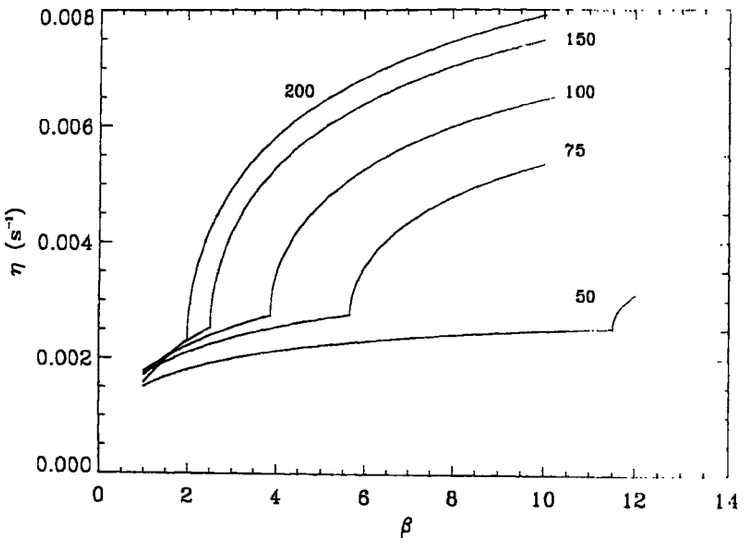

Figure 3.6: Growth rates η of overstable and convective modes as a function of β for different values of the sizes of the tubes. The polytropic index $m = 3.85$ and $\gamma = 1.1$

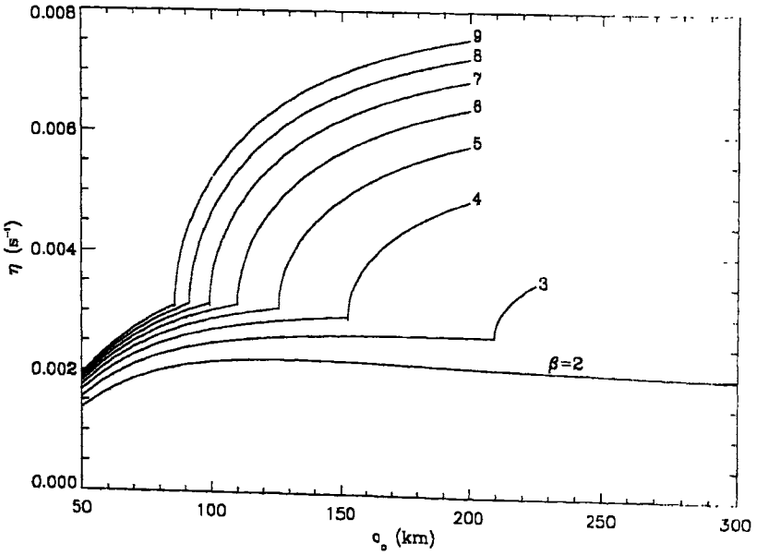

Figure 3.7: Growth rates η of overstable and convective modes as a function of a_o for different values of β.

value of the non-adiabaticity parameter α used for this set of curves is 0.02.

To understand better the effects of non-adiabaticity due to radiation, we plot in Fig. (3.8) the growth rates for a tube of radius 100 km for different values of α as a function of β. Here we have shown only the overstable and the normal convective mode parts of the curves. Lower the value of α (or equivalently, the smaller the value of radiative conductivity and hence the radiative flux), less the non-adiabaticity. The curves in Fig. (3.8a) demonstrate the suppression of the convective instability by radiation: for $\alpha = 0.05$ a tube of radius 100 km does not undergo convective collapse in the relevant range of β values, while for smaller values of $\alpha = 0.02$ or 0.01 there are convective modes present. The larger the non-adiabaticity due to radiation the more stable is the tube against the convective instability. The curves in Fig. (3.8a) are for values of $m = 1.5$ and $\gamma = 1.3$. A similar comparison is shown in Fig. (3.8b) for values of $m = 3.85$ and $\gamma = 1.1$.

Size(flux)-strength relation for the tubes

The influence of size on convective collapse of tubes is evident from the relative positions of the bifurcation by which the overstable mode is transformed into two monotonically unstable convective modes, as shown in the Fig. (3.4)-(3.8). Moreover, the values of β and hence the field strength for which the tube is convectively unstable, are a function of the size. Therefore, by assuming that tubes which collapse attain a final stable equilibrium state with higher field strengths, we can derive a relation between the size and strength for tubes which are formed by this collapse process. We do this by locating the positions on the curves shown in Fig. (3.4)-(3.8), that mark the onset of convective instability. The corresponding flux-strength relations are plotted in Fig.(3.9): Fig. (3.9a) shows such relations for a polytropic index $m = 1.5$ and $\gamma = 1.3$ for three different values of the non-adiabaticity parameter α, and Fig. (3.9b) for the case of polytropic index $m = 3.85$ and $\gamma = 1.1$. For larger values of α the non-adiabaticity due to radiation is more and therefore a tube of given field strength will require a larger radius to be convectively unstable. This behaviour is evident in the flux-strength relations presented in the figures: for larger values of α, it is seen that the field strength for stability is smaller and thus for a given amount of magnetic flux the field strength for stability is higher for smaller values of α. Thus for example, considering the case presented in Fig. (3.9b), if we choose a initial weak field (uncollapsed) concentration containing a flux of 4×10^{17} Mx, the strengths corresponding to the convectively stable limit after the collapse in atmospheres having different amounts of non-adiabaticity as parameterized by α are given by the points on the curves intersected by a straight line drawn parallel to the x-axis for a flux $\Phi = 4 \times 10^{17}$ Mx. Here, we see that $\alpha = 0.02$ corresponds to a stable state of strength $B_{ph} \approx 1400$ G, whereas $\alpha = 0.05$ corresponds to $B_{ph} \approx 1200$ G and $\alpha = 0.1$ corresponds to $B_{ph} \approx 1100$ G. Since α can

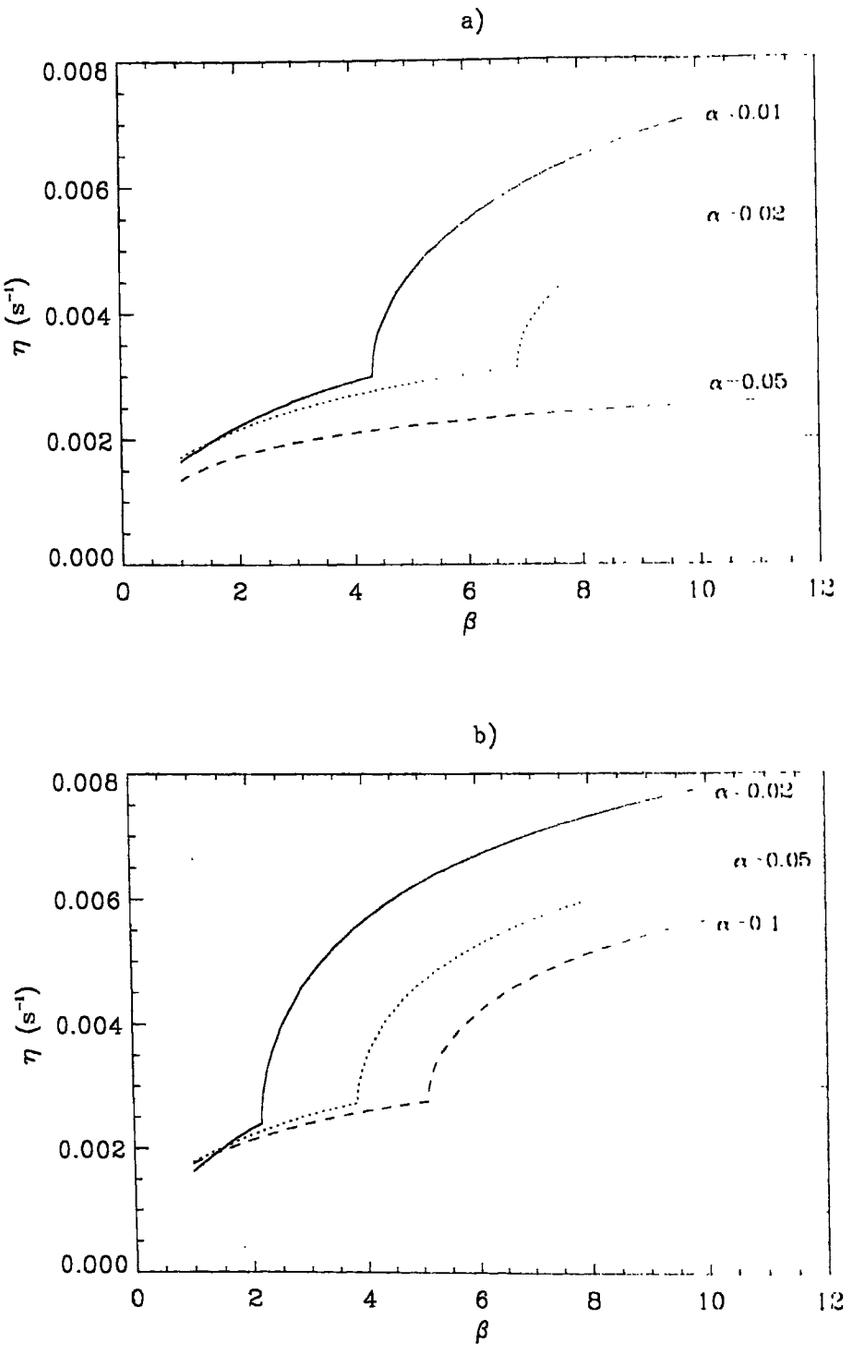

Figure 3.8: Comparison of instability behaviour for a tube of surface radius 100 km for different values of the non-adiabaticity parameter α; a) $m = 1.5$ and $\gamma = 1.3$ yielding a super-adiabaticity $\delta = \nabla - \nabla_a = 0.17$. b) $m = 3.85$ and $\gamma = 1.1$, which yield $\delta = \nabla - \nabla_a = 0.115$

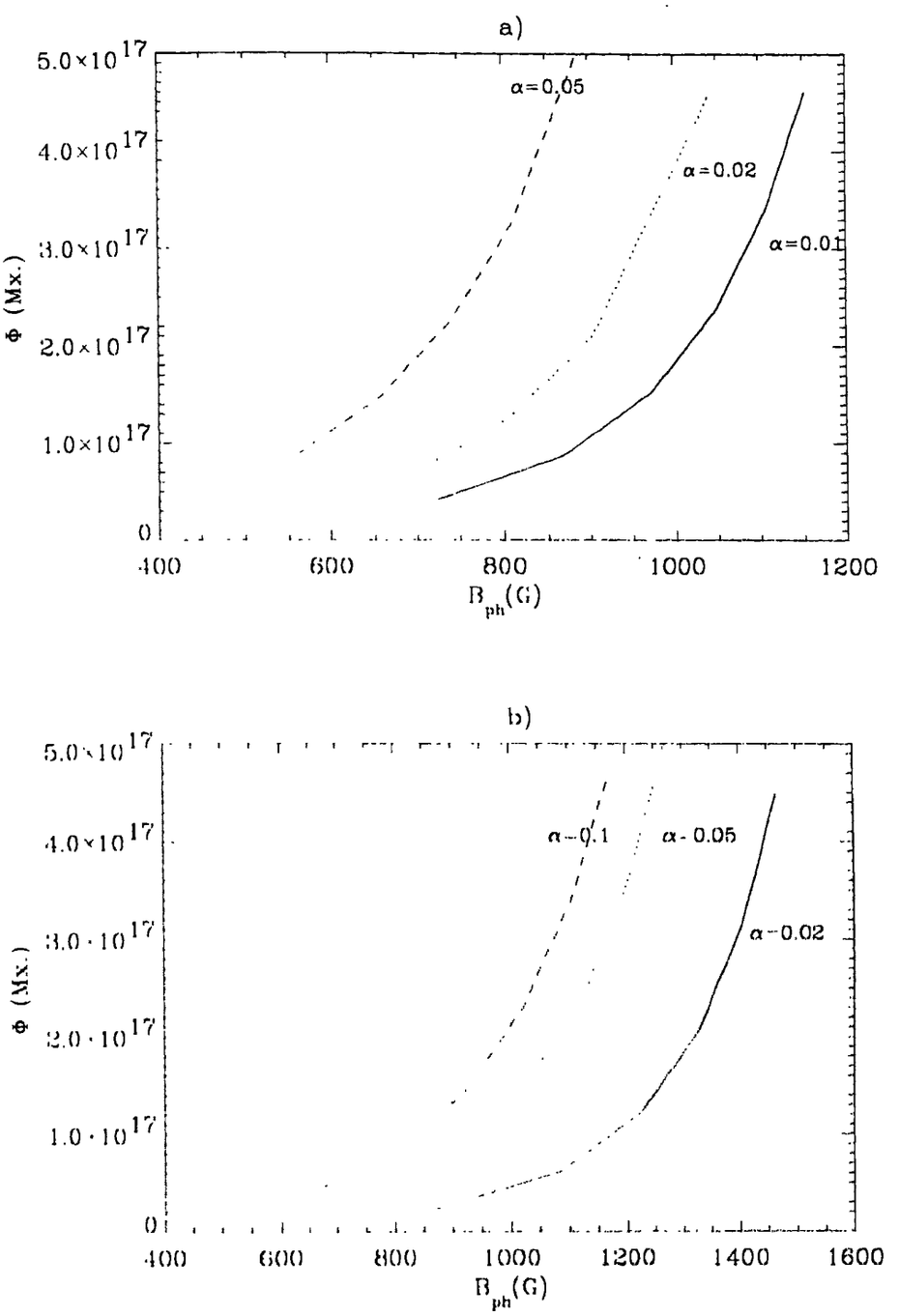

Figure 3.9: Flux-strength relations for three different values of the non-adiabaticity parameter α; a) $m = 1.5$ and $\gamma = 1.3$. b) $m = 3.85$ and $\gamma = 1.1$

also be considered as an average over depth of the changing fraction of the radiative flux to the convective flux in a real star, we can say from the above results that convectively stable tubes embedded in atmospheres where the fraction of convective to radiative energy fluxes is higher must have stronger field strengths

3.3.4 Overstability

The existence of overstability and the dependence of the growth rates on α for a convectively stable adiabatic stratification ($m = 1.5$ and $\gamma = 5/3$) were shown in Section 3.3.1. Here, we calculate the growth rates of the overstable modes for super-adiabatic stratifications. For this purpose, we choose a polytrope of index $m = 3.85$ and $\gamma = 1.1$ (which provide a good match for the super-adiabatic layers of the Sun). The results for a convectively stable (collapsed) strong tube of $\beta = 1$ for different values of its sizes (surface radius a_o) are shown in Fig. (3.10). The dependence of the growth rates on the non-adiabaticity parameter α are similar to that of a adiabtically stratified polytrope [Fig. (3.1)]. But it should be noted, that in the present case the growth rates are typically around $10^{-3}s^{-1}$ in contrast with the values of the order of $10^{-6}s^{-1}$ found for the adiabatic polytrope. Another difference between the two cases is the absence of damping (negative growth rates) in the present case of a convectively unstable stratification. There is overstability even for very small values of α (≈ 0.01). We note that the finding in the Chapter 2 of the damping of the wave mode, even for super-adiabatic stratifications, is mainly a consequence of non-zero divergence of the radiative flux (radiative non-equilibrium) and thus is due to vertical radiative losses. Here such effects are absent as a polytropic equilibrium is constrained to have a constant radiative flux and thus is in radiative equilibrium.

As regard the dependence of the overstability on the polytropic index (super-adiabaticity) and the field strength, we refer to Fig. (3.3), which contains also the overstability criteria (the dashed curves) in the $\beta - m$ plane. It is seen that the overstability criteria always lie in the region of sub-adiabatic stratifications and the critical values of the polytropic index for the onset of overstability are weakly dependent on plasma β. The regions between the dashed curves and the dotted vertical line in these figures are those which correspond to the sub-adiabatic stratifications which are overstable. Interestingly, this sub-adiabatic overstable region's area in the $\beta - m$ space shrinks as the amount of non-adiabaticity increases, i.e. as the tube size decreases and as α increases. This behaviour corresponds to the non-linear dependence of the growth rates on α and tube size, which are shown in Fig. (3.1).

Finally, we show in Fig. (3.11) the dependence of the growth rates on the tube size, for typical values of α and β. Depending on α, there is an optimum value for the size of the tube (a_o) at which

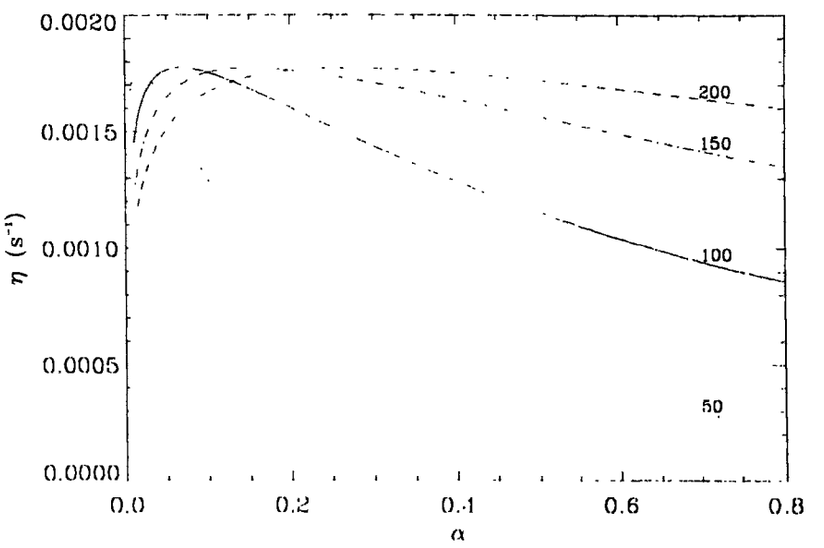

Figure 3.10: Growth rates of the overstable mode (fundamental mode) as a function of α under a super-adiabatic stratification (m = 3.85 and γ = 1.1). The numbers by the side of the curves denote the surface radii in km and the results shown are for a tube of $\beta = 1$

the oscillations have a maximum growth rate. The corresponding frequencies of the overstable mode are shown in Fig. (3.12). It was explained in Section (3.3.1) that the size dependent horizontal radiative exchange was the cause of the growth rates peaking at a particular value of α. The growth rates of the convectively overstable mode shown in Fig. (3.11) further clarifies such an influence of horizontal exchange.

3.4 Conclusions

- We have demonstrated that radiative transport has a marked effect on the size-field strength relation for magnetic flux tubes. By introducing a parameter that controls the amount of non-adiabaticity due to radiation we have performed numerical experiments which bring out the pattern of stabilizing action of radiation on the convective instability of the tubes. The greater the nonadiabaticity due radiation, or equivalently the larger the radiative conductivity and the radiative flux in the atmosphere, the smaller the field strength required for stability against convective collapse and consequently it is demonstrated that convectively stable tubes embedded in atmospheres where the fraction of convective to radiative energy fluxes is higher are stronger.

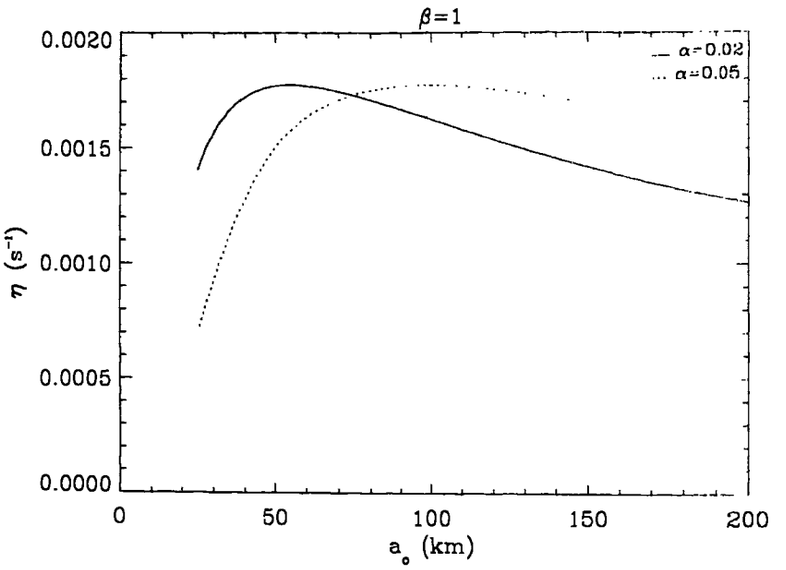

Figure 3.11: Growth rates of the overstable mode (fundamental mode) as a function of the surface radius a_o (km) for $\beta = 1$ and two different values of α.

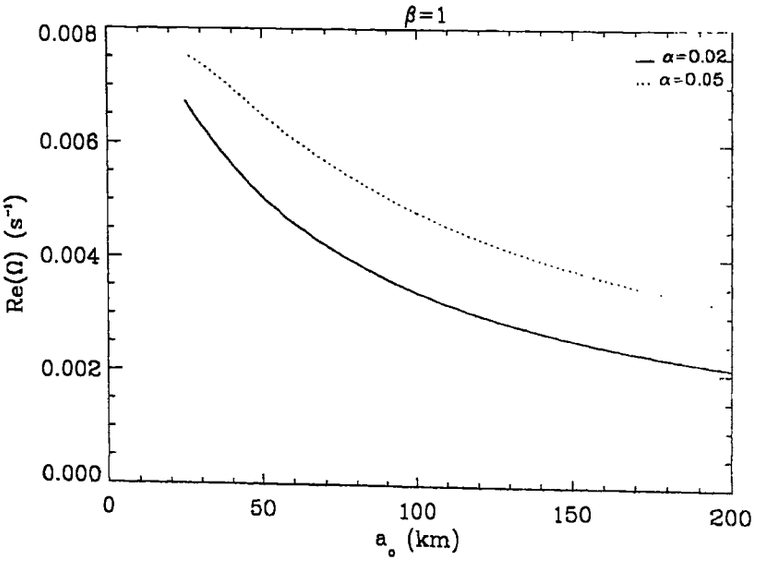

Figure 3.12: The corresponding frequencies of fundamental overstable mode shown in the previous graph

- We have generalized the necessary condition for the onset of convective instability in the presence of radiative heat diffusion. We find that radiative diffusion has a stabilizing influence which is greater for tubes with small radius.

- The critical value of the polytropic index for the onset of overstability has been determined for different values of β. This value depends weakly on β. It is also demonstrated that a adiabatically stratified convectively stable tube has overstability depending on the amount of non-adiabaticity which is determined by the amount of radiative flux, as well as the size and strength of the tube.

Chapter 4

Radiative Diffusion and Unstable Motions in Slender Magnetic Flux Tubes. III. Small-scale Solar Magnetic Structures

4.1 Introduction and motivation

The magnetic elements that constitute about 90% of the magnetic flux on the Sun's surface outside of sunspots have been shown, observationally, to posses field strengths in the range of 1-2 kGauss and sizes of 100-300 km (Howard and Stenflo 1972, Stenflo 1973). These strong field flux elements are found preferentially at the supergranular downflow regions and form the so called *network* which is observed to be a prominent feature in the chromosphere and play a crucial role in the dynamics of the chromospheric and coronal gas. These network elements share uniform properties, such as their strength and the other observational signatures, be it in the active region plages or in the quite regions of the Sun(Schussler 1991,1993). Most importantly it has been found that the field strengths of these strong field structures show a very weak dependence on the flux per element, Φ: the active region network elements have Φ much higher than the quite region ones, yet the field strengths are almost the same. This observational fact suggests that the formation and equilibrium of these structures is unique and global. On the other hand, there are the inner network mixed polarity weak field structures, whose field strengths have been measured recently(Keller et al. 1994; Lin 1995; Solanki et al. 1996) to have a typical value of 500 G, with the property that they have Φ typically less than 1×10^{17} Mx and with strengths strongly dependent on the flux: Φ changes only slightly but the field strengths show a large range from about the equipartition values of 300-400 G to about 1000 G. If the convective collapse of a weak field tube is the global process responsible for the formation

of the strong field tubes(Parker 1978; Webb and Roberts 1978; Spruit and Zweibel 1979; Spruit 1979; Hasan 1983, 1984; Venkatakrishnan 1985; Steiner 1996), that comprise the network with strengths weakly dependent on Φ, then, it should be explained why tubes with smaller fluxes viz., the inner network elements do not collapse to kG strength. Efficient radiative exchange with the surroundings by a small flux tube(Hasan 1986; Venkatakrishnan 1986) offers a natural explanation, as we also have shown in the last chapter in a general way for tubes having a linear temperature profile, i.e. for polytropic stratifications. In particular, Venkatakrishnan(1986), from a simplified treatment of such effects of radiation on the convective collapse, derived a size-strength relation for tubes choosing numbers appropriate for the Sun. Such a relation has been shown, recently, to match well with the observations (Solanki et al 1996). Apart from inhibiting the convective instability of a tube, radiative exchange also makes the longitudinal tube mode overstable (Hasan 1986). This was also established in our study in the last chapter for polytropic stratifications. Here in this Chapter, having in mind a quantitative comparison with the above explained observationally established properties of the solar flux tubes, we employ a model atmosphere for the photosphere and the convection zone of the sun and study in detail the effects of radiation on the convective instability and the wave motions in the tube. We retain the diffusion approximation for the treatment of the radiative transport, as we did for the polytropic models in the last chapter. We mention here that equilibrium models of small-scale solar flux tubes under the diffusion approximation have been constructed by Spruit (1977).

The chapter is organised as follows: Section 4.2 describes the equilibrium model of the sun used and presents the relevant equations, along with the boundary conditions. Section (4.3) contains a general discussion on the action of radiation on the evolution of structures on the surface of the sun. The results and discussions are presented in Section (4.4): we first obtain the numerical solution of the adiabatic system of equations for the solar case and compare them with those obtained by Spruit and Zweibel (1979), in order to assess the differences on the stability due to the background model atmosphere. Also an analysis of the effects of nature of the boundary conditions is presented, which clarifies the role of horizontal radiative exchange in rendering the oscillations overstable. Finally, solutions of the full non-adaibatic system are discussed. Size-strength relations for the solar tubes are derived and overstability criteria are obtained. In the final section, the results are summarized with conclusions.

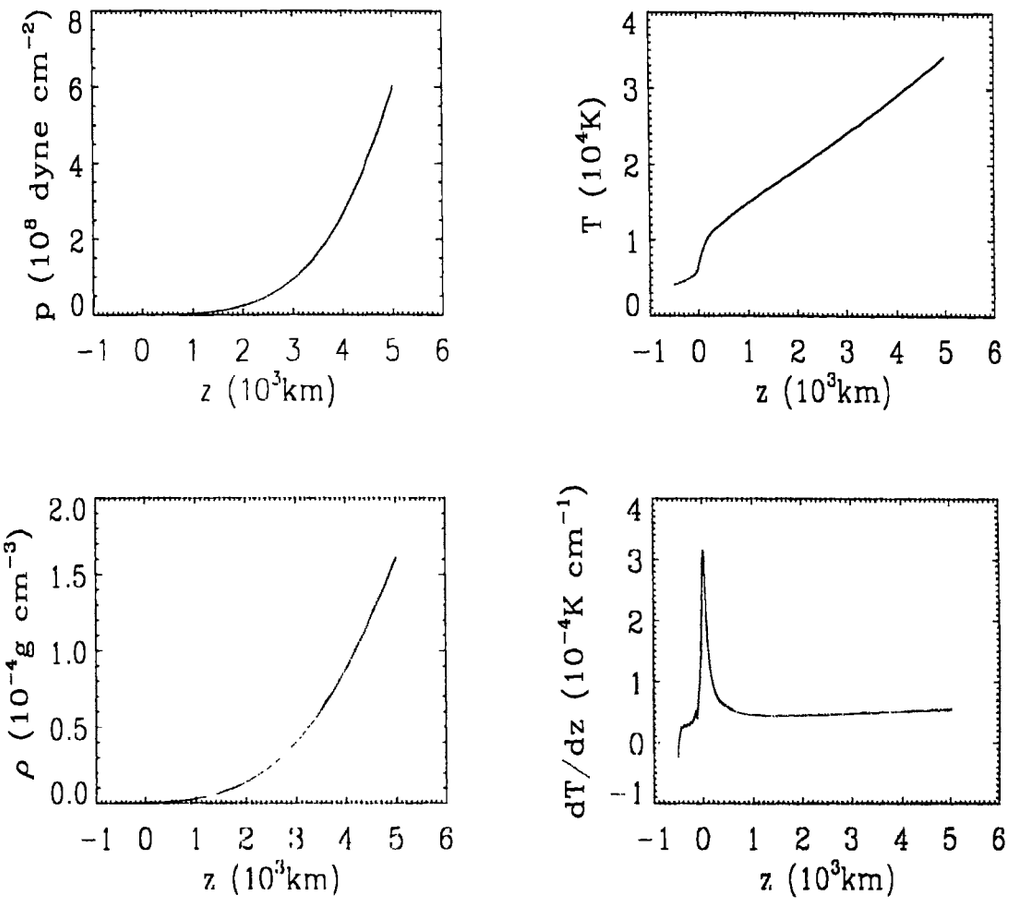

Figure 4.1: Equilibrium profiles of temperature, pressure, density and the temperature gradient for the external quiet sun model constructed as explained in Section 4.2

4.2 Equilibrium model of the Sun

The equilibrium stratification of the external medium that is used here is the one determined to match the $VAL-C$ (Vernazza et al. 1981) model for the photosphere and the higher layers whereas in the convection zone, the atmosphere is constructed as explained in Hasan and Kalkofen (1994) and Hasan, Kneer and Kalkofen (1998). The convection zone structure in this model differs slightly from that of Spruit (1977), owing to refinements in the treatments of radiative transfer and mixing length formalism. This model satisfies the hydrostatic and energy equilibrium conditions (2.6) and (2.7) presented in Chapter 2. The vertical energy fluxes in the external atmosphere and flux tube respectively, $F_{z,e}$ and F_z, in equations (2.7) and (2.3) respectively, are the total energy fluxes which contain contributions from both radiative and convective transport. The profiles of temperature, pressure and density of the model are shown in Fig. (4.1). Saha's equation is used to determine μ-the mean molecular weight and the various thermodynamic quantities like C_v are determined following Mihalas (1967). The Rosseland mean opacities are calculated by interpolation from the tables of Kurucz (1993) for the upper layers and from those of Rogers and Iglesias (1992) for the deeper regions. The depth dependence of adiabatic temperature gradient ∇_a and the logarithmic temperature gradient ∇ are shown in Fig. (4.2a) and that of superadiabaticity $\delta = \nabla - \nabla_a$ is shown in Fig. (4.2b). The superadiabaticity δ, which drives the convective instability, peaks at about 75 km below $z = 0$ and much of the deeper layers are almost adiabatic. This character of the real sun is distinctly different from polytropic stratifications used in the last chapter where the superadiabaticity is depth-independent.

4.3 Linear stability equations and boundary conditions

The general set of equations derived in Chapter 2, namely the equations (2.16), (2.17), (2.18) and (2.19), applies for background equlibria with arbitrary stratifications and variable ionization, superadiabaticity, mean molecular weight etc.. For convenience we give them again hereunder:

$$\frac{d\xi}{dr} = \frac{1}{H}\left(\frac{dH}{dr} - \frac{1}{2}\right)\xi - \left(\frac{\beta}{2} + \frac{1}{\chi_\rho}\right)\frac{p'}{p} + \frac{\chi_T}{\chi_\rho}\frac{T'}{T} \tag{4.1}$$

$$\frac{d}{dr}\left(\frac{p'}{p}\right) = \frac{\Omega^2}{H}\xi - \frac{(\chi_\rho - 1)}{\chi_\rho H}\frac{p'}{p} - \frac{\chi_T}{\chi_\rho H}\frac{T'}{T} \tag{4.2}$$

$$\frac{d}{dr}\left(\frac{T'}{T}\right) = \frac{dlnT}{dr}\left[\kappa_p + \frac{1}{\chi_\rho}\right]\frac{p'}{p} - \frac{dlnT}{dr}\left[4 - \kappa_T + \frac{\chi_T}{\chi_\rho}\right]\frac{T'}{T} + \frac{dlnT}{dr}\frac{F_z'}{F_z} \tag{4.3}$$

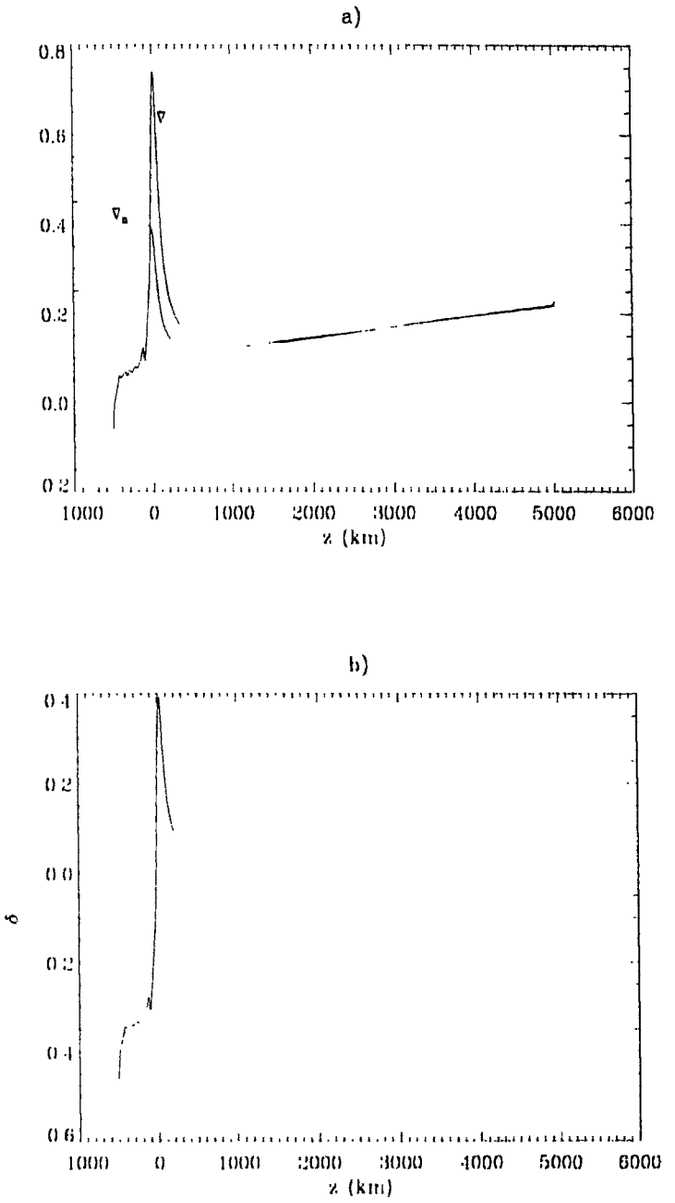

Figure 4.2: The depth dependence of a) ∇ and ∇_a, and b) superadiabaticity δ=$\nabla - \nabla_a$

$$C\frac{d}{dr}\left(\frac{F_z'}{F_z}\right) = -i\Omega\frac{N^2\Gamma_1}{\chi_T}\xi + i\Omega\frac{(\gamma-1)}{\chi_T}\frac{p'}{p} + (4\epsilon - i\Omega\gamma)\frac{T'}{T} - C\frac{dlnF_z}{dr}\frac{F_z'}{F_z} \tag{4.4}$$

The various quantities appearing in the above equations have the same meaning as explained in Chapter 2.

As was pointed out in Chapter 3, the effect of the mechanical boundary conditions, especially for the bottom boundary of the tube, has non-trivial physical consequences when the driving forces for the unstable motions studied are not uniform over the vertical extension of the atmosphere in the tube. Thus it is important to analyse such effects in the present case of realistic model stratifications. Accordingly we choose the following combinations of the boundary conditions:

Closed or Rigid Boundaries:

$$\xi = 0, \qquad at\ z = z_{top}\ \ and\ at\ \ z = z_b \tag{4.5}$$

with the thermal conditions,

$$\frac{F_z'}{F} = 4\frac{T'}{T}, \qquad at\ z = z_{top} \tag{4.6}$$

and

$$\frac{T'}{T} - \frac{\gamma-1}{\gamma}\frac{p'}{p} = 0, \qquad at\ z = z_b \tag{4.7}$$

Mixed (open and closed) boundaries:

i)

The Lagrangian pressure perturbation is zero at z_{top}:

$$\frac{\delta p}{p} = \frac{p'}{p} + \xi = 0 \tag{4.8}$$

and

$$\xi = 0, \qquad at\ z = z_b \tag{4.9}$$

ii)

$$\xi = 0, \qquad at\ z = z_{top} \tag{4.10}$$

and

$$\frac{d\xi}{dz} = 0, \qquad at\ z = z_b \tag{4.11}$$

Open boundaries:

$$\frac{\delta p}{p} = \frac{p'}{p} + \xi = 0, \qquad at\ z = z_{top} \tag{4.12}$$

$$\frac{d\xi}{dz} = 0, \qquad at \ z = z_b \tag{4.13}$$

The thermal boundary conditions for the above two sets are the same as that for the first set. The second thermal condition is the adiabatic condition which is applied at the lower boundary. We mainly consider the differences between the cases of the lower boundary mechanical condition being open and closed, choosing two different locations one at 5000 km and the other at 10000 km from the photospheric surface ($z = 0$). The numerical procedure of solving the system of equations is the same as explained in the previous chapter.

4.4 Influence of radiation on the surface structures- a general discussion

The balance of momentum of material motions on the sun's surface layers is strongly coupled to the energy transport by radiation: much of the visible structures, like the granulation, on these layers are due to radiative heating (or cooling) from the deeper layers where convective transport is more efficient; such a coupling is even more prominent in the presence of magnetic fields; the structure, the size-dependent intensity contrasts and the critical sizes for the transition from bright to dark pores for the magnetic structures are all determined by the action of radiation (Spruit and Zwaan 1981, Spruit 1991). The size distribution and the observed scale of solar granulation is explained by radiative transfer effects (Nelson and Musman 1978 and references therein). In fact, these authors conclude that efficient horizontal radiative smoothing of temperature fluctuations limits the sizes of structures on the sun to a minimum of about 500 km: for structures smaller than this the horizontal optical thickness of the phtospheric material is low enough for the radiation to smooth out the temperature fluctuations on a dynamical time scale. Thus, though adiabatic growth rates of linear modes increase monotonically as the horizontal scale of the perturbations decreases, the above discussed damping due to radiation increases faster as the scale decreases and thus scales greater than a certain critical value only will dominate.

On the other hand, the small-scale magnetic structures are inferred to have sizes 100 km or even smaller. This suggests that the physical processes that create these strucures are located somewhat deeper in the convection zone where the matter is optically thick and hence the radiation allows smaller size fluctuations. The convective instability of a weak field magnetic tube is driven by the superadiabatic stratification which peaks roughly about 75 km below the photospheric surface. This location for the driving force for the convective instability is deeper than the location where the radiative losses, which greatly influence the granular evolution, peak. Thus, at the photospheric surface, the radiative smoothing is very efficient and this explains the lower limit of 500 km that

Nelson and Musman(1978) have obtained for the granulation. Our study here of the effects of radiation on the convective instability of a solar magnetic flux tube is with such an aim of obtaining a lower limit for the size of the tube, which is otherwise formed by expelling convective flows to strength of equipartition values.

4.5 Results and discussion

Before presenting the solutions to the full non-adiabatic set of equations (2.16) -(2.19), we examine the behaviour of the solutions of the adiabatic system (2.27) & (2.28) and those of equations (2.39) & (2.40) which apply for radiative exchange under Newton's law of cooling, for the solar model considered. We especially examine and clarify the role of open lower boundary on the eigenvalues and eigenfunctions, and bring out the physical significance of horizontal radiative exchange in rendering the oscillations overstable.

4.5.1 Adiabatic solution

As noted in Chapter 2, the adiabatic system of equations has the property that the eigenvalues ω^2 are real: ω is either real or purely imaginary. With our convention of choosing the time variation as $exp(-i\omega t)$ for the perturbations, a purely imaginary value for ω represents the monotonically growing or damped convective mode with the growth rate or damping rate equal to the value taken by ω: positive ω^2 represents stable oscillations while a negative value for ω^2 represents a growing convective mode. The parameter which determines the stability characteristics of the system here is the plasma β. With a model background atmospheric structure for the convection zone and the photosphere, Spruit and Zweibel(1979) solved the system (2.27) and (2.28): they found the critical value for stability β_c to be 1.83. This corresponds to a value of 1350 G for the field strength at $\tau = 1$ inside the tube. Thus tubes with fields stronger than this are stable to convective motions and exhibit stable oscillations. Tubes of smaller strength than this limit are convectively unstable and collapse to form tubes with strengths larger than 1350 G. For the solar model used here, which is slightly different from the one used by Spruit and Zweibel (1979), we obtain a value of $\beta_c = 1.64$ for convective stability (assuming rigid boundary conditions). The atmospheric model covers the regions from the temperature minimum in the chromosphere, which is at $z_{top} = -500$ km, to a convection zone depth of $z_b = 5000$ km. The value of $\beta_c = 1.64$ corresponds to a strength 1430 G at $\tau = 1$ inside the tube. Now we extend the lower boundary to a depth of 10,000 km and with the same closed conditions we find the critical β to be 1.48, marginally different from the earlier case. This demonstrates that the deeper layers make a small contribution to the unstable

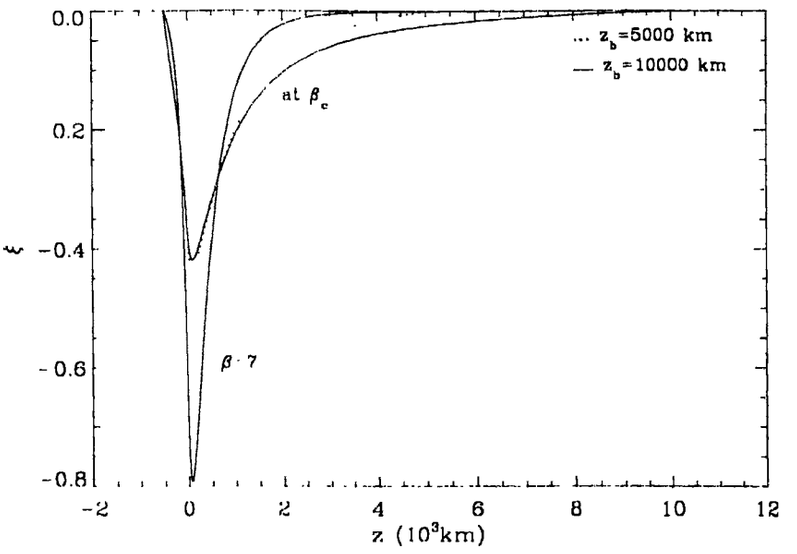

Figure 4.3: Comparison of the displacement eigen-functions ξ for the two different depths of the lower boundary which is closed. The dotted curve is for a depth of 5000 km while the full curve is for 10000 km. For $\beta = 7$, i.e. for a weak field(equipartition) tube the two cases are indistinguishable

motion which is mainly driven by the superadiabatic region confined to about 1000 km below the surface(z=0.). This is also evident from the shape of the displacement eigen-functions ξ shown in Fig. (4.3) where the dotted curves are for the case of a bottom boundary at a depth of 5000 km and the full curves for 10,000 km. We have shown the adiabatic displacement eigenfunctions (ξ) for two different values of the field strengths for the tubes: $\beta = 7$ (a weak equipartition strength tube) and $\beta = \beta_c$. For the former case of weak tube, the dotted and solid curves are indistinguishable. This shows that the sensitivity to the nature of the lower boundary mechanical condition is greater for a stronger tube. Since, before collapsing to form stronger tubes, all tubes are expected to be at a initial strength of roughly about the equipartition value (around $\beta = 7$), we can conclude that the influence of the nature of the lower boundary mechanical condition is inconsequential provided the location of the bottom boundary is far away from the driving regions.

The plot of the complex eigenvalues $\omega = \sigma + i\eta$, where η are the growth rates and σ are the frequencies of the modes, as a function of β is shown in Fig. (4.4). The values we refer to here, as also that of Spruit and Zweibel, are for the fundamental mode which is also the most unstable; all higher harmonics have smaller growth rates . It is easily noticed that the displacement eigen function peaks at about 120 km below the surface, which is the same location where the superadiabaticity peaks. Also shown in Fig. (4.4) are the growth rates and frequencies when a open flow-through condition,

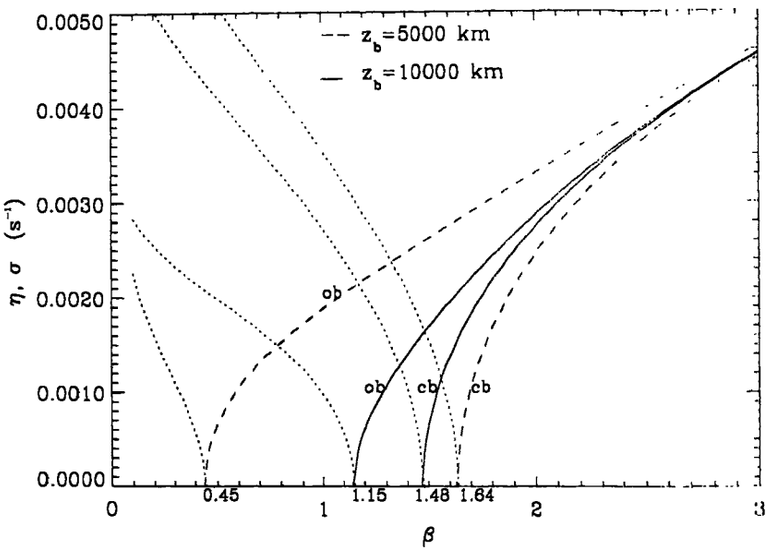

Figure 4.4: Comparison of the growth rates and frequencies (dotted lines) for the adiabatic case for different boundary conditions;'ob' and 'cb' refer to open and closed boundaries, respectively

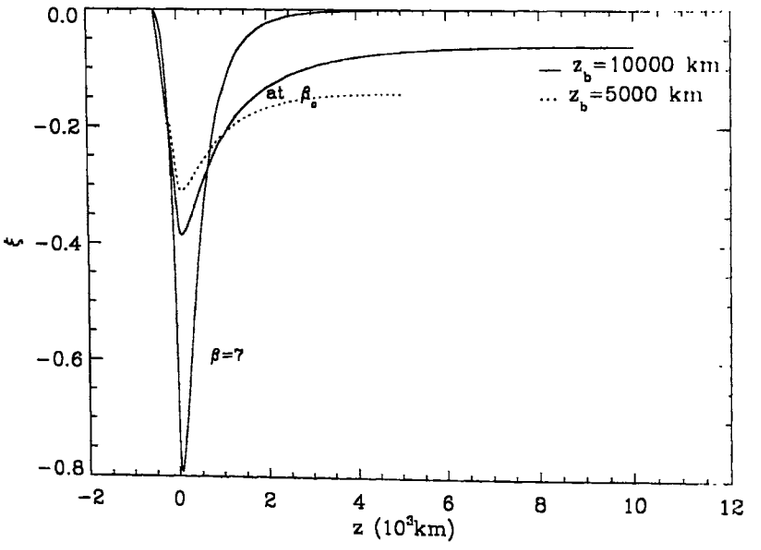

Figure 4.5: Comparison of the displacement eigenfunctions ξ for an open bottom boundary at two different depths as indicated in the figure

i.e. $d\xi/dz = 0$ is used at the lower boundary. We have marked the curves with *'ob'* for open boundary and with *'cb'* for closed boundary. We find that the difference in the values of critical β between the cases of closed and open lower boundaries is larger for the lower boundary location at 5000 km than that for the lower boundary at 10,000 km. Thus the stability limit is $\beta = 0.45$ for the lower open boundary at 5000 km, much different from the closed boundary limit of 1.64, whereas for the case of lower boundary at 10,000 km the stability limit is $\beta = 1.15$ for open boundary and 1.48 for closed boundary, the difference being smaller than that for the former case. The corresponding eigen-function comparison for open lower boundary is shown in Fig. (4.5). In general, we find that *the shallower the tube, i.e. the closer the lower boundary to the driving regions, the larger the difference between the cases of open and closed conditions.* This is easily understood, because the deeper layers are very close to adiabatic conditions and thus are stable. Thus the nature of the lower boundary conditions are inconsequential provided they are located deep enough and far away from the regions driving the instability.

4.5.2 Newton's law of cooling - (only lateral heat exchange)

Here we present the solution of the system of equations (2.39) and (2.40) that describe the flux tube behaviour when the only energy exchange is due to lateral heat exchange based on Newton's law of cooling. This system has been studied earlier (Hasan 1986). We reproduce such a study to facilitate a comparison with the results that are obtained for the full non-adiabatic system of equations that include the vertical radiative losses and presented in the following section. Also we study the influence of the boundary conditions on the overstable and convective behaviour: we especially clarify that the overstability is the physical consequence of the lateral exchange of radiation by the tube with the surroundings rather than as that due to reflection associated with a closed mechanical condition at the bottom boundary as claimed by (Takeuchi 1995). This is established by demonstrating the presence of overstability even when a open flow-through boundary condition is used at the bottom boundary.

In Fig. (4.6) a comparison of the growth rates and frequencies of the modes is presented for the cases of closed and open lower boundaries. Here, the growth-rates are plotted as a function of β for a tubes of surface radius $a_o = 100$ km. The bottom boundary is located at a depth of $z_b = 5000$ km. The dotted curves are for the case when the bottom boundary is open and the solid ones are for closed bottom boundary. As in the adiabatic case, the major effect to emerge is the destabilizing action of the open boundary on the convective motions as could be seen from the shift of the bifurcation, that mark the onset of the convective instability, towards smaller β. It is also seen that the overstability persists even for the open boundary though there is a small

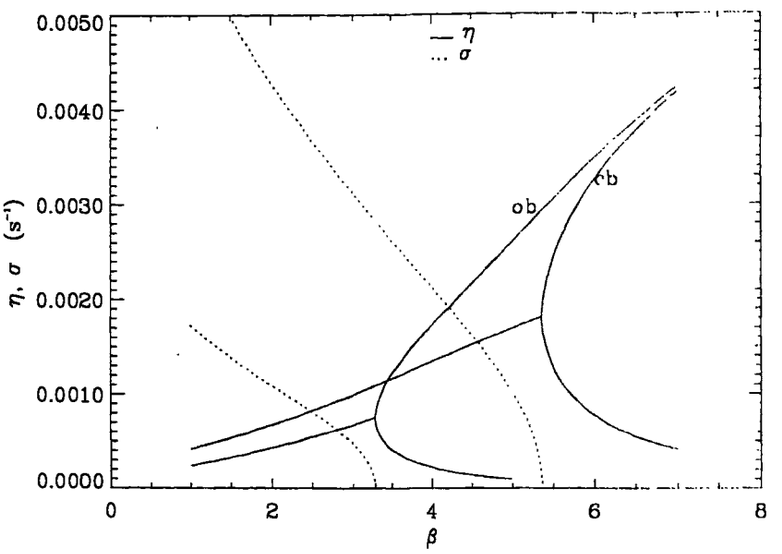

Figure 4.6: Comparison of the growth rates (solid curves) and frequencies (dotted curves) of the modes for closed (cb) and open (ob) bottom boundaries.

reduction in the growth rates from those that are obtained for the closed boundary case. This behaviour is in contradiction with the damped wave-motions reported by Takeuchi (1995) (i.e. negative growth rates) for the case of open bottom boundary, leading him to the conclusion that the overstability is an artifact of the reflection associated with a closed boundary. Our finding here of the overstability (i.e. positive growth rates) even when a open flow-through condition is used demonstrates that the boundary effects are *not* the cause of the overstability and, combined with the fact that the adiabatic oscillations are stable, that it is the lateral exchange of radiation of the vertically oscillating fluid elements of the tube that causes the amplification of the oscillations. The physical explanation of this overstability mechanism (Cowling 1957, Moore and Spiegel 1966) relies on the interactions of three different processes: a destabilizing force which drives the system away from equilibrium, a restoring force which brings it back to equilibrium and a dissipative process such as radiative exchange which acts against the destabilizing force thereby reducing the driving. Here, the driving force is the bouyancy associated with the superadiabatic temperature gradient, the restoring force is the magnetic pressure plus the gas pressure and the dissipative process is the horizontal radiative exchange between the flux tube and the surroundings. When the magnetic field is strong enough to restore the bouyantly moving gas element, it oscillates in the adiabatic limit as we showed in the last section. The radiative exchange, which is controlled by the flux tube size, reduces the driving due to bouyancy in such a way that the net restoring force is greater during

the return toward equilibrium than it was during the departure from equilibrium: a downward moving element is cooler and receives heat from the surroundings resulting in its temperature rise and a consequent reduction in its density, on account of the pressure equilibrium which is, by assumption, attained instantaneously; hence on its return to its equilibrium, the element will have a smaller density excess than what it had when it last left the equilibrium. Therefore the downward bouyancy force on its downward passage is greater than on its upward passage. A similar difference in bouyancy force will occur during the upward swing. This results in the gas element returning to its equilibrium position faster than when it left on each swing downward and this same effect, but with opposite signs, operates on the upward swings. The amplitude of the oscillations builds up exponentially, in this manner. Here, since the heat exchange time τ_r is larger for a bigger size tube, one would expect the overstability growth rate to decrease as the tube size increases. But, the results shown in Fig. (4.6) and Fig. (4.7) (the dotted curves) reveal the following feature: the growth rates increase slowly as the size increases (the overstability growth rates, in these figures, are those parts of the curves which are to the left of the cusps which represent the transition to the convective mode). This is due to the fact that the oscillation period of the mode increases at a higher rate than the growth rates, as a function of size. This more than compensates the increase in the heating time because the fluid element is spending now more time in its passage out of equilibrium.

4.5.3 Solution of the full non-adiabatic system of equations

The full non-adiabatic system of equations (2.16), (2.17), (2.18) and (2.19) includes the vertical radiative losses also. Thus, the major difference from the set of equations that we solved for the polytropic case in the last chapter is the appearance of the radiative loss term $dlnF_z/dz$ in the perturbed energy equation (2.19). This term arises due to radiative non-equilibrium which is a realistic representation of the solar sub-photospheric regions where there is a strong gradient in the radiative energy flux. The results presented in this section show a strong influence of the radiative losses. With regard to the situation of Section 4.4, the main contribution for the non-adiabaticty from the lateral influx of radiation is now coupled to the vertical radiative transport. Due to finite radiative relaxation time in the vertical direction, heating or cooling associated with the lateral heat exchange is now coupled to the vertical transport. This is reflected in the appearance of the ratio $\epsilon = \tau_r/\tau_{th}$ in equation (2.19). Physically this accounts for the fact that the vertical outward flux of radiation in a typical time-scale of τ_{th} reduces the heating experienced, in a time scale τ_r, by the displaced fluid element.

As explained in the last section, the important effects of radiation, namely the flux tube size-

dependent stabilizing influence of the radiation on the convective instability and also the rendering of the oscillations of the convectively stable tube overstable, are brought out in a simple way when just the lateral exchange is allowed. The last section also gave a discussion of the comparison between open and closed bottom boundaries on such radiative effects and it was demonstrated that overstability is only marginally reduced for open flow-through condition at the bottom. The major difference was the destabilizing influence of the open boundary on the convective instability. But drawing on the results that were obtained for the adiabatic case, it is clear that such differences between the closed and bottom boundaries for the convective instability would become negligible, even in the presence of non-adiabaticity due to radiation, for a sufficiently deep location of the bottom boundary. Also the adiabatic stability limits for the closed boundaries at 5000 km and at 10,000 km are not very different, being respectively at $\beta = 1.64$ and 1.48. Hence, and also for computational reasons, we integrate the fourth-order system of non-adiabatic equations only upto a depth of 5000 km with a closed mechanical boundary. The results are presented in Fig. (4.7). The dotted curves are for the case of lateral exchange alone under the Newton's law of cooling and the full curves present the results when the full non-adiabaticity due to vertical losses are taken into account. These plots show the growth rates as a function of the surface radius a_0 for various values of the plasma β.

Convective Instability

The heating by radiation from the surroundings reduces the degree of adiabaticity of the down-flowing gas resulting in its deceleration and this effect is, as one would naturally expect, dependent on the horizontal optical thickness of the tube. The radius as well as the initial field strength of the tube determine the horizontal optical thickness of the tube: a stronger tube has less dense gas inside because, in the present assumption of temperature equilibrium, the reduction in the gas pressure inside required for pressure equilibrium with the surroundings is achieved mainly through a reduction in the density. Due to the reduction in the gas pressure and density inside the tube, stronger fields lower the opacity κ of the gas inside the tube. The variation of the tube's optical thickness $\kappa\rho a$, at about a depth of 100 km (from the surface $z = 0$) where roughly the superadiabaticity peaks, as a function of β is shown in Fig. (4.8). Thus there are two aspects to the stabilizing action of the radiation against the bouyancy forces that drive the convective instability: (i) for a given initial field strength (i.e. for a curve in Fig. [4.7] for a fixed β) the lateral radiative heating which acts against the convective force is more for tubes with smaller radii and hence the growth rate of the convective instability decreases as the radius decreases until a critical value for the tube radius where the convective mode is tranformed into an oscillatory overstable mode. This

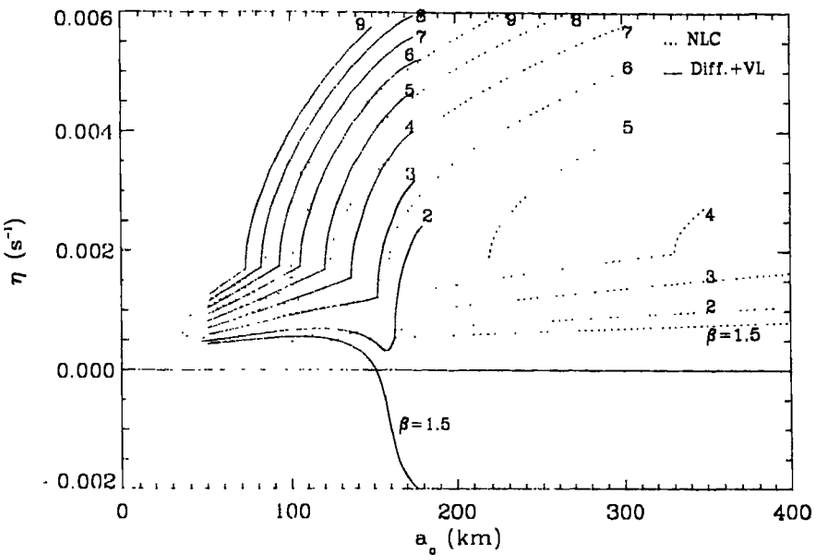

Figure 4.7: Growth-rates of the convective and overstable modes as a function of surafce radius a_o for various values of β; the dotted curves are for the case of lateral exchange alone in the Newton's law of cooling while the full ones are obtained when full non-adiabaticity due to vertical losses is also taken into account.

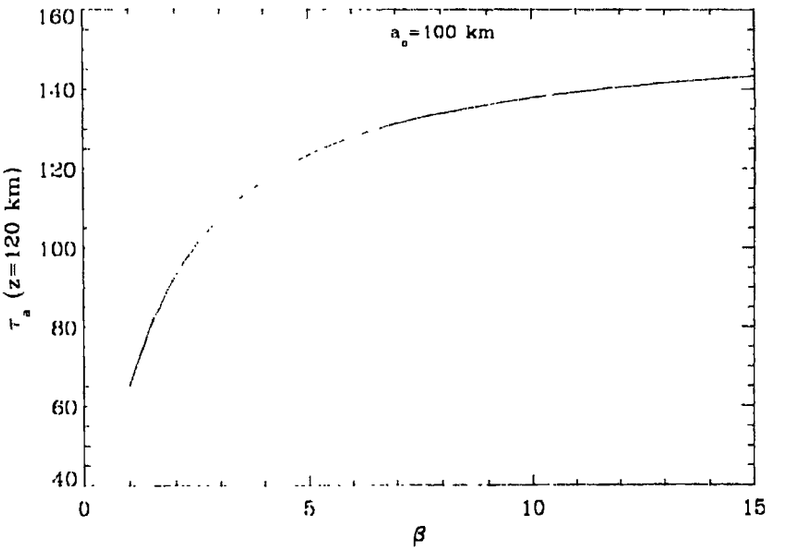

Figure 4.8: The variation of the horizontal optical thickness $\kappa\rho a$ at a depth of 100 km for a tube of surface radius 100 km as a function of β

transition in the tube's behaviour corresponds to the cusps in the curves of Fig. (4.7). (*ii*) secondly, for a given tube radius the lateral radiative exchange time is smaller for stronger tubes leading to an increased stabilizing action of the radiation. This requires that the critical radii, $a_{0,c}$, for the onset of the convective instability increase as the field strength increases, as could be seen in the Fig. (4.7).

The above two aspects are related to the horizontal radiative exchange which counteracts the convective instability. The differences brought out in the present study, as shown in Fig. (4.7), are mainly due to the vertical exchange and the radiative losses. As is evident in the figure, the vertical losses tend to enhance the convective instability: the cooling of the gas associated with the vertical radiative losses accelerate the downflow perturbation and hence the tube is more unstable than the situation where the only radiative interaction is the heating due to the lateral influx of radiation. Indeed it is the cooling associated with the radiative losses that trigger the downflow, as first discussed by Parker (1978). As such, in the absence of vertical radiative losses, the convective perturbations are bi-directional: an upflow perturbation is equally unstable as a downflow and thus an initial tube configuration is equally liable for a dispersal or a collapse. But in the presence of a net radiative loss in the vertical direction, a fluid element is always cooled irrespective of whether it moves downward or upward. This means that the motion in a direction opposite to the direction of radiative losses, i.e. the downward motion is more unstable than the upward. As a result downflow perturbations are amplified faster. From Fig. (4.7), it is seen that the convective instability growth rates are larger for the case where the vertical radiative transport is included (solid curves) than when only horizontal exchange is included (dotted curves). Thus it can be concluded that in the presence of vertical radiative losses a weak field tube preferably undergoes a collapse resulting in its field intensification rather than an upward convective perturbation which tends to further weaken and disperse the tube. We note here, however, that the radiative losses calculated here using the diffusion approximation are overestimated in the upper photospheric and higher layers which are optically thin and thus the instability rate is overestimated. We check this overestimate in the next Chapter when we refine our our analysis by using the generalised Eddington approximation.

Size(flux)-Strength Relation

The way the critical radii ($a_{0,c}$), equivalently the critical fluxes $\Phi = \pi B_c a_{0,c}^2$, vary as a function of the strength is shown in Fig. (4.9). Such a size-strength relation, first produced by Venkatakrishnan(1986) for the solar case (also contained in the results of Hasan[1986] for a real model atmosphere similarly to the results obtained here) based on a simplified treatment employing isothermal

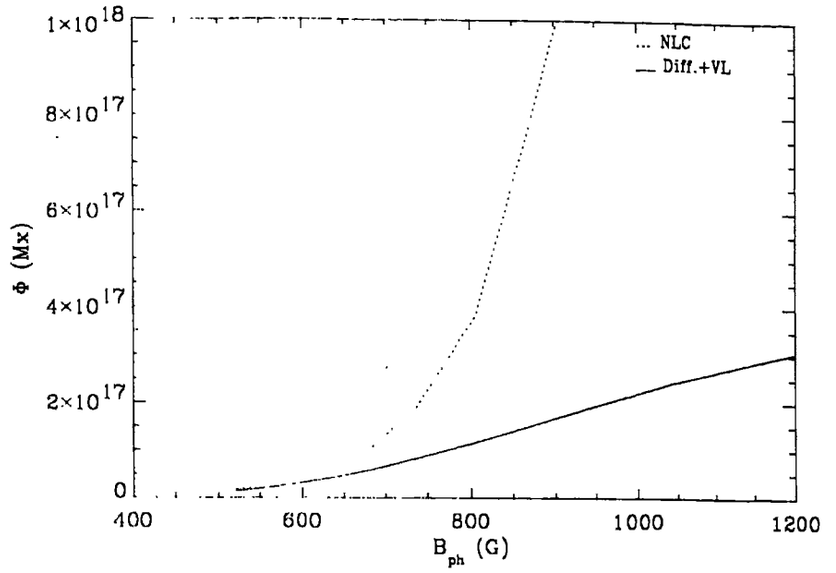

Figure 4.9: The magnetic flux-strength relation for the convectively stable tubes. The dotted curve is obtained for the case of lateral exchange under Newton's law of cooling while the solid curve is for the full non-adiabatic case including the vertical losses.

stratifications, reveals that weaker tubes, with strength less than about 900 G, show very weak dependence on the size(flux) while stronger tubes have sharply increasing sizes(fluxes). We have obtained this size-strength dependence from the field strength dependent critical radii for the onset of the convective instability (i.e. from the positions of the cusps in the growth rate curves of Fig. (4.7)) and thus the tubes which satisfy the derived relation represent a stable (convectively) limit: tubes of strengths and sizes which fall to the right of the flux(size)-strength relation curve of Fig. (4.9) are stable.

Realistically, the initial strengths for the tubes are set by the equipartition limit given by $B_{eq} \approx v_e(4\pi\rho)^{1/2}$, which is roughly about 500 G($\beta \approx 9$) at the solar photosphere. All higher strengths for the tubes are assumed to result after the equipartition strength initial tubes undergo the convective collapse. From the growth rate curve for $\beta = 9$ in Fig. (4.7) it is seen that the minimum size for the tube to undergo convective collapse is a radius of 84 km at the photospheric surface. A better understanding and a size-strength relation for the tubes could be derived by comparing the size-dependent growth time with the size-dependent lateral radiative exchange time scale τ_r at a depth of about 120 km where the convective diplacement (and hence the convective downflow) eigenfunction peaks. Such a comparison shows that, for $\beta = 9$, the growth time is equal to the radiative exchange time at a value of about 88 km for the tube radius and decreases as the tube size increases. It

is plausible that tubes of initial sizes greater than this value collapse fast enough to the adiabatic stable limit of $\beta \approx 1.64$ without much hindrance due to the radiation and all smaller size tubes are subject to the efficient radiative heating and would stop at those strengths and sizes which correspond to the convective onset points shown in Fig. (4.7).

Overstability

Overstable oscillations are characterized by the appearance of the complex conjugate pairs of eigenvalues for Ω. In Fig. (4.7), the growth rates for the overstable modes are to the left of the cusps in the curves. The mechanism by which the overstability is achieved has already been explained in Section (4.5.2). Here we concentrate on the effects imparted by the vertical radiative transport. The horizontal heating or cooling of the downward or upward moving gas element is now subject to a net radiative loss in the vertical direction. This introduces an asymmetry between the downward and upward swings of the oscillating fluid element: the upward return passage of a initial downward swing of the is now not as fast as that it obtains in the absence of vertical losses. In other words, a part of the energy gained by the fluid element from the radiation due to horizontal exchange is now lost out and hence the amount of amplification of the oscillation is reduced. This is nothing but the well known process of radiative damping. From the results shown in Fig. (4.7), we see that such radiative damping associated with the vertical losses are more for a stronger tube. Since a stronger tube is more evacuated than a weaker one, its vertical loss time scale is now much shorter resulting in the increased influence of the above discussed damping effect on the oscillations. This effect is further enhanced as the tube size increases which reduces the horizontal heating effects. Thus, taking the example of $\beta = 1.5$ in Fig. (4.7), it is seen that the radiative damping wins over the amplifying mechanism of overstability at about a value of $a_o = 100$ km, and then the growth rates start decreasing. At a critical value of a_o they cross zero and thus the oscillations get damped. Thus tubes which are strong enough with sizes larger than a certain critical value are subject to the severe radiative damping associated with the vertical radiative losses and thus are stable.

4.6 Conclusions

The results and discussions of the previous section lead to the following conclusions:

- The overstability of the wave-motions of a convectively stable tube is mainly a consequence of the horizontal radiative exchange of the tube with the surroundings. A closed mechanical boundary condition at the bottom is not the cause of the overstability though overstable

growth rates are slightly reduced for a open boundary.

- The influence of the open bottom boundary is negligible on the convective instability of the tube provided the location of the bottom boundary is deep enough and far away from the driving regions.

- The vertical radiative losses increase the acceleration of downflowing gas and thereby enhance the convective instability. Thus vertical losses compensate the stabilizing influence of the radaitive heating from the surroundings. This leads to a size(flux)-strength relation for convectively stable tubes which leads to higher field strengths at a relatively lower flux than those obtained when there are no vertical radiative losses.

- The vertical radiative losses, for oscillatory motions, reduce the growth rates of the overstable modes thereby leading to a severe damping of the slow mode in strong and thick magnetic flux tubes, such as those in the network of the Sun.

Chapter 5

Convective Instability and Wave motions in a slender tube- Radiative Transfer in the Generalised Eddington Approximation

5.1 Introduction

The structure of intense magnetic flux tubes is greatly influenced by radiative energy exchange at the photospheric level and above owing to their comparable or smaller spatial scales than the photon mean free path and hence a sophisticated treatment of the radiation field is necessary to correctly account for the intrinsically non-local nature of the radiation field and thus determine the basic atmospheric structure inside such tubes. Radiative energy exchange is also believed to decisively influence the nature of waves which play a crucial role in the energy budget of the overlying non-radiatively heated chromospheric and coronal regions. In the previous Chapters we have examined the effects of radiation on the convective instability and the wave motions in the tubes, treating the radiation in the diffusion approximation. This approximation is justifiable only for optically thick regions and thus is valid for the regions below the photospheric level. The superadiabaticity, which is the source of unstable motions that are the focus of this study, peaks just below the photospheric layers at a depth of around 75 km and is thus at the transition from the optically thin upper photospheric layers to the optically thick lower convection zone. These intermediate optical depth regions require a more accurate treatment of radiation than the one provided by the diffusion approximation, and this requirement is even more necessary for dynamically active magnetic fields which tend to increase the transparency of the gas confined by them, on account of their pressure effects. Another shortcoming of using the diffusion approximation is that it overestimates the

radiative losses in the optically thin higher layers. This can be remedied by using the generalized Eddington approximation for the radiation field, first introduced by Unno and Spiegel (1966). This more general approach has been shown by the above authors to yield both optically thick and thin limits correctly and also to give accurate results in the intermediate range. We, thus, extend our earlier treatments by adopting the generalised Eddington approximation to study the stability and wave motions of a flux tube atmosphere under the influence of radiative energy exchange.

The driving of overstable oscillations in a magnetic flux tube due to the horizontal radiative transfer (Roberts 1976, Spruit 1979, Hasan 1985, 1986; Venkatakrishnan 1985; Massaglia et al. 1989) needs to be ascertained when vertical radiative losses are self- consistently taken into account. In the last chapter, we established the importance of the vertical radiative losses, both for the convective and oscillatory modes. The diffusion approximation overestimates the vertical losses in the optically thin layers which we quantify through a comparison of the results obtained in Chapter 4 with those obtained using the general Eddington approximation. Moreover we show, using this approximation, that the departure from the Planck function, for the mean intensity, has a strong stabilizing influence.

5.2 Mathematical formulation

5.2.1 Radiative transfer in a thin tube

We utilize the three dimensional generalization of the Eddington approximation(Unno and Spiegel 1967, Hasan 1988) to derive a transfer equation appropriate for a thin magnetic flux tube; the radiative flux in this approximation is written as,

$$\mathbf{F}_R = -\frac{4\pi}{3\kappa\rho}\nabla J \tag{5.1}$$

where J is the mean intensity and κ is the Rosseland mean opacity; as suggested by Unno and Spiegel we use the above expression in the following exact relation to derive the needed equation which provides the closure for the system of equations that we deal with:

$$\nabla.\mathbf{F}_R = 4\pi\kappa\rho(S - J) \tag{5.2}$$

where S is the source function which we equate to the Planck function. Hence $S = \sigma T^4/\pi$ where σ is the Stefan-Boltzmann constant. In the present case of our slender tube the zeroth-order reduction of the above two equations yields (Hasan 1988)

$$\frac{1}{3}\frac{\partial^2 J}{\partial \tau^2} + \frac{4}{3}\left(\frac{J_e - J}{\tau_a^2}\right) = J - S \tag{5.3}$$

where $d\tau = \kappa\rho dz$, $\tau_a = \kappa\rho a$, and J_e is the mean intensity in the external medium. Assuming the external atmosphere to be plane-parallel with hydrostatic and energy equilibrium and disregarding the boundary layer which separates the interior of the tube from the exterior we have for J_e, in the Eddington approximation, the equation

$$\frac{1}{3}\frac{\partial^2 J_e}{\partial \tau_e^2} = J_e - S_e \tag{5.4}$$

The calculation of the radiation field fluctuations and their coupling to the hydrodynamic perturbations are done conveniently when we write the above forms of second order equations for the mean intensity as two first order equations in terms of the moments of the radiation field that were introduced in Chapter 1; thus we have the transfer equation (5.3) for the tube taking the following forms,

$$\frac{dJ}{d\tau} = -3\mathcal{H} \tag{5.5}$$

$$\frac{d\mathcal{H}}{d\tau} - \frac{4}{3}\left(\frac{J_e - J}{\tau_a^2}\right) = S - J \tag{5.6}$$

while that for the external medium, equation (5.4), is written as,

$$\frac{dJ_e}{d\tau_e} = -3\mathcal{H}_e \tag{5.7}$$

$$\frac{d\mathcal{H}_e}{d\tau_e} = S_e - J_e \tag{5.8}$$

Here $\mathcal{H}$ is the Eddington flux and is related to the radiative flux F_R by

$$\mathbf{F}_R = 4\pi\mathcal{H} \tag{5.9}$$

5.2.2 Equilibrium solution

The background atmosphere that we use here is the same as the one used in the previous Chapter and its construction has already been explained. The mean radiation intensity as a function of depth for this model, in our present treatment using the Eddington approximation, can be determined by solving equation (5.4). This we do numerically, using finite differences with the following upper and lower boundary conditions

$$\frac{1}{\sqrt{3}}\frac{\partial J_e}{\partial \tau_e} = J_e \tag{5.10}$$

and

$$\frac{1}{\sqrt{3}}\frac{\partial J_e}{\partial \tau_e} = -J_e + I_e^+ \tag{5.11}$$

respectively, where I_e^+ is the radiation intensity in the upward direction which, in the diffusion approximation, is

$$I_e^+ = S_e + \frac{1}{\sqrt{3}}\frac{1}{\kappa_e \rho_e}\frac{\partial S_e}{\partial z} \tag{5.12}$$

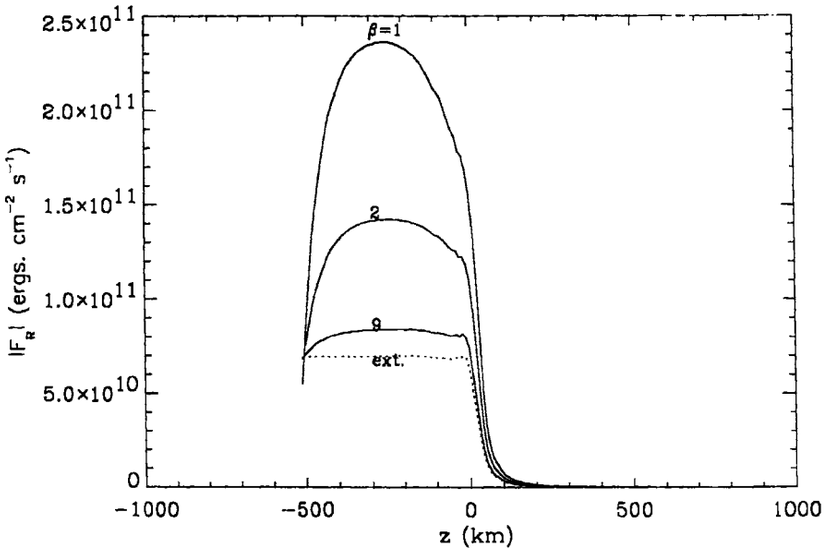

Figure 5.1: The magnitude of the radiative flux F_R in the Eddington approximation for three different values of β. The dotted curve is for the external mean atmosphere

We again assume temperature equilibrium, $T = T_e$, which implies that β, defined as $\beta = 8\pi p/B^2$, is constant with z (if the dependence of μ is neglected). The pressure and density are thus determined from

$$p = \frac{\beta}{1+\beta} p_e \tag{5.13}$$

$$\rho = \frac{\beta}{1+\beta} \rho_e \tag{5.14}$$

Once the mean intensity J_e for the external medium is found it is used in equation (5.3) which is solved to find the mean intensity J inside the tube with the same set of boundary conditions as that for the external medium. The region of integration of the equilibrium equations cover the atmosphere from the temperature minimum in the chromosphere to a depth of 5000km in the convection zone with the photospheric surface ($\tau = 1$) chosen at $z = 0$. We measure z as positive downwards. The radiative flux as given by equation (5.1) with the mean intensity calculated as explained above is shown in Fig. (5.1) for three different values of β along with that for the external background solar model used for a_o =100 km. The stronger the field in the tube the greater is the vertical radiative flux, owing to the enhanced lateral influx of radiation. The departure from radiative equilibrium, i.e. the non-zero divergence of the radiative flux, is a measure of non-radiative energy transport such as through convection below the photosphere. Fig. (5.2) shows the variation of $\nabla.\mathbf{F_R}$ calculated in the Eddington approximation. For the sake of comparison Fig. (5.3) shows

$\nabla.\mathbf{F_R}$ calculated in the diffusion approximation. It is seen that the layers around optical depth unity ($z = 0$) are those which are in a state of radiative non-equilibrium and since the driving regions for the convective motions are at about the same locations it is expected that such a state would have important consequences for the convective instability of the tube. The radiative flux inside the tube calculated here is a crude representation of the real situation for which one should set up the atmospheric structure inside the tube consistently by solving the (magneto)hydrostatic equation along with the radiative transfer equations. Since our main concern here is not on the detailed equilibrium structure, we have assumed the temperature structure inside to be the same as that outside. This is not very different from the real situation, as it has been known from more sophisticated treatments of radiative transfer (Steiner 1990, Hasan and Kalkofen 1994, Hasan, Kalkofen and Steiner 1999) that the temperature difference at equal geometrical levels is small except close to the surface layers. The effect of such a temperature difference is likely to be negligible in our stability calculations. The main uncertainty in our calculations is the constancy of β over depth, an artifact of our assumption of temperature equilibrium, which yields field strengths which are possibly too strong in the deeper layers. An important difference between the present case with the Eddington approximation and the diffusion approximation is in the quantity ∇_c, which measures the departure of the mean intensity from the Planck function. This quantity is always small and finite only in the upper photospheric layers of optical depth near unity and is zero in the optically thick deeper layers. Yet, as we show later in this chapter, this quantity shows an appreciable stabilizing influence on the unstable modes of the tube. Such a stabilizing influence of the difference between J and S has been found also in the studies of the radiative transfer effects on the stability of the solar p-modes (Dalsgaard and Fransden 1983). We show a plot of ∇_c in Fig. (5.4). The stronger the magnetic field in the tube the larger is the departure from the Planck function for the mean intensity inside the tube as is evident from this figure. This behaviour is also related to the assumption $T = T_e$. Another quantity of interest here for the tube is ∇_t, which appears in the stability equations derived in the next section, which is the ratio of the difference in the mean intensities between the tube and the exterior to the Planck function. This quantity is also a small quantity which depends on the plasma β and the radius of the tube and is shown in Fig. (5.5) for representative values of β and a. We also show the run of the thermal time-scale τ_{th}, the lateral radiative cooling time τ_r and the radiative relaxation time τ_N that one obtains in the optically thin limit(Spiegel 1957). The depth dependence of various other equilibrium quantities which determine the stability pattern and the characteristics of the unstable motions are the same as those shown in the Chapter 4.

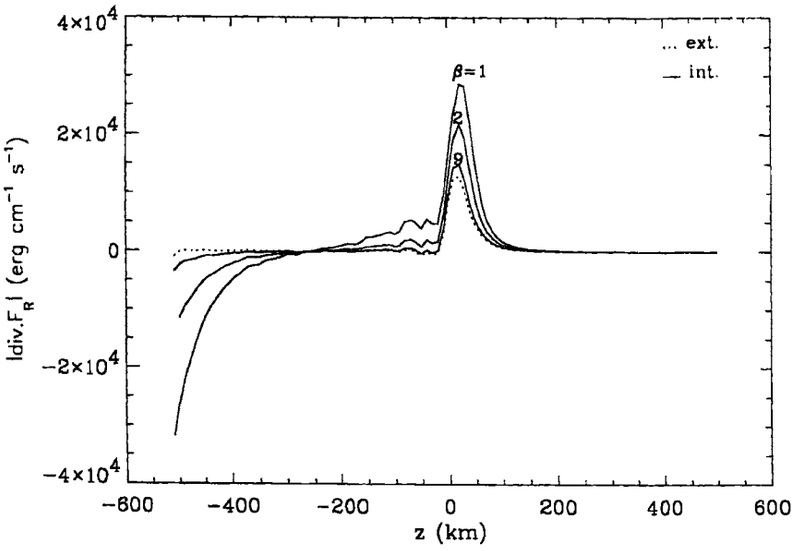

Figure 5.2: The magnitude of $\nabla.\mathbf{F_R}$, in the Eddington approximation, which is a measure of radiative non-equilibrium as a function of depth for different values of β

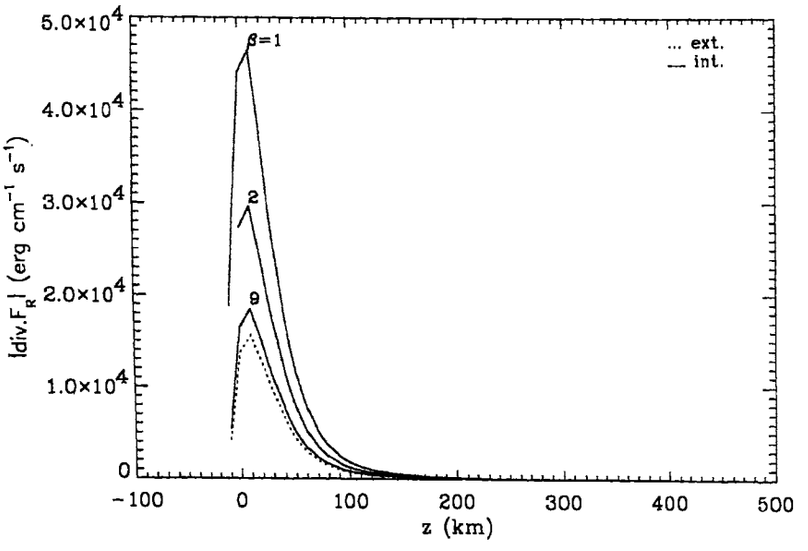

Figure 5.3: The magnitude of $\nabla.\mathbf{F_R}$ in the diffusion approximation

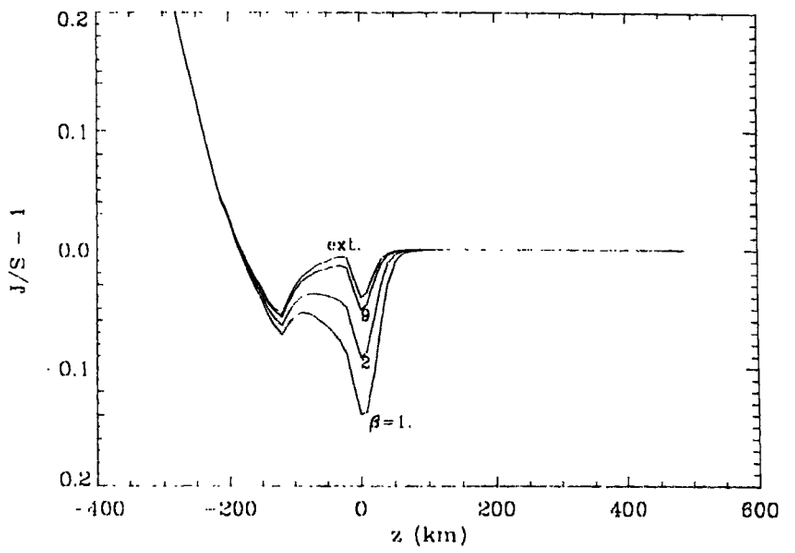

Figure 5.4: The depth dependence of $\nabla_r = J/S - 1$, which measures the departure of the mean intensity from the Planck function, for three representative values of β

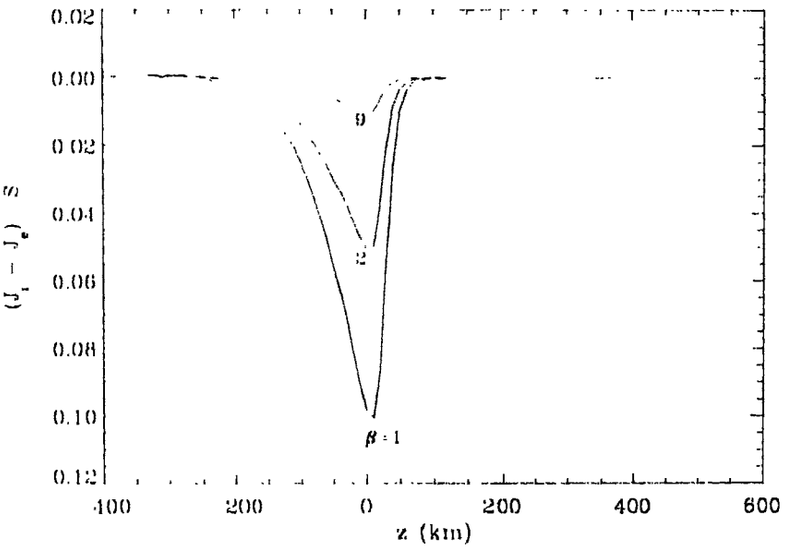

Figure 5.5: The fraction of the mean intensity difference between the tube and the external atmosphere to the Planck function, ∇_f, as a function of depth for different values of β

5.2.3 Linear Stability: Perturbation equations

Since the only difference between the present treatment and that in Chapter 4 relates to radiative transfer equations, the linearized equations (2.16), (2.17) other than the one derived from the energy equation are the same. The perturbed energy equation yields:

$$\frac{\partial}{\partial t}\left(\frac{p'}{p}\right) - \Gamma_1 \frac{\partial}{\partial t}\left(\frac{\rho'}{\rho}\right) + \left[\frac{d\ln p}{dz} - \Gamma_1 \frac{d\ln \rho}{dz}\right]\frac{\partial \xi}{\partial t} = -\frac{\chi_T}{\rho c_v T}\nabla.\mathbf{F}' \tag{5.15}$$

The perturbation in the radiative flux and its divergence have to be calculated by solving the perturbed radiative transfer equations. The perturbation of equation (5.2) can be done in a straightforward manner:

$$\nabla.\mathbf{F}'_{\mathbf{R}} = \frac{dF'_R}{dz} = 4\kappa_a \rho(S' - J') + \nabla.\mathbf{F}_{\mathbf{R}}\left(\frac{\kappa'}{\kappa} + \frac{\rho'}{\rho}\right) \tag{5.16}$$

The perturbations ρ'/ρ and κ'/κ can be expanded in terms of T'/T and p'/p as

$$\frac{\rho'}{\rho} = \frac{1}{\chi_\rho}\frac{p'}{p} - \frac{\chi_T}{\chi_\rho}\frac{T'}{T} \tag{5.17}$$

$$\frac{\kappa'}{\kappa} = \kappa_p \frac{p'}{p} + \kappa_T \frac{T'}{T} \tag{5.18}$$

where

$$\kappa_p = \left(\frac{\partial \ln \kappa}{\partial \ln p}\right)_T, \kappa_T = \left(\frac{\partial \ln \kappa}{\partial \ln T}\right)_p \tag{5.19}$$

χ_ρ and χ_T can be determined from the equation of state. Since the Planck function S is an explicit function of T, S' is immediately found as

$$S' = \frac{dS}{dT}T' = 4S\frac{T'}{T} \tag{5.20}$$

The equation (5.16) becomes

$$\nabla.\mathbf{F}'_{\mathbf{R}} = \nabla.\mathbf{F}_{\mathbf{R}}\left(\frac{1}{\chi_\rho} + \kappa_p\right)\frac{p'}{p} + \nabla.\mathbf{F}_{\mathbf{R}}\left(\kappa_T - \frac{\chi_T}{\chi_\rho}\right)\frac{T'}{T} - 4\kappa\rho J' \tag{5.21}$$

the substitution of which in the perturbed energy equation (5.15) yields the desired equation which relates the mean intensity perturbations to the thermodynamic perturbations. With $e^{-i\omega t}$ dependence for time, this equation becomes algebraic and is given by,

$$\left[i\omega(1-\gamma) + \omega_R \Delta_c \chi_T\left(\frac{1}{\chi_\rho} + \kappa_p\right)\right]\frac{p'}{p} + \{i\omega\gamma\chi_T -$$
$$\omega_R\chi_T\left[4 - \nabla_c\left(\kappa_T - \frac{\chi_T}{\chi_\rho}\right)\right]\}\frac{T'}{T} + i\omega\frac{\Gamma_1 N^2}{g}\xi + \frac{\omega_R\chi_T}{S}J' = 0 \tag{5.22}$$

where

$$\nabla_c = \frac{J}{S} - 1 \tag{5.23}$$

and N^2 is the Brunt-Väisälä frequency. The above equation is used to replace the temperature perturbations in the rest of the equations. The perturbation in the mean intensity J' is determined by perturbing and linearizing the transfer equation (5.3). Here we use the equivalent two first order moment equations (5.5) and (5.6) whose perturbations in terms of the dimensionless variables J'/J and $\mathcal{H}'/\mathcal{H}$ are:

$$\frac{d}{dz}\left(\frac{J'}{J}\right) = \frac{dlnJ}{dz}\frac{\Lambda'}{\Lambda} - \frac{dlnJ}{dz}\frac{J'}{J} + \frac{dlnJ}{dz}\frac{\mathcal{H}'}{\mathcal{H}} \tag{5.24}$$

$$\frac{d}{dz}\left(\frac{\mathcal{H}'}{\mathcal{H}}\right) = \left(\frac{\nabla_t}{2\epsilon H_p} - \frac{dln\mathcal{H}}{dz}\right)\frac{\Lambda'}{\Lambda} + \frac{\nabla_t}{2\epsilon H_p}\frac{a'}{a} - \frac{(1+\nabla_c)(4+3\tau_a^2)}{16\epsilon H_p}\frac{J'}{J} + \frac{1}{qH_p}\frac{T'}{T} - \frac{dln\mathcal{H}}{dz}\frac{\mathcal{H}'}{\mathcal{H}} \tag{5.25}$$

where $\Lambda = \kappa\rho$, a is the radius of the tube, H_p is the pressure scale-height at the bottom and the various other quantities are as defined below:

$$\nabla_t = \frac{J - J_e}{S} \tag{5.26}$$

is the ratio of the excess of the mean intensity inside the tube to the Planck function. ϵ and q are the ratios,

$$\epsilon = \frac{\tau_r}{\tau_{th}} \tag{5.27}$$

$$q = \frac{\tau_N}{\tau_{th}} \tag{5.28}$$

where

$$\tau_{th} = \frac{\rho c_p T H_p}{\mathcal{H}} \tag{5.29}$$

is the radiative relaxation time over one pressure scale-height at the bottom,

$$\tau_r = \frac{\rho c_p a^2}{K}, \qquad K = \frac{16\sigma T^3}{3\kappa\rho} \tag{5.30}$$

is the radiative relaxation time across the tube in the optically thick limit and

$$\tau_N = \frac{c_p T}{4\kappa S} \tag{5.31}$$

is the radiative relaxation time that one obtains in the optically thin limit with Newton's law of cooling (Spiegel,1957) and,

$$\tau_a = \kappa\rho a \tag{5.32}$$

is the depth dependent optical thickness of the tube. The perturbations in the radius a of the tube are found using the flux conservation condition Ba^2 =constant:

$$\frac{a'}{a} = -\frac{1}{2}\frac{B'}{B} = \frac{\beta}{4}\frac{p'}{p} \tag{5.33}$$

The perturbations in the quantity $\Lambda = \kappa\rho$ can be written in terms of the pressure and temperature perturbations as follows:

$$\frac{\Lambda'}{\Lambda} = \frac{\kappa'}{\kappa} + \frac{\rho'}{\rho} = \left(\kappa_p + \frac{1}{\chi_\rho}\right)\frac{p'}{p} + \left(\kappa_T - \frac{\chi_T}{\chi_\rho}\right)\frac{T'}{T} \tag{5.34}$$

The use of above two equations along with the equation (5.22) in the equations (2.16), (2.17), (5.24) and (5.25) yields the final set of four equations for the four variables ξ, p'/p, J'/J and $\mathcal{H}'/\mathcal{H}$. It is easy to check that the above set of equations get reduced to the correct forms for the optically thick and optically thin limits. The optically thick reduction of the set of equations corresponds to taking the limit τ tending to infinity and replacing the mean intensity by the Planck function. The optically thin case is got in the limit τ_{th} approaching zero. This proven validity of the generalised Eddington approximation(Unno and Spiegel 1967) for both the limits makes the analysis of the present problem realistic.

5.2.4 Boundary Conditions

The upper boundary is placed at 500 km above the photospheric surface ($\tau = 1$) in the ambient medium, which coincides with the temperature minimum, and the lower boundary is at a depth of 5000 km in the convection zone below the surface. We use closed mechanical conditions at both the boundaries. This is justified here because the boundaries are far away from the regions which drive the convective motions. The other boundary conditions for the present fourth order system are thermal: at the top boundary we require that there is no incoming radiation from above and at the bottom we assume that the perturbations are adiabatic. Thus in mathematical form the set of boundary conditions is:

Mechanical conditions:
Rigid or closed boundaries:

$$\xi = 0, \qquad at\ z = z_{top}\ \ and\ \ at\ \ z = z_b \tag{5.35}$$

Open boundaries:
The Lagrangian pressure perturbation is zero at z_{top}:

$$\frac{\delta p}{p} = \frac{p'}{p} + \xi = 0 \tag{5.36}$$

where ξ is the dimensionless displacement scaled by the pressure scale-height H_0 at the top. At the bottom boundary we have

$$\frac{d\xi}{dz} = 0 \tag{5.37}$$

Thermal conditions:

The condition that there is no incoming radiation from above at the top boundary is expressed as,

$$\mathcal{H} = \frac{J}{\sqrt{3}} \tag{5.38}$$

with the linearised form

$$\frac{\mathcal{H}'}{\mathcal{H}} - \frac{J'}{J} = 0 \tag{5.39}$$

At the bottom boundary, since the matter is optically thick, we assume that the perturbations are adiabatic and we simply require that the flux perturbations are zero which amounts to the case of mean intensity perturbations being exactly equal to the perturbations in the Planck function:

$$\frac{\mathcal{H}'}{\mathcal{H}} = \frac{B'}{B} - \frac{J'}{J} = 0 \tag{5.40}$$

5.3 Results and discussion

We found in our earlier treatment which used the diffusion approximation that the radiative transfer tends to inhibit the convective instability of the tube which is the same behaviour as seen in studies of convective instability in a nonmagnetised atmosphere(Spiegel 1964,1968): radiative smoothing of the fluctuations associated with the bouyant motion of the gas blobs. It was found that while the lateral exchange of radiation from the surroundings always acted to smooth out the convective perturbations, the vertical radiative exchanges and losses help to accelerate the convective downflows. This was demonstrated by our numerical experiments where we compared the results when there is only lateral heat exchange with the case where vertical exchange was also included self-consistently. On the other hand, for convectively stable tubes i.e., for tubes of strong enough field strength or for those small enough tubes which are prevented from collapsing by the lateral influx of radiation, the slow magneto-acoustic oscillatory mode of the tube experiences two competing and opposing influences from the vertical losses and the lateral exchange of radiation; while the lateral exchange drives the oscillations overstable the vertical losses tend to stabilize the oscillations: this is the familiar *radiative damping* of the wave motions studied extensively in the literature. The use of diffusion approximation for the radiative transfer is justified only when the gas is optically thick. The vertical extent of the flux tube in our case also includes the optically thin regions upto the temperature minimum, the intermediate optical depth regions of

the photosphere and the sub-photosphere and down to the optically thick convection zone depth of about 5000 km. In such a situation the use of the generalised Eddington approximation is more appropriate for a realistic comparison of the calculations with the observations. Moreover, in the regions of intermediate optical depth the use of diffusion approximation underestimates the amount of radiative flux and consequently the radiative smoothing effects on the convective instability are also underestimated, whereas for the optically thin regions the radiative flux is overestimated. This discrepancy for the optically thin regions does not have appreciable influence on the results as the the superadiabtic region which drives the instability is located in the intermediate optical depth sub-photosphere.

Fig. (5.6) depicts the growth rates of the fundamental mode as a function of the tube radius a_0 at the surface $z = 0$, for various values of the β; superposed on the solid curves, which represent the results of the present chapter, are the results for the diffusion approximation (dotted curves) case of last chapter. The corresponding frequencies of the mode as a function of radius is shown in Fig. (5.7). The qualitative behaviour of the mode remains the same as the one we found in the diffusion approximation. However, the locations, in the parameter space, where the overstable mode gets transformed into the convective modes, the growth rates and the frequencies that we obtain here are different.

5.3.1 Convective Instability

Let us first focus on the pattern of the convective instability of the tube as a function of the tube radius and plasma β (field strength). As explained in the earlier chapters the onset of convective instability corresponds to a bifurcation in η-a_0 space where the frequency of the overstable mode becomes zero and the growth rate curve bifurcates into two curves which correspond to two convective modes. Here, as shown in Fig. (5.6), for a given value of β the parameter varied is the radius of the tube. Comparing the curves in Fig. (5.6), in Fig. (5.6), it is seen that the diffusion approximation overestimates the degree of instability: the growth rates obtained with the present more accurate treatment of radiation are appreciably smaller. Moreover, for a given value of β, i.e. for a tube of given field strength the onset of convective instability requires the size of the tube to be greater in the present case than that required when the diffusion approximation is used. This is exemplified by a shift in the positions of the bifurcations towards larger radii as compared to those in the diffusion approximation. These shifts or in other words the differences between the two approximations are larger for lower values of β, i.e. for stronger tubes. This is easily explained because stronger tubes are more transparent than the weaker ones: the density and pressure differences between the tube and the ambient medium are larger for stronger tubes resulting in the reduction of the optical

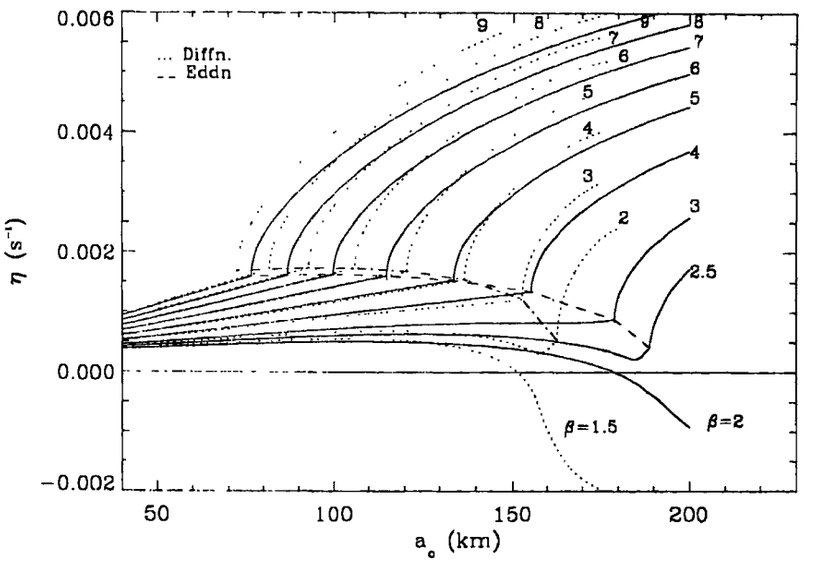

Figure 5.6: Growth rates of the fundamental mode as a function of the tube radius a_0 at the surface $z = 0$ for various values of the plasma β. Solid curves are for the Eddington approximation and dotted curves are for the diffusion approximation. Dashed line connects the convective mode onset points for the Eddington approximation while the dot-dashed line connects the onset points for the diffusion approximation

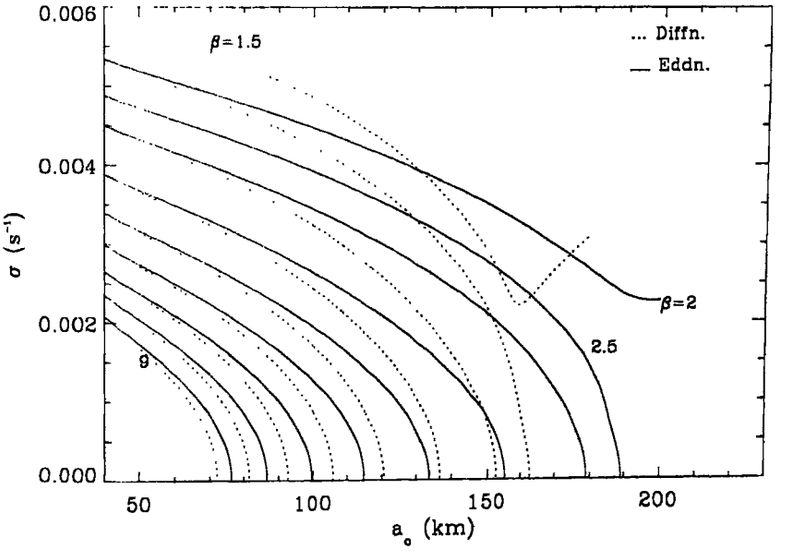

Figure 5.7: The frequencies of the fundamental mode as a function of the tube radius a_0 at the surface $z = 0$ for various values of the plasma β.

thickness of the gas inside. This makes the deviation from the diffusion approximation larger. As noted earlier, one of the quantities which measures the deviation from the diffusion approximation is ∇_c which is the ratio of difference between the mean intensity and the Planck function to the Planck function. The variation of this quantity over depth for different values of β is shown in Fig. (5.2). This quantity is larger for smaller values of β, i.e. for stronger tubes. The appearance of ∇_c in the equations is purely an effect of including the vertical radiative losses in the Eddington approximation and it is *zero* if $\nabla.F_R$ is zero, which means that, in the Eddington approximation, the gas is in radiative equilibrium if the mean intensity is equal to the Planck function. Thus ∇_c is also a measure of radiative non-equilibrium. In contrast, in the diffusion approximation, $\nabla.F_R$ is completely determined by the temperature field and the radiative conductivity; thus the use of the diffusion formula to calculate the radiative flux in the photospheric and higher layers yields, mainly due to the very high radiative conductivity of these optically thin layers, values for F_R and $\nabla.F_R$ which are too high and thus radiative non-equilibrium is overestimated. As is evident from the results presented in Fig. (5.6), the physical effect of the above mentioned differences between the cases of diffusion approximation and the Eddington approximation is that the convective instability is more vigorous in the former owing to the higher amount of radiative losses that it yields. It is also seen that the growth rates of the overstable mode also are overestimated in the diffusion approximation. More discussion of this behaviour is presented in the *section* on overstability.

To enable a better comparison of the above explained differences between the different approximations the growth rates of the convective and overstable modes are plotted for tubes of different strength in Figs. (5.8), (5.9) and (5.10) for β values of 2, 4 and 9 respectively. For stronger tubes the differences are larger. For the case of $\beta = 2$ [Fig. (5.8)] the tube is stable against convective instability and also against overstability for sizes greater than a certain critical value in the Eddington approximation, whereas in the diffusion approximation the tube exhibits convective instability and in the case of lateral exchange under Newton's law of cooling the tube is always overstable. For a weak field tube, e.g. for $\beta = 9$ [Fig. (5.10)], the differences are small.

The convective instability is completely suppressed for tubes with β smaller than 2.45 irrespective of its radius. This corresponds to a field strength of about 1160 G at $\tau = 1$ inside the tube. This has to be compared with the value of 1310 G ($\beta = 1.9$) that we obtained in the diffusion approximation and the value of 1430 G ($\beta = 1.6$) for the adiabatic case. The above numbers clearly demonstrate the stabilizing aspects of the radiation on the convective instability of the tube. We should point out that the field strength of 1160G that we obtain here does not necessarily imply that the collapse of tubes with weaker fields will attain this unique value and become stable. This value represents a necessary strength for stability against convective collapse and thus can be considered as a minimum

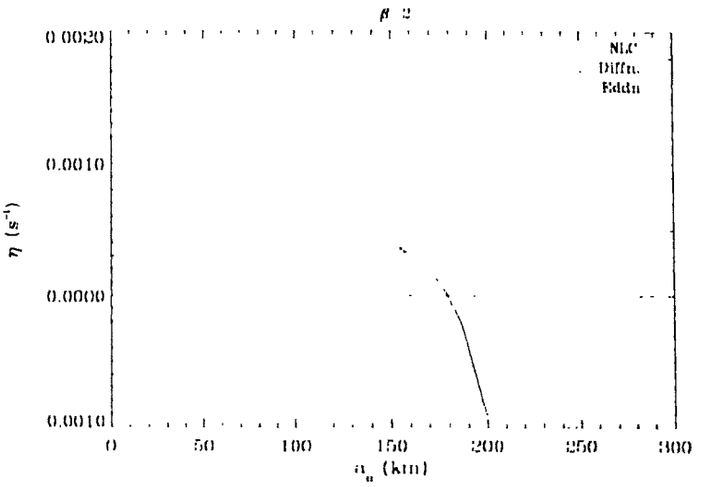

Figure 5.8: Growth rates for a tube with $\beta = 2.$, for comparison of the different approximations. Shown are results for Newton's law of cooling (dashed curves), diffusion approximation (dotted curves) and Eddington approximation (solid curves)

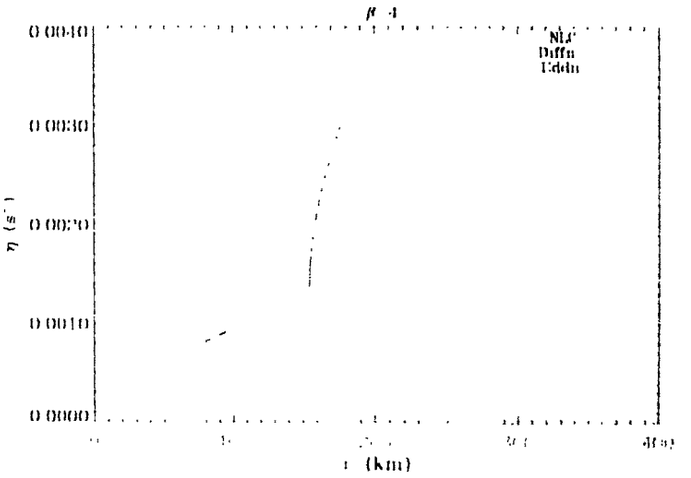

Figure 5.9: Growth rates for a tube of $\beta = 4.$

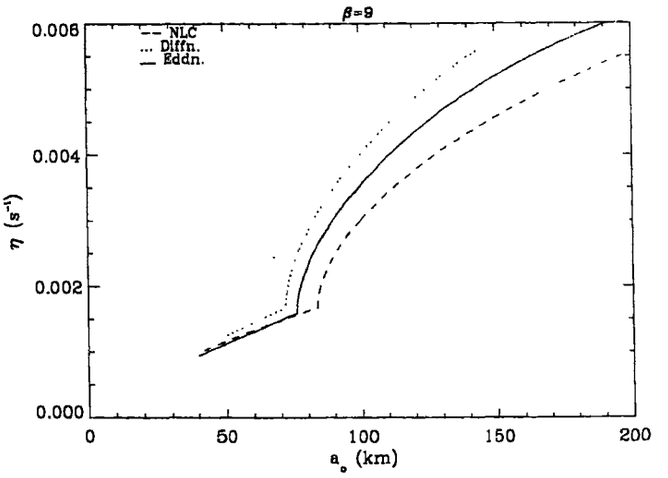

Figure 5.10: Growth rates for a tube of $\beta = 9$.

strength for stability. A collapsing weak tube of sufficient size can of course attain an equilibrium collapsed state of field strength higher than this value (Spruit 1979). Another interesting aspect to be noted from the results shown in Fig. (5.6) is the variation of the growth rate at the points of bifurcation, i.e. at the onset of convective instability, as a function of the tube radius and the field strength (β). This variation represents the relative importance of the magnetic field and the radiation in preventing the convective instability. For larger radii the stabilizing influence of radiation is smaller, yet the growth rates at the points of onset go down sharply as the field strength increases. The maximum onset growth rate is at about a tube radius of 100 km for a strength of about 600 G ($\beta = 9$). For tubes with size and strength greater than these values the main stabilizing influence thus is the magnetic field. On the other hand, as the tube size decreases, i.e. as the radiative influence increases we do not see a remarkable decrease in the onset growth rates as that happens when the magnetic field strength is increased. This just shows that the dominant stabilizing agent against the convective instability is the magnetic field.

5.3.2 Size-strength distribution for the solar tubes

As was done in the earlier chapters we derive a size(flux)-strength relation for the tubes from the curves shown in Fig. (5.6). On account of the present improved treatment of the radiation field the relation between the sizes and strengths of the tubes that we derive here offers a better comparison with the observations (Solanki et al. 1996, Lin 1996). From the positions of the bifurcations in the curves of Fig. (5.6), i.e. from the positions that mark the onset of the convective instability we

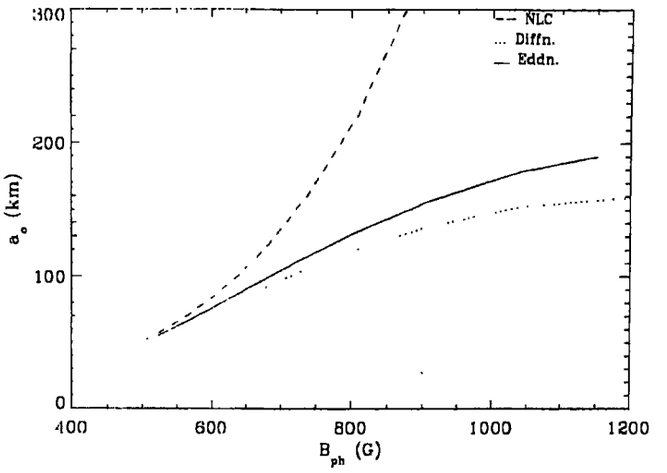

Figure 5.11: Size-strength relation for the tubes which demarcate the stable and unstable tubes. Region above the curves is unstable and that below is stable

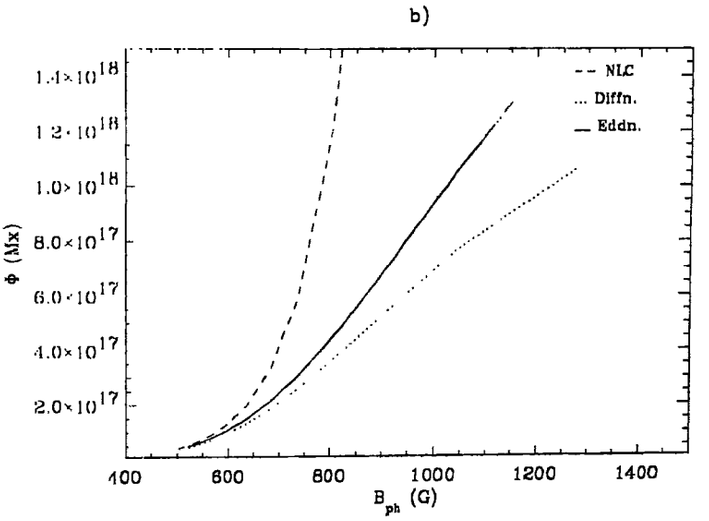

Figure 5.12: The magnetic flux-strength relation corresponding to the size-strength relation shown in Fig. (5.11)

note the values of the plasma β and the radius a_0. The resulting radius-field strength dependence is shown in Fig. (5.11) (solid curve). Superposed on this curve are the relations obtained for the case with only lateral exchange under Newton's law of cooling (dashed curve) and that for the diffusion approximation (dotted curve). In deriving such relations between the size and the field strength and comparing with the observed distribution on the Sun's surface, the following scenerio is implicitly assumed: an initial weak field tube of size big enough to be convectively unstable, i.e. a tube on a location beyond the bifurcation towards larger radii on the curves of Fig. (5.6) would collapse leading to an increase in its strength (lower β) and a decrease in its size in conformity with the flux conservation condition; if, in this process, the collapsing tube attains a size and strength such that it crosses the bifurcation points of the curves of Fig. (5.6) and reaches the convectively stable regions then the collapse is assumed to cease and attain its final equilibrium state thereby leading to the predicted distribution from the curves of Fig. (5.6). It is found that the maximum possible initial field strength up to which a tube can be subject to the convective instability is about 1160 G corresponding to $\beta = 2.45$ and the critical size of $a_o = 190$ km, i.e. a tube of strength 1160 G can still collapse to a higher strength if its size is greater than $a_o = 190$ km. Thus, from these numbers, it can be said that *the minimum amount of flux above which all flux concentrations attain always a collapsed state of strong kG field above* 1160 *G is* $\pi B_c a_c^2 = 1.31 \times 10^{18}$ Mx. This result is in good agreement with the observational results (Solanki et al.. 1996, Lin 1996, Keller et al.. 1994). Realistically, in the absence of any other mechanism to form stronger tubes, the maximum attainable field strength (corresponding to the maximum observed speed of about 3 km/sec for the granular flows) is the equipartition strength of approximately 500 G corresponding to a value of $\beta = 9$. Thus all initial equipartition strength magnetic flux concentrations with fluxes less than the above obtained limit of about 10^{18} Mx are subject to the radiative inhibition effects as brought out in the present study and consequently they would exhibit the $size - strength$ relation that is obtained here.

Since the observations only measure the magnetic fluxes and the strengths and their distribution(Solanki et al. 1996) we give the corresponding flux-strength distribution in Fig. (5.12). For the sake of better comparison, we have superposed the flux-strength relation calculated in the Eddington approximation (solid curve), in Fig. (5.13), with that observationally produced (histogram); the plot of histogram in Fig. (5.13) has been taken from the observational results of Solanki et al. (1996). There is a remarkable agreement between the predictions and the observations leading to the conclusion that indeed the convective collapse is the cause of the formation of the flux elements on the Sun's surface. Our refined, realistic, and exact treatment of the convective collapse process on the Sun reinforces the conclusions drawn from earlier simplified treatments (Venkatakrishnan

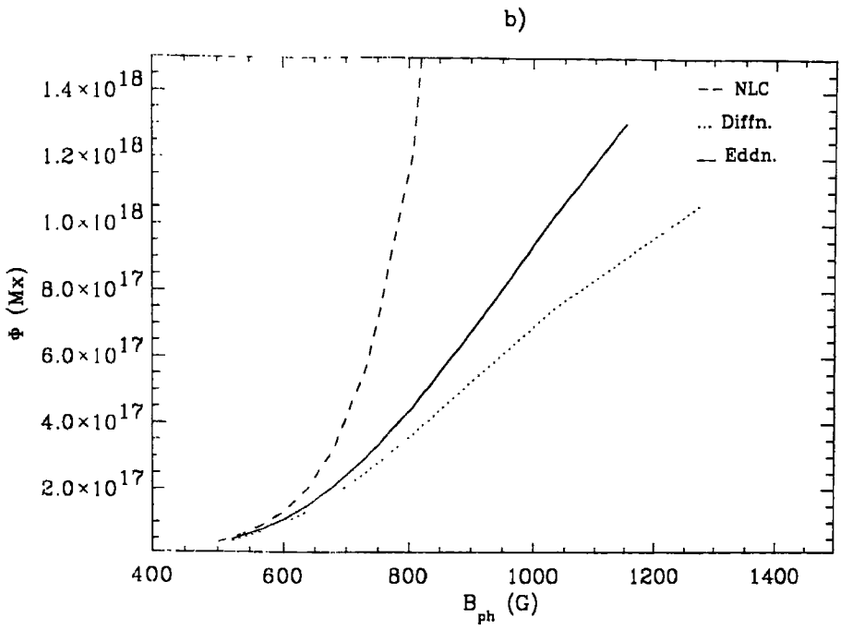

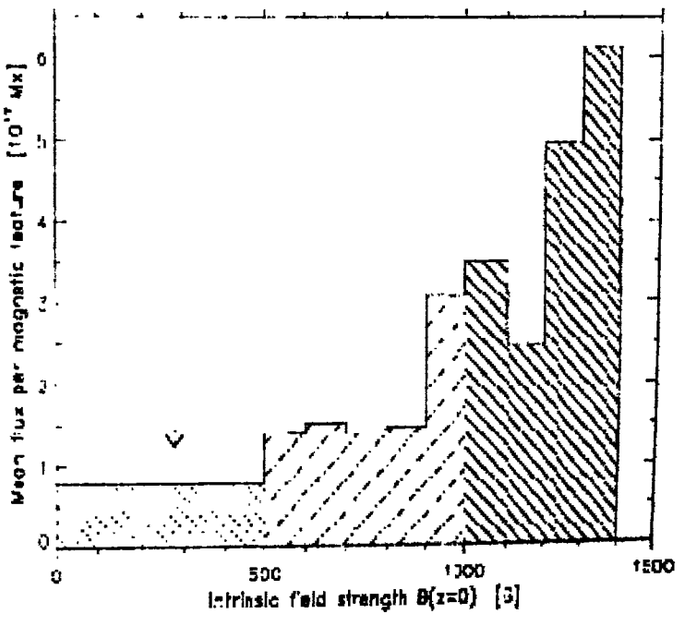

Figure 5.13: Comaparison of the calculated flux-strength relations in the Eddington approximation (solid curve) with the observed flux-strength distribution (histogram) of Solanki et al. (1996) for the solar tubes.

1986, Hasan 1986) and verifies the original suggestion and the physical explanation by Parker (1978) for the concentrated small scale magnetic structures on the Sun.

5.3.3 Overstability

The characteristics of the overstable mode are explained with the help of the Fig. (5.6) again. The mechanism by which overstability of the longitudinal slow mode of the tube is brought in has been already explained in the previous chapter. Here we only compare the growth rates obtained in the present case with that of the earlier treatments. To facilitate such a comparison we plot in Fig. (5.14) the growth rates of the overstable mode obtained based on the diffusion approximation (dotted curves) and the Eddington approximation (solid curves). The chosen β values here correspond to tubes which are strong enough to be stable against the convective instability and are relevant for the magnetic network on the Sun. It is seen that the growth rates in the present Eddington approximation are smaller than those obtained in the diffusion approximation. Also shown are the growth rates when only lateral exchange is allowed. The differences between the curves for the diffusion and the Eddington approximations clearly show that overstability is overestimated in the former case as already mentioned. It was noted in the last chapter, by a comparison between the cases of diffusion approximation including the vertical losses and the lateral exchange alone under Newton's law of cooling, that there existed a destabilizing effect on the osillatory motions, the same as the classical κ-mechanism, due to the perturbations associated with the opacity. This happens as a consequence of the inclusion of the vertical radiative exchanges. This destabilizing mechanism is countered, in the present Eddington approximation, by the above mentioned effect of ∇_e leading to the result that the growth rates get closer to those obtained in the Newton's law of cooling limit.

Another important difference between the present analysis and that in Chapter 4 is the location in the η-a_o plot at which the overstability sets in First of all, we note that whereas in the diffusion approximation the critical value of β above which the tube is always overstable irrespective of its size, provided it is convectively stable, is 1.9, in the present Eddington approximation this value has increased to 2.45. Secondly, for β values smaller than these critical values, in each case, the critical radii at which the overstability sets in are different in the two cases for a given β. As can be seen from Fig. (5.14), in the present case the overstability sets in at a larger radius than in the diffusion approximation because the diffusion approximation underestimates the lateral effects of radiation. But since the diffusion approximation is valid for the optically thick regions, we conclude that there is an appreciable influence of the intermediate optical depth and optically thin regions of the top layers of the tube, which are modelled correctly in the present Eddington approximation, in driving the oscillations overstable.

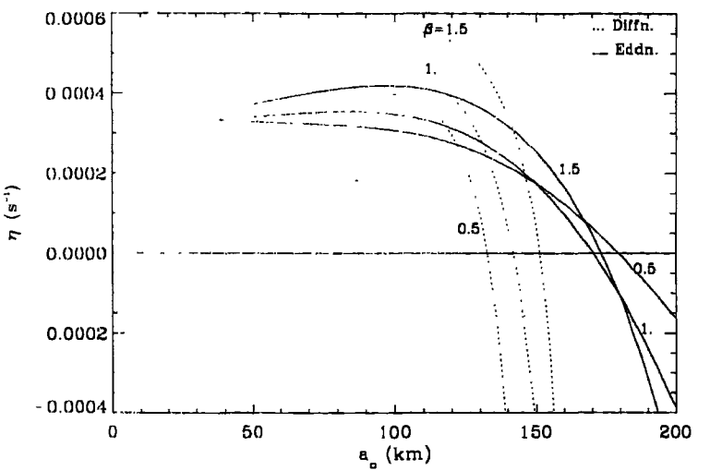

Figure 5.14: Variation of η with a_o for values of β typical of solar network tubes. The solid lines are for the Eddington approximation and the dotted ones for diffusion approximation

We point out that while there is no damping of oscillations when only lateral exchange takes place and the growth rate of the oscillation only asymptotically goes to zero in the limit of large radii, i.e. in the adiabatic limit, the inclusion of vertical radiative losses make the oscillations to damp out for radii greater than a particular finite value which is determined by the β. Thus our calculations support the classical physical explanations for the mechanism of overstability(Cowling 1957,Chandrasekhar 1960), that the horizontal exchange between vertically oscillating fluid elements acts to amplify the oscillations, and that vertical losses always try to smooth out the fluctuations thereby introducing damping. This radiative damping is quite severe for the overstable mode of an intense flux tube on the Sun that it gets completely damped out for tubes of radii larger than a certain critical value. We note here that the onset of overstability at a critical value of the tube radius, for a tube of strong enough field strength to be convectively stable, is through a Hopf bifurcation as we have here a pair of complex conjugate eigenvalues the imaginary part of which changes sign at the critical value of the parameter (See Appendix B.2 for further discussion).

Finally we note that a tube, which is convectively unstable at some value for its radius for a given strength, is always overstable. In other words, a tube which can undergo convective collapse for radii greater than a critical value for a given field strength remains overstable for all smaller radii that it can take.

5.4 Conclusions

We have modelled the interaction between the radiation and the dynamical instabilities of the gas confined inside the dynamically active magnetic flux tubes located vertically in the surface layers (upper convection zone + photosphere) on the Sun with sufficient refinement in the treatment of radiation to make a quantitaive comparison with the observations. The results of this chapter, in comparison with the results of the earlier chapter, clearly demonstrate the importance of the accurate modelling of the radiation in layers of widely varying optical depth, viz. the intermediate optical depth regions in the photopshere, the optically thick convection zone and the optically thin upper photospheric and higher layers. It has been demonstrated that the use of diffusion approximation overestimate the radiative effects in the optically thin layers thereby yielding growth rates which are larger than the correct values.

We have obtained a critical limit for the magnetic flux which demarcates the flux concentrations into two groups: (i) flux concentrations with fluxes above this limit, which is $\approx 10^{18}$ Mx, collapse unhindered to a stable tube of strength above about 1160 G to a stable value, which is bounded from above at the limit of a completely evacuated tube, with a very weak dependence between the fluxes and strengths; (ii) flux concentrations with fluxes smaller than the above limit are subject to the inhibiting action of the radiation leading lead to a strong dependence between the fluxes and strengths as brought out in the present study. This theoretical prediction of the existence of the two groups of magnetic structures finds excellent observational verification leading to the conclusion that the convective collapse is a global process operating on the surface layers of the Sun forming the highly inhomogeneous small-scale structured magnetic fields. By analogy, this same process is highly likley to be operative in other stars like the Sun with the similar structuring of the magnetic field, which is so fundamental to a varied forms of activity and non-thermal heating of the higher layers.

We have also established improved stability criteria for the overstable mode of the tube. It is demonstrated that strong tubes of large enough sizes are subject to the radiative damping associated with the vertical radiative losses leading to the damping of the slow magnetoacoustic mode of the tube. This leads to the conclusion that a thick network tube (of surface radius greater than about 150 km) is not subject to the overstability due to the horizontal radiative exchange.

Chapter 6

Conclusions

In this final Chapter, we conclude by summarizing the main results obtained in this thesis and by highlighting their contribution on our understanding of certain aspects of the physics of small-scale magnetic flux tubes on the Sun. We also critically assess the strengths and limitations of the present work and highlight the directions for future research.

6.1 Summary of the main results

The influence of radiative energy transport on wave motions and instability in a magnetic flux tube extending vertically through the solar photosphere and convection zone has been investigated. An analytical dispersion relation has been derived for the complex frequencies that describe the evolution of convective and oscillatory perturbations of the flux tube gas, generlizing previously known results which consider only the horizontal radiative influences. This relation is based on a quasiadiabatic treatment of vertical radiative transport. A local stability analysis has revealed that vertical radiative losses have a destabilizing influence on the convective instability of a flux tube and a stabilizing influence on the oscillatory motions in a convectively stable tube.A criterion for the oscillations to be overstable in the presence of vertical radiative losses has been derived; oscillations in thick and tubes with strong field are shown to damp out owing to the radiative damping associated with the radiative losses. The more the vertical radiative losses, i.e. the more the departure from radiative equilibrium in the driving regions, the larger are the convective growth rates implying a faster downflow and thus a faster collapse of a initial weak field tube. Thus, this result shows that the trigerring of a convective collapse of the tube could be due to the vertical losses, as first suggested by Parker (1978).

Numerical solutions of the full fourth order system of non-adiabatic equations have been obtained in Chapter III for tubes embedded in polytropes. By introducing a parameter that controls the

amount of non-adiabaticity due to radiation we have performed numerical experiments which bring out the pattern of stabilizing action of radiation on the convective instability of the tubes; the greater the radiative interaction, the smaller the field strength required for stability against convective collapse and consequently it is demonstrated that convectively stable tubes embedded in atmospheres where the fraction of convective to radiative energy fluxes is higher are stronger. A necessary condition for the onset of convective instability in the presence of radiative heat diffusion, which generalizes the previously known such conditions for adiabatic motions, has been numerically obtained demonstrating the size dependent stabilizing action of the radiation. Critical values of the polytropic index for the onset of overstability has been determined for different values of β, based on typical values for γ(the ratio of specific heats). These values depend weakly on β. It has also been demonstrated that a adiabatically stratified convectively stable tube exhibits overstability depending on the amount of non-adiabaticity which is determined by the amount of radiative flux, as well as the size and strength of the tube.

Turning to small-scale magnetic structures on the Sun, in Chapter IV and V, we have obtained results which provide a physical explanation for the size-dependent (thus magnetic flux dependent) relation for the observed field strengths. It has been clarified that the nature of the bottom boundary mechanical condition is inconsequential provided the location of the bottom boundary is deep enough and far away from the driving regions which are mainly confined to the top 1000 km. The overstability of the wave-motions of a convectively stable tube is shown to emerge mainly as a consequence of the horizontal radiative exchange of the tube with its surroundings; a closed mechanical boundary condition at the bottom is shown not to be the cause of the overstability, though overstable growth rates are slightly reduced for a open boundary. The comparison of the results obtained in Chapter IV in the diffusion approximation with those of Chapter V where an improved treatment of radiation based on the Eddington approximation is used shows that the diffusion approximation overestimates both the convective and oscillatory growth rates; this is explained because diffusion approximation overestimates the radiative flux in the optically thin higher layers and thus the radiative losses, resulting in the faster cooling of the gas thereby helping to the stronger acceleration of the convective downflows as found.

The study in Chapter V, with a sufficiently realistic treatment of radiation in the Eddington approximation to enable a meaningful comparison with observations, has led to the following results: (i) flux concentrations with fluxes above a limit of around 1×10^{18}Mx are subject to convective collapse with negligible hindrance due to radiation, and they result in stable tubes of strength above 1160 G, which is the stable minimum limit, with a very weak dependence between the fluxes and strengths. The strong field tubes observed in the *network* outlining the supergranular boundaries

are identified with such collapsed tubes; thus the minimum flux contained in a network tube is given by the above value which is consistent with the observations; (ii) flux concentrations with fluxes smaller than the above limit are subject to the inhibiting action of the radiation leading to a strong dependence between the fluxes and strengths as shown in Fig. (5.12) and (5.13a)(the solid curves). This theoretical prediction of the existence of the two groups of magnetic structures finds excellent observational verification (Solanki et al 1996; Lin 1995) leading to the conclusion that the convective collapse is a global process operating on the surface layers of the Sun forming the highly inhomogeneous small-scale structured magnetic fields. By analogy, this same process is likley to be operative in other stars like the Sun with similar atmospheric stratification and structuring of the magnetic field.

The improved stability criteria obtained in Chapter V for the overstable mode of the tube demonstrate that strong tubes of large enough sizes are subject to vertical radiative losses leading to a damping of the slow magnetoacoustic mode of the tube, which is otherwise driven overstable by the horizontal exchange of radiation. This leads to the conclusion that a flux tube of surface radius greater than about 150 km is not subject to the overstability due to the horizontal radiative exchange.

6.2 Limitations and Future Directions

A shortcoming of the analysis in the thesis is due to the assumption that in the equilibrium the temperatures in the tube and its surroundings are equal which lead to a depth independent plasma β. This results in magnetic field strengths which are too high at deeper layers; consequently the stabilizing action of the magnetic field is overestimated. Thus the field strengths that we have derived for convective stability are likely to be smaller than actual values. Another limitation is the use of the thin flux tube approximation which is basically one- dimensional reduction of the MHD equations. Although this approximation is valid at the photospheric base and below, in the higher layers it breaks down when the tube radius exceeds the local pressure scale height. Also, radiative transfer effects are intrinsically multidimensional in the photospheric layers and the analysis in this thesis lacks a proper treatment of this situation. The modelling of the horizontal exchange in this thesis is quasi-one-dimensional as could be achieved within the thin tube approximation. Lastly, it should be emphasized that the results presented in this thesis are based on a linear treatment of the MHD equations, which are inherently non-linear, though the stability criteria obtained are most likely to remain valid even in the non-linear regime.

Having delineated the basic physical mechanisms governing the interaction of radiation with mo-

tions in magnetic flux tubes, a next step would be to include the mechanical coupling of the outside motions to those inside. Recent high resolution observations have revealed the highly dynamic (Berger et al. 1997) nature of the flux elements, showing a vigorous shuffling and fast displacements of their footpoints due to the surrounding convective motions. These externally imposed motions and also the periodic pressure perturbations due to the p-modes travelling in the external atmosphere are potential sources for the excitation of motions inside the tubes. We have not included such effects in this thesis. In view of the important implications that the flux tube guided outward propagating waves and motions have for chromospheric and coronal heating, a question of relevance here is the effects of radiation on externally excited flux tube motions and oscillations. It is also useful to study radiative damping effects, which are shown to limit the growth of overstable modes, for the case of externally excited motions.

Appendix A

Derivation of Key Equations

A.1 Derivation of the Thin Flux Tube Equations

The *thin flux tube equations* (1.13)-(1.17) given in Chapter 1 are derived from the MHD equations (1.6)-(1.8) and the equation (1.12) without the viscous and Joule dissipation terms, through an general expansion approach which is valid for axisymmetric magnetic flux tubes in which all the physical variables have a radial scale of variation that is much less than the vertical scale. Thus, if L is a typical vertical length scale, e.g. the pressure scale height $L = H = p/\rho g$, it is assumed that at each level z, $r << L$ over the cross section of the tube. The small terms in the expansion are conveniently described in terms of a small order parameter ϵ, taken to be $r(z)/L(z)$ at a suitable depth z where the condition $\epsilon << 1$ is satisfied. The requirement that the variables are regular on the axis of the tube makes this expansion to be of a Taylor series around $r = 0$. This scheme was first developed by Roberts and Webb (1978)(see also Ferriz-Mass and Schussler 1989). In a compact notation, each physical variable is expanded,

$$f(r,z,t) = \sum_{n=0}^{\infty} \frac{(\epsilon L)^n}{n!} \left(\frac{\partial^n f(0,z,t)}{\partial r^n} \right) |_{r=0} \cdot \tag{A.1}$$

Here f represents each dependent variable in turn, i.e. p, T, ρ, B, etc. As a consequence of symmetry with respect to the axis of flux tube, the radial and azimuthal components of vector variables $\mathbf{v}$ and $\mathbf{B}$ have only odd terms, while the axial components v_z and B_z as well as the scalar functions p and ρ have only even terms in the expansion. Inserting the series expansion (A.1) into the MHD equations (1.6)-(1.8) and the equation (1.12) without the viscous and Joule dissipation terms, and arranging separately the contributions to equal powers in ϵ, a system of expanded magnetohydrodynamic equations in the variables z and t are obtained. The *thin flux tube approximation* amounts to retaining only the zeroeth order terms in this expansion. Denoting partial differentiation with respect to z by primes, the zeroeth-order equations are:

the continuity equation (1.6),

$$\frac{\partial \rho_0}{\partial t} + (\rho_0 v_{z0})' + 2\rho_0 v_{r1} = 0, \tag{A.2}$$

the axial component of the momentum equation (1.7),

$$\rho_0 \left(\frac{\partial v_{z0}}{\partial t} + v_{z0} v_{z0}' \right) + p_0' + \rho_0 g = 0, \tag{A.3}$$

the axial component of the induction equation (1.8),

$$\frac{\partial B_{z0}}{\partial t} + v_{z0} B_{z0}' + 2 B_{z0} v_{r1} = 0, \tag{A.4}$$

and the energy equation (1.12) without the viscous and Joule dissipation terms,

$$\frac{\partial p_0}{\partial t} + v_{z0} p_0' - \frac{\Gamma_1 p_0}{\rho_0} \left[\frac{\partial \rho_0}{\partial t} + v_{z0} \rho_0' \right] = -\frac{\chi T}{\rho_0 c_v T_0} (\nabla . \mathbf{F})_0, \tag{A.5}$$

where $(\nabla . \mathbf{F})_0$ is the zeroth order contribution to the divergence of the energy flux and is found to be,

$$(\nabla . \mathbf{F})_0 = 2F_{r1} + \frac{dF_z}{dz}. \tag{A.6}$$

In all the above equations the quantities with subscript '0' refer to the axial values and those with subscript '1' refer to the first order terms in the expansion. The boundary between the magnetized gas inside the flux tube and the external medium represents a tangential discontinuity at which it is required that the total (gas plus magnetic) pressure is continuous (Landau and Lifshitz, 1984):

$$p_0 + \frac{B_{z0}^2}{8\pi} = p_e \tag{A.7}$$

where p_e is the external gas pressure. The radius $a(z)$ of the flux tube is determined by the requirement of magnetic flux conservation, which up to second order yields:

$$B_{z0} a^2 = const. \tag{A.8}$$

We note that the radial component of the induction equation, to zeroeth order, simply determines the first order component B_{r1} in terms of v_{z0} and B_{z0} through the continuity equation (A.2). And, the zeroeth order radial component of the momentum equation determines p_1 once B_{z0} and B_{r1} are known.

The final set of thin flux tube equations (1.13)-(1.17) given in Chapter 1 are arrived at by eliminating the unknown v_{r1} using equations (A.2) and (A.4) in the set of equations derived above and by dropping the subscripts '0' and 'z' in all the variables.

A.2 Derivation of the Perturbation Equations

Here, details of the derivation of the perturbation equations that describe the linear evolution of the small amplitude fluctuations imposed on a thin flaring vertical flux tube are presented; the radiation field is treated in the diffusion approximation. The equations to be perturbed and linearized are the thin tube equations (1.13), (1.14), (1.15) and (1.16) given in Chapter 1. The variables are assumed to acquire small fluctuations about their time-independent equilibrium values; the perturbations as seen in a fixed frame of reference i.e., the Eulerian perturbations are denoted by primes while the Lagrangian perturbations, which are those as seen in the frame moving along with the fluid, are denoted with the symbol δ preceding them. Perturbation of equation (1.13) :

$$\frac{\rho'}{\rho} = \frac{B'}{B} - \frac{d\xi}{dz} - \left[\frac{dln\rho}{dz} - \frac{dlnB}{dz}\right]\xi \tag{A.9}$$

where ξ is the vertical displacement perturbation satisfying

$$v' = \frac{d\xi}{dt} \tag{A.10}$$

Perturbation of equation (1.15) with the assumption that the Eulerian perturbation in the external pressure is negligible yields,

$$\frac{B'}{B} = -\frac{\beta}{2}\frac{p'}{p} \tag{A.11}$$

where $\beta = 8\pi p/B^2$. Using the above eqn. (A.11) to replace the magnetic field perturbation in eqn. (A.9) we have,

$$\frac{d\xi}{dz} = -\frac{\beta}{2}\frac{p'}{p} - \frac{\rho'}{\rho} - \left[\frac{dln\rho}{dz} - \frac{dlnB}{dz}\right]\xi \tag{A.12}$$

The vertical gradients of density and magnetic field appearing in the above equation can be expressed in terms of the pressure scale-height,

$$H = \frac{p}{\rho g} \tag{A.13}$$

as follows:

$$\frac{dln\rho}{dz} = \frac{1}{\rho g}\frac{d}{dz}\left(\frac{p}{H}\right) = \frac{1}{H}\left(1 - \frac{dH}{dz}\right) \tag{A.14}$$

Differentiating the pressure balance condition (1.15) with respect to z we have,

$$\frac{dlnB}{dz} = \frac{\beta}{2}\frac{(\rho_e - \rho)g}{p} = \frac{1}{2H_e} + \frac{\beta}{2}\frac{(H - H_e)}{HH_e} \tag{A.15}$$

where the subscript 'e' stands for the external medium. If the tube is in temperature equilibrium with the surroundings or more specifically if

$$\frac{T}{\mu} = \frac{T_e}{\mu_e} \tag{A.16}$$

we have $H = H_e$ and hence,

$$\frac{dlnB}{dz} = \frac{1}{2H} \tag{A.17}$$

Therefore we have

$$\frac{dln\rho}{dz} - \frac{dlnB}{dz} = \frac{1}{H}\left(\frac{1}{2} - \frac{dH}{dz}\right) \tag{A.18}$$

For an equation of state of the form,

$$p = p(\rho, T) \tag{A.19}$$

we have,

$$\frac{\rho'}{\rho} = \frac{1}{\chi_\rho}\frac{p'}{p} - \frac{\chi_T}{\chi_\rho}\frac{T'}{T} \tag{A.20}$$

where

$$\chi_\rho = \left(\frac{\partial lnp}{\partial ln\rho}\right)_T, \chi_T = \left(\frac{\partial lnp}{\partial lnT}\right)_\rho \tag{A.21}$$

Use of the above two equations in eqn. (A.12) yields,

$$\frac{d\xi}{dz} = \frac{1}{H}\left(\frac{dH}{dz} - \frac{1}{2}\right)\xi - \left(\frac{\beta}{2} + \frac{1}{\chi_\rho}\right)\frac{p'}{p} + \frac{\chi_T}{\chi_\rho}\frac{T'}{T} \tag{A.22}$$

Perturbation of the momentum eqn. (1.14) yields,

$$\frac{d^2\xi}{dt^2} = -\frac{p}{\rho}\frac{d}{dz}\left(\frac{p'}{p}\right) - g\frac{p'}{p} + g\frac{\rho'}{\rho} \tag{A.23}$$

With $e^{-i\omega t}$ time dependence and replacing the density perturbations, we have,

$$\frac{d}{dz}\left(\frac{p'}{p}\right) = \frac{\omega^2}{Hg} + \frac{(1-\chi_\rho)}{H\chi_\rho}\frac{p'}{p} - \frac{\chi_T}{H\chi_\rho}\frac{T'}{T} \tag{A.24}$$

The perturbation of the energy equation (1.16):

$$i\omega(1-\gamma)\frac{p'}{p} + i\omega\gamma\chi_T\frac{T'}{T} + i\omega\frac{\Gamma_1 N^2}{g}\xi = \frac{\chi_T}{\rho c_v T}\nabla.\mathbf{F}' \tag{A.25}$$

where

$$N^2 = g\left[\frac{1}{\Gamma_1}\frac{dlnp}{dz} - \frac{dln\rho}{dz}\right] = \frac{g}{H}\left[\frac{dH}{dz} - \frac{(\Gamma_1 - 1)}{\Gamma_1}\right] \tag{A.26}$$

is the squared Brunt-Vaisala frequency and

$$\gamma = \frac{\Gamma_1}{\chi_\rho} = \frac{c_p}{c_v} \tag{A.27}$$

The divergence of the flux perturbations that appear in the RHS of the equation (A.25) can be written as

$$\nabla.\mathbf{F}' = 2\frac{F_r'}{r} + \frac{dF_z'}{dz} \tag{A.28}$$

In the present thin-tube approximation, the components F_r and F_z are given as

$$F_r = -r\frac{8\sigma(T_e^4 - T^4)}{3\kappa\rho a^2} \tag{A.29}$$

$$F_z = -\frac{16\sigma T^3}{3\kappa\rho}\frac{\partial T}{\partial z} \tag{A.30}$$

where a is the radius of the tube. Since the tube has the same temperature as the external medium in the equilibrium state, the perturbation in the radial component of the flux is found as,

$$F_r' = 2r\frac{KT}{a^2}\frac{T'}{T} \tag{A.31}$$

Substituting the above relation and rewriting the equation (A.28),

$$\nabla.\mathbf{F}' = \frac{4KT}{a^2}\frac{T'}{T} + F_z\frac{d}{dz}\left(\frac{F_z'}{F_z}\right) + \frac{dF_z}{dz}\frac{F_z'}{F_z} \tag{A.32}$$

With the use of the above equation we rewrite the perturbed energy equation (A.25) in the following form:

$$\frac{d}{dz}\left(\frac{F_z'}{F_z}\right) = -i\omega\tau_{th}\frac{N^2\Gamma_1}{g\chi_T Z_d}\xi + i\omega\tau_{th}\frac{(\gamma-1)}{\chi_T Z_d}\frac{p'}{p} + \left[\frac{4}{\epsilon Z_d} - i\frac{\omega\tau_{th}\gamma}{Z_d}\right]\frac{T'}{T} - \frac{dlnF_z}{dz}\frac{F_z'}{F_z} \tag{A.33}$$

where Z_d is the depth down to which the tube extends and we have introduced the following time-scales:

$$\tau_{th} = \frac{\rho c_v T Z_d}{F} \tag{A.34}$$

is a thermal time-scale in which the radiative relaxation takes place over the length of the tube; here F is the magnitude of the vertical component of the flux;

$$\tau_r = \frac{\rho c_v a^2}{K} \tag{A.35}$$

is the lateral radiative exchange time-scale for the tube of radius a and ϵ is a ratio as defined below,

$$\epsilon = \frac{\tau_r}{\tau_{th}} \tag{A.36}$$

The other equation that closes our system of equations is got by perturbing the expression for the vertical radiative flux. Noting that, to linear order in the perturbations,

$$(T+T')^3 \approx T^3 + 3T^3\frac{T'}{T} \tag{A.37}$$

$$\frac{1}{\eta+\eta'} \approx \frac{1}{\eta} - \frac{1}{\eta}\frac{\eta'}{\eta} \tag{A.38}$$

where

$$\eta = \kappa\rho \tag{A.39}$$

we have for the perturbations in the vertical component of the flux,

$$\frac{F_z'}{F_z} = \left(\frac{dlnT}{dz}\right)^{-1} \frac{d}{dz}\left(\frac{T'}{T}\right) + 4\frac{T'}{T} - \frac{\eta'}{\eta} \tag{A.40}$$

The perturbations in η can be written as,

$$\frac{\eta'}{\eta} = \frac{\kappa'}{\kappa} + \frac{\rho'}{\rho} \tag{A.41}$$

The opacity perturbations can be expressed in terms of the pressure and the temperature perturbations as

$$\frac{\kappa'}{\kappa} = \kappa_p \frac{p'}{p} + \kappa_T \frac{T'}{T} \tag{A.42}$$

where

$$\kappa_p = \left(\frac{\partial \ln \kappa}{\partial \ln p}\right)_T, \kappa_T = \left(\frac{\partial \ln \kappa}{\partial \ln T}\right)_p \tag{A.43}$$

Use of equations (A.20) and (A.42) in the equation (A.40) yields the vertical flux perturbation as a function of pressure and temperature perturbations:

$$\frac{F_z'}{F_z} = \left(\frac{dlnT}{dz}\right)^{-1} \frac{d}{dz}\left(\frac{T'}{T}\right) - \left[\kappa_p + \frac{1}{\chi_\rho}\right]\frac{p'}{p} + \left[4 - \kappa_T + \frac{\chi_T}{\chi_\rho}\right]\frac{T'}{T} \tag{A.44}$$

We rewrite the above equation in the following convenient form:

$$\frac{d}{dz}\left(\frac{T'}{T}\right) = \frac{dlnT}{dz}\left[\kappa_p + \frac{1}{\chi_\rho}\right]\frac{p'}{p} - \frac{dlnT}{dz}\left[4 - \kappa_T + \frac{\chi_T}{\chi_\rho}\right]\frac{T'}{T} + \frac{dlnT}{dz}\frac{F_z'}{F_z} \tag{A.45}$$

The equations (A.22), (A.24), (A.33) and (A.45) form a complete set for the four variables ξ, p'/p, F_z'/F_z and T'/T.

Appendix B

Discussions on Validity of Diffusion Approximation and Overstability

B.1 Validity of the Diffusion Approximation

The treatment of radiative transfer in Chapters 2 - 4 is based on the diffusion approximation. This approximation is introduced in Chapter 1, Section 1.3.2, along with a brief description. Here, we provide a further discussion on its applicability and justification in the present context. The diffusion approximation is valid when the radiation mean free path is much smaller than the scales over which thermodynamic quantities vary. In this situation, the radiation field does not lose its isotropy and homogeneity, and the gaseous medium is said to be 'locally homogeneous'. This happens at locations where large optical depths are obtained, and as is well known, interiors of stars satisfy this condition. In the solar atmosphere, the photosphere corresponds to a optical depth surface of $\tau = \kappa\rho z = 1$. Hydrogen ionizes immediately below the photosphere, at $T = 10^4 K$; this drastically increases the opacity of the gas beneath. Thus the solar atmosphere attains a condition wherein the radiation *diffuses*, rather than streaming as in the photosphere and above, immediately beneath the photosphere, starting at depths as shallow as 50 km. The depth extent of the embedded magnetic flux tubes that are studied in the thesis is about 5000 km, and thus most mass of the gas confined in them lie in the regions that are optically thick. This justifies the use of the diffusion approximation for the study of gas motions in magnetic flux tubes. But, however, as discussed in Chapter 5, the regions which drive the convective instability in a magnetic flux tube is confined very close to the surface, and this region has a depth of about 50 - 100 km. Hence, a better treatment than the diffusion approximation is needed to accurately describe the radiation and gas interactions in these intermediate optical depth regions. Such a remedy is provided by the Eddington approximation, which has been adopted in Chapter 5. The diffusion approximation,

however, has the advantage of mathematical simplicity: the radiative flux is completely determined by the temperature field which is known from the model atmospheres; and also, all the essential effects of interaction between radiation and gas are brought out even in this simple treatment.

B.2 Overstability

Further to a brief discussion on the origin of overstability given in Chapter 2, Section 2.1, we explain here some finer points associated with this process of wave amplification in a gaseous medium. It is clarified that in treatments based on *Boussinesq approximation*, as was first studied by Chandrasekhar (1961), where bouyancy forces can maintain internal gravity waves in an incompressible medium, the inclusion of radiative dissipation leads to the amplification of these waves and thus overstability. In a compressible medium, the presence of radiative dissipation can amplify the acoustic waves driven by the pressure forces, and this happens even in the absence of gravity. Thus, in essence, the overstability of wave motions is achieved by the interaction of a dissipative mechanism with any restoring force that supports a wave motion. Mere presence of dissipation, without any restoring force that acts to restore a machanically perturbed fluid element, cannot lead to overstability.

With reference to the nature of onset of overstabilty in a magnetic flux tube as its size (radius a) is varied, it was noted in Chapter 5, Section 5.3.3 (page 105) that the onset occurs through a Hopf bifurcation. Physically, this bifurcation corresponds to the situation where the wave motions change from a state of being damped (stable to wave-like perturbations) to a state of amplification, through the neutral stability (zero growth rate) point, as a parameter that controls the dynamics is varied. Here, the tube size (photospheric radius a_o) is the control parameter, and as a_o decreases, from a point where the growth rates (η, the imaginary part of the complex eigen-value $\omega = \sigma + i\eta$) are negative corresponding to damping (refer to Fig. 5.14), η increases and it crosses zero at a critical value $a_{o,c}$ marking the location of Hopf bifurcation. For values of a_o smaller than this critical value, η are positive representing growing wave motions. Here, it should be noted that the real part σ of the eigen-value remains non-zero maintaining the perturbations wave-like. Thus, as is generic to Hopf bifurcations, the loss of stability is through oscillatory motions. The control parameter a_o (tube radius) basically dictates the extent of interaction of radiative dissipation with the tube wave motions, and thereby leads to the above described character of the onset of overstability.

Bibliography

[1] Abramowitz, M., Stegun, I.A., 1965, Handbook of Mathematical Functions, Dover, New York.

[2] Antia, H.M, Chitre, R., 1978, Sol. Phys., 60, 31

[3] Antia, H.M, Chitre, R., 1979, Sol. Phys., 63, 67

[4] Auer, L.H., Mihalas, D., 1970, 149, 65

[5] Babcock, H.W., Babcock, H.D., 1952, Publ. Astron. Soc. Pacific, 64, 282

[6] Beckers, J.M., Schröter, E.H., 1968, Solar Phys., 4, 142

[7] Berger, T.E., Loefdahl, M.G., Shine, R.S., Title, A.M., 1998, ApJ, 495, 973

[8] Biermann, L., 1941, Vierteljahrsschr. Astron. Ges., 76, 194

[9] Böhm, K.H., Richter, 1959, Zeitschrift fur Astrophysik, 48, 231

[10] Bogdan, T.J., Hindman, B., Cally, P.S., Charbonneau, P., 1996, ApJ, 465, 406

[11] Braginsky, S.I., 1965, Rev. of Plasma Phys., 1, 605

[12] Brault, J.W., 1978, in G.Godoli, G.Noci, A.Righini (eds.): Proc. JOSO Workshop Future Solar Optical Observations- Needs and Constraints, Osserv. Mem. Oss. Astrofis. Arcetri No. 106, p.33

[13] Chandrasekhar, S., 1939, An Introduction to the Study of Stellar Structure, Chicago, Ill., The University of Chicago Press[1939].

[14] Chandrasekhar, S., 1961, Hydrodynamic and Hydromagnetic Stability, Clarendon, Oxford

[15] Chou, D.-Y., Fisher, G.H., 1989, ApJ, 341, 533

[16] Christensen-Dalsgaard, J., Proffitt, C.R., Thompson, M.J., 1993, ApJ, 403, L75

[17] Christensen-Dalsgaard, J., Frandsen, S., 1983, Sol. Phys., 82, 165

[18] Cowling, T.G., 1951, ApJ, 114, 272

[19] Cowling, T.G., 1953, in G.P.Kuiper, (ed.), The Sun, Chicago: University of Chicago Press, p.569.

[20] Cowling, T.G., 1957, Magnetohydrodynamics, Wiley, New York.

[21] Cox, J.P., 1980, Theory of Stellar Pulsation, Princeton University Press.

[22] Defouw, R.J., 1970, ApJ, 160, 659

[23] Deinzer, W., Hensler, G., Schüssler, M., Weisshaar, E., 1984, A& A, 139, 435

[24] Deinzer, W., Knölker, M., Voigt, H.H. (eds.): 1986, Small Scale Magnetic Flux Concentrations in the Solar Photosphere, Abh. der Akad. Wiss. Göttingen, Math.-Phys. Klasse, Folge 3, Nr. 38, Vandenhoeck und Ruprecht, Göttingen.

[25] Feautrier, P., 1964, Proc. 1st Harvard-Smithsonian Conf. on Stellar Atmospheres, S.A.O. Special Report No. 167, p.110.

[26] Ferriz-Mas, A., Schüssler, M., 1989, Geophys. Astrophys. Fluid Dyn. 48, 217

[27] Frazier, E.N., Stenflo, J.O., 1972, Sol. Phys., 27, 330

[28] Galloway, D.J., Proctor, M.R.E., Weiss, N.O., 1978, J. Fluid Mech. 87, 243

[29] Gough, D.O., Taylor, R.J., MNRAS, 1966, 133, 85

[30] Grossmann-Doerth, U., Knölker, M., Schüssler, M., Weisshaar, E., 1989a, in R.J.Rutten and G.Severino (eds.), Solar and stellar granulation, NATO ASI Series C Vol. 263, Kluwer, Dordrecht

[31] Grossman-Doerth, U., Schüssler, M., Solanki, S.K., 1989b, A& A, 221, 338

[32] Grossman-Doerth, U., Schüssler, M., Steiner, O., 1998, A& A, 337, 928

[33] Hale, G.E., 1908, ApJ, 28, 315

[34] Hale, G.E., 1922a, Proc. National Acad. Sci., 8, 168

[35] Hale, G.E., 1922b, MNRAS, 82, 168

[36] Hasan, S.S., 1983, in J.O.Stenflo (ed.), Solar and Stellar Magnetic Fields: Origin and Coronal Effects, IAU-Symp. No. 102, Reidel, Dordrecht, p.73

[37] Hasan, S.S., 1984, ApJ, 285, 851

[38] Hasan, S.S., 1985, A& A, 143, 39

[39] Hasan, S.S., 1986, MNRAS, 219, 357

[40] Hasan, S.S., 1988, ApJ, 332, 499

[41] Hasan, S.S., Kalkofen, W., 1994, ApJ, 436, 355

[42] Hasan, S.S., Kneer, F., Kalkofen, W., 1998, A&A, 332, 1064

[43] Hasan, S.S., Kneer, F., Kalkofen, W., in Solar Polarization: Proc. of SPW2, K.N.Nagendra, J.O.Stenflo (eds.), 1999, ASSL, Kluwer (in press), Dordrecht.

[44] Hasan, S.S., Schüssler, M., 1985, A& A, 151, 69

[45] Herbold, G., Ulmschneider, P., Spruit, H.C., Rosner, R., 1985, A& A, 145, 157

[46] Howard, R.W., Stenflo, J.O., 1972, Solar Phys., 22, 402

[47] Hurlburt, N.E., Toomre, J., 1988, ApJ, 327, 920

[48] Jones, C.A., 1970, MNRAS, 176, 145

[49] Kalkofen, W., 1996, ApJ, 468, L69

[50] Kalkofen, W., 1997, ApJ, 486, L145

[51] Kato, S., 1966, PASJ, 18, 201

[52] Kerswell, R., Childress, S., 1992, ApJ, 385, 746

[53] Kiepenheuer, K.O., 1953, ApJ, 117, 447

[54] Keller, C.U., Deubner, F.-L., Egger, U., Fleck, B., Povel, H.P., 1994, A&A, 286, 626

[55] Knölker, M., Grossmann-Doerth, U., Schüssler, M., Weisshaar, E., 1991, Adv. Space Res., 11, 285

[56] Kraichnan, R.H., 1976, J. Fluid Mech., 77, 753

[57] Kurucz, R.L., 1993 (private communication, Hasan, S.S., Kalkofen, W., 1994)

[58] Landau, L., Lifshitz, E., 1984, Electrodynamics of Continuous Media, Pergamon Press.

[59] Ledoux, P., in Handbuch der Physik, Band LI, 1958, p.678, Springer-Verlag, Berlin.

[60] Lin, H., 1995, ApJ, 446, 421

[61] Livingston, W.C., 1991, in L.November (ed.), Solar Polarimetry, National Solar Observatory, Sunspot, p.356

[62] Massaglia, S., Bodo, G., Rossi, P., 1989, A&A, 209, 399

[63] Meneguzzi, M., Frisch, U., Pouquet, A., 1981, Phys. Rev. Lett., 47, 1060

[64] Meunier, N., Solanki, S.K., Livingston, W.C., 1998, A&A, 331, 771

[65] Mihalas, D., 1967, in Methods in Comp. Phys., Vol.7, (eds.) Adler, B., Fernbach, S., Rotenburg, M., Academic Press, New York.

[66] Moreno-Insertis, F., 1986, A&A, 166, 291

[67] Moreno-Insertis, F., 1992, in J.H.Thomas and N.O.Weiss (eds.), Sunspots: Theory and Observations, NATO ARW, Kluwer, Dordrecht.

[68] Moore, D.W., Spiegel, E.A., 1966, ApJ, 143, 871

[69] Musman, S., Nelson, G.D., 1976, ApJ, 207, 981

[70] Nelson, G.D., Musman, S., 1978, ApJ, 222, L69

[71] Nordlund, A., 1976, Highlights of Astronomy, 4 part II, remark on p.272.

[72] Nordlund, A., 1983, in J.O.Stenflo (ed.), Solar and Stellar Magnetic Fields: Origin and Coronal Effects, IAU-Symp. No. 102, Reidel, Dordrecht, p.79.

[73] Nordlund, A., 1984a, in T.D.Guyenne and J.J.Hunt (eds.), The Hydromagnetics of the Sun, ESA SP-220, p.37.

[74] Nordlund, A., 1984b, in S.L.Keil (ed.), Small-scale Processes in Quiet Stellar Atmospheres, Sacramento Peak Observatory, Sunspot, p.174.

[75] Nordlund, A., 1986, in Deinzer et al. (1986), p.83

[76] Orszag, S., Tang, C.-H., 1979, J. Fluid Mech., 90, 129

[77] Parker, E.N., 1955, ApJ, 121, 491

[78] Parker, E.N., 1963, ApJ, 138, 552

[79] Parker, E.N., 1978, ApJ, 221, 368

[80] Parker, E.N., 1984, ApJ, 283, 343

[81] Pizzo, V.J., 1990, ApJ, 365, 764

[82] Pizzo, V.J., McGregor, K.B., Kunasz, P.B., 1993, ApJ, 404, 788

[83] Proctor, M.R.E., Gilbert, A.D., (eds.) Lectures on Solar and Planetary Dynamos, 1994, Publications of the Newton Institute, Cambridge University Press, Cambridge.

[84] Proctor, M.R.E., Weiss, N.O., 1982, Rep. Progr. Phys., 45, 1317

[85] Roberts, B., 1976, ApJ,204, 268

[86] Roberts, B., 1986, in Deinzer et al. (1986), p.169

[87] Roberts, B., 1991, in Ulmschneider et al. (1991), p.494

[88] Roberts, B., Webb, A.R., 1978, Solar Phys., 56, 5.

[89] Rogers, F.J., Iglesias, C., 1992, ApJS, 79, 507

[90] Rüedi, I., 1991, Measurement of Solar Magnetic Fields with Infrared Lines, Diplomarbeit, Institut fur Astronomie, ETH Zurich.

[91] Rüedi, I., Solanki, S.K., Livingston, W., Stenflo, J.O., 1992, A&A, 263, 368

[92] Ryutova, M.P., 1990, in Stenflo (1990), p.229.

[93] Schmidt, H.U. (ed.), 1985, Theoretical Problems in High Resolution Solar Physics, MPA 212, Max-Planck-Institut fur Physik und Astrophysik, Munchen.

[94] Schüssler, M., in J.O.Stenflo, 1990, p.161.

[95] Schüssler, M., 1991, Habilitationsschriff, Universität Göttingen

[96] Schüssler, M., 1992, in The Sun - a Laboratory for Astrophysics, J.T.Schmelz, J.C.Brown (eds.), Kluwer, Dordrecht, p.191

[97] Sheeley, Jr., N.R., 1966, ApJ, 144, 723

[98] Sheeley, Jr., N.R., 1967, Sol. Phys., 1, 171

[99] Sivaraman, K.R., Livingston, W.C., 1982, Sol. Phys., 80, 227

[100] Solanki, S.K., 1986, A&A, 168, 311

[101] Solanki, S.K., 1987a, The photospheric layers of solar magnetic fluxtubes, Dissertation, Institut fur Astronomie, ETH Zurich.

[102] Solanki, S.K., 1987b, in L.Hejna, M.Sobotka (eds.), Proc. Tenth European Regional Astronomy Meeting of the IAU. Vol. 1: The Sun, Publ. Astron. Inst. Czechosl. Acad. Sci., p.95.

[103] Solanki, S.K., 1987c, in E.-H.Schröter et al. (1987), p.67.

[104] Solanki, S.K., 1989, A&A, 224, 225

[105] Solanki, S.K., 1990, in Stenflo (1990), p.103

[106] Solanki, S.K., 1993, Space Sci. Rev., 61, 1

[107] Solanki, S.K., Stenflo, J.O., 1984, A&A, 140, 185

[108] Solanki, S.K., Zufferey, D., Lin, H., Ruedi, I., Kuhn, J.R., 1996, A&A, 310, L33

[109] Spiegel, E.A., 1957, ApJ, 126, 202

[110] Spiegel, E.A., 1960, ApJ, 132, 716

[111] Spiegel, E.A., 1963, ApJ, 138, 216

[112] Spiegel, E.A., 1964, ApJ, 139, 959

[113] Spiegel, E.A., 1972, ARAA, 10, 261

[114] Spruit, H.C., 1977, Ph.D Thesis.

[115] Spruit, H.C., 1979, Sol. Phys., 61, 363

[116] Spruit, H.C., 1981a, in S.Jordan (ed.), The Sun as a Star, CNRS/NASA Monograph Series on Nonthermal Phenomena in Stellar Atmospheres, NASA SP-450, p.385.

[117] Spruit, H.C., 1981b, A&A, 98, 155

[118] Spruit, H.C., 1981c, A&A, 102, 129

[119] Spruit, H.C., 1983, in J.O.Stenflo (ed.), Solar and Stellar Magnetic Fields: Origin and Coronal Effects, IAU-Symp. No. 102, Reidel, Dordrecht, 41

[120] Spruit, H.C., 1991, in C.P.Sonett, M.S.Giampapa, M.S.Mathews, (eds.), The Sun in Time, University of Arizona Press, The University of Arizona, Tucson.

[121] Spruit, H.C., Roberts, B., 1983, Nature, 304, 401

[122] Spruit, H.C., Schüssler, M., Solanki, S.K., 1991, in The Solar Interior and Atmosphere, W.C.Livingston and A.N.Cox (eds.), University of Arizona Press, The University of Arizona, Tucson.

[123] Spruit, H.C., Zwaan, C., 1981, Sol. Phys., 70, 207

[124] Spruit, H.C., Zweibel, E.G., 1979, Sol. Phys., 62, 15

[125] Steiner, O., 1990, Model calculations of solar magnetic fluxtubes and radiative transfer, Dissertation, Institut fur Astronomie, ETH Zurich.

[126] Steiner, O., 1994, in Infrared Solar Physics: IAU Symposium 154, D.M.Rabin, John T. Jefferies, and C.Lindsey (eds.), Kluwer Academic Publishers, Dordrecht, p.407

[127] Steiner, O., 1996, in Solar and Galactic Magnetic Fields, D.Schmidt (ed.), Nachrichten der Akademie der Wisenschaften, Göttingen.

[128] Steiner, O., Grossmann-Doerth, U., Knoelker, M., Schüssler, M., 1998, ApJ, 495, 468

[129] Steiner, O., Stenflo, J.O., 1990, in Stenflo (1990), p.181.

[130] Stenflo, J.O., 1973, Sol. Phys., 32, 41

[131] Stenflo, J.O., 1989, Astron. Astrophys. Rev., 1, 3

[132] Stenflo, J.O., (ed.), 1990, Solar Photosphere: Structure, Convection and Magnetic Fields, IAU-Symp. No. 138, Kluwer, Dordrecht.

[133] Stenflo, J.O., Harvey, J., 1985, Sol. Phys., 95, 99

[134] Stenflo, J.O., Solanki, S.K., Harvey, J.W., 1987a, A&A, 171, 305

[135] Stenflo, J.O., Solanki, S.K., Harvey, J.W., 1987b, A&A, 173, 167

[136] Syrovatskii, S.I., Zhugzhda, Y.D., 1968, Soviet Astr. A.J., 11, 945

[137] Takeuchi, 1993, PASJ, 45, 811

[138] Takeuchi, 1995, PASJ, 47, 331

[139] Thomas, J.H., in Schmidt (1985), p.126

[140] Thomas, J.H., 1990, in Physics of Magnetic Flux ropes, C.T.Russell, E.R.Priest, L.C.Lee (eds.), Geophysical Monograph 58, American Geophys. Union, Washington DC, p.133

[141] Title, A.M., Tarbell, T.D., Topka, K.P., 1987, ApJ, 317, 892

[142] Unno, W., Ando, H., 1979, Geophys. Astrophys. Fluid Dyn., 12, 107

[143] Unno, W., Spiegel, E.A., 1966, PASJ, 18, 85

[144] Van Ballegooijen, A., 1984a, in Small-scale Dynamical Processes in Quiet Stellar Atmospheres, S.L.Keil (ed.), National Solar Obs., Sunspot, NM, p.260

[145] Van Ballegooijen, A., 1984b, Sol. Phys., 91, 195

[146] Venkatakrishnan, P., 1983, J. Astrophys. Astron., 4, 135

[147] Venkatakrishnan, P., 1985, J. Astrophys. Astron., 6, 21

[148] Venkatakrishnan, P., 1986, Nature, 322, 156

[149] Vernazza J.E., Avrett, E.H., Loeser, R., 1981, ApJS, 45, 635

[150] Webb, A.R., Roberts, B., 1978, Sol. Phys., 59, 249

[151] Weiss, N.O., 1966, Proc. Roy. Soc. A, 293, 310

[152] Weiss, N.O., 1981a, J. Fluid Mech., 108, 247

[153] Weiss, N.O., 1981b, J. Fluid Mech., 108, 273

[154] Weiss, N.O., Brownjohn, D.P., Hurlburt, N.E., Proctor, M.R.E., MNRAS, 1990, 245, 434

[155] Wiehr, E., 1985, A&A, 149, 217

[156] Wilkinson, J.H., Reinsch, C., 1971, in Handbook for Automatic Computation, Vol.2, Springer-Verlag, Berlin

[157] Zayer, I., Solanki, S.K., Stenflo, J.O., 1989, A&A, 211, 463

[158] Zayer, I., Solanki, S.K., Stenflo, J.O., Keller, C.U., 1990, A&A, 239, 356

[159] Zhang, J., Lin, G., Wang, J., Wang, H., Zirin, H., 1998, Sol. Phys., 178, 245

[160] Zwaan, C., 1979, Sol. Phys., 60, 3